NASA Contractor Report 3620

Analysis of an Existing Experiment on the Interaction of Acoustic Waves With a Laminar Boundary Layer

M. R. Schopper

CONTRACT NAS1-16572
NOVEMBER 1982

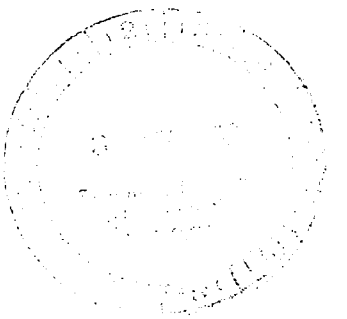

NASA

ERRATA

NASA Contractor Report 3620

ANALYSIS OF AN EXISTING EXPERIMENT ON THE INTERACTION OF ACOUSTIC WAVES WITH A LAMINAR BOUNDARY LAYER

M. R. Schopper
November 1982

The following corrections should be made to this report:

Page 30, lines 3 and 6 of third full paragraph: Change equation (41) to equation (11)

Page 43, line 11: Change figure 10 to figure 8

Page 51, last line before equation (16): Change eq. (9) to eq. (15)

Page 57, third line after equation (25): Change equation (26) to equation (25)

Page 59, first line after equation (37): Change equation (28) to equation (34)

Page 62: Equation (41) should read:

$$k_x = \left[\left(\frac{\omega}{c}\right)^2 - \left(\frac{m\pi}{w}\right)^2 - \left(\frac{n\pi}{h}\right)^2 \right]^{1/2}$$

Page 64, line 12 should read: The rms value of the signal is $\tilde{s} = \sqrt{1/2\ \hat{s}\ \hat{s}^*}$

Page 65, ninth line from bottom of page: Change the first part of the line to read

$$\delta_a = 1.55\sqrt{2\nu/\omega}.$$

Page 69, last line before equation (44): Change (ref. 41) to (ref. 48)

Pages 74-75: Change reference numbers 40 through 46 to 47 through 53

Page 75: Change reference numbers 47 through 53 to 40 through 46

Date issued: March 1983

NASA Contractor Report 3620

Analysis of an Existing Experiment on the Interaction of Acoustic Waves With a Laminar Boundary Layer

M. R. Schopper
Systems and Applied Sciences Corporation
Hampton, Virginia

Prepared for
Langley Research Center
under Contract NAS1-16572

National Aeronautics
and Space Administration

**Scientific and Technical
Information Branch**

1982

SUMMARY

The primary purpose of the present study is the reevaluation of the hot-wire anemometer amplitude data contained in the 1977 subsonic flat plate acoustic-boundary layer instability investigation report of P. J. Shapiro entitled, "The Influence of Sound Upon Laminar Boundary Layer Instability." As shown here, the low-Reynolds number boundary layer disturbance data were misinterpreted and the present effort was made to improve the corresponding disturbance growth rate curves. The data show a standing wave pattern along the plate and it is known that this can be satisfactorily explained as being due to the superposition of the free-stream sound waves and the laminar boundary layer instability Tollmien-Schlichting (TS) waves. To extract the TS wave amplitude and phase velocity information the data were modeled as the sum of acoustic waves and a wave representing the TS wave. Using the free-stream disturbance data, the sound field was modeled by a primary downstream traveling sound wave, a weak reflected upstream traveling wave, and nonpropagating "noise" terms representing possible decaying evanescent sound fields at each end of the test section. The amplitude and phase velocity of the TS wave were then adjusted so that the total signal reasonably matched the amplitude and phase angle from hot-wire data along the laminar boundary layer on the plate.

Except for the region upstream of the rapid increase in boundary layer disturbance growth, the resulting phase velocity variation was within 2% of the theoretical two-dimensional TS phase speed. In the upstream region the speeds were about 10% higher than the flat plate values, but the increase is qualitatively consistent with the adverse pressure gradient existing in this region. The TS wave amplitude at the earliest measurement station was 0.25 times the sound field amplitude near the leading edge. Shapiro's TS growth rate curves showed growth ahead of the theoretical flat plate stability neutral point, and the revised rates show growth occurring even further upstream. It appears that the premature growth is due to the adverse pressure gradient created by the shape of the plate. One of the purposes of Shapiro's investigation was to determine if the sound could be affecting TS wave growth along the plate, but the pressure gradient has prevented such a determination. Comparison of the measured pressure distribution with published theoretical distributions for plate leading edge shapes similar to Shapiro's shows considerable disagreement. Obviously, it would be desirable to reduce the pressure gradients in future experiments.

Acoustic excitation experiments are important to the boundary layer transition problem because sound pervades the flow environment of aircraft and wind tunnels. But these experiments are difficult ones to satisfactorily conduct because of the problem of establishing a controlled acoustic field; a complicated wave field is invariably present. Sound field measurements are an important part of tunnel experiments which use sound. Some of the basic elements of sound propagation in ducts have been reviewed in the present report.

Shapiro did expend a considerable effort monitoring and altering the test section sound field. The acoustic data presented in the report, however, appears to have been taken with the flat plate absent. Because the plate would effectively divide the test section into two channels, the presence of the plate would likely affect the sound field for the higher of the two frequencies used in the investigation because of changes in the modal characteristics of the sound passages. For the lower frequency case (500 Hz),

the condition modeled in the present work, the presence of the plate may not have significantly altered the sound field. Study of the acoustic stability experimental literature reveals that researchers need to be more diligent in reporting tunnel size and model location so that readers can better assess the standing wave situation.

TABLE OF CONTENTS

INTRODUCTION

The laminar boundary layer is a rather discriminating listener. Sounds which it rejects are quashed with little more than a ripple. But those it finds mellifluous are accepted with waves of enthusiasm which soon burst into turbulent pandemonium. Boundary layer transition--what a fascinating, fickle, unpredictable, and important fluid phenomenon it is. And indeed, sound often plays an important role in the process. In fact, it is not unusual to find that in acoustic-transition experiments the location of transition on simple models can be controlled using the sound from a loudspeaker (e.g., refs. 1 and 2). Sound is residually present in low-speed wind tunnels, is prominently present in the form of engine noise in subsonic flight, and, in the form of noise radiated from the turbulent nozzle boundary layers, is the predominant disturbance in supersonic wind tunnels. Only in supersonic flight are there laminar boundary layers in regions out of the reach of sound--and these regions are also generally out of the reach of the experimenters. It is no wonder, then, that the acoustic-transition problem has attracted and fascinated the researcher. It has certainly challenged and frustrated him as well as the designer of wind tunnels and laminar flow control aircraft.

Tollmien-Schlichting boundary layer instability waves (TS waves) and their amplification frequently form one of the early stages of the boundary layer transition process. It is known that when a moderate acoustic field is present the existence of the TS waves is intimately related to the field. But while the behavior of TS waves in the absence of sound waves can be calculated, it is not entirely understood just how a sound field interacts with a boundary layer to produce TS waves and to what extent, if any, the sound field subsequently affects these waves. Does the sound field simply set up the initial conditions of the TS waves? Does the sound field alter the growth rate of the TS waves by feeding energy into the waves as they travel along the boundary layer? In the experimental investigation of Shapiro (ref. 3) an attempt was made to confront these issues.

Using a low-speed wind tunnel Shapiro studied the effects of acoustic excitation on the Tollmien-Schlichting waves. In the experiment the subsonic flat plate laminar boundary layer was excited acoustically by the sound field from a loudspeaker located upstream of the tunnel test section. Shapiro found that Tollmien-Schlichting instability waves were generated with the same frequency as the excitation sound field. Using a hot-wire anemometer, the TS wave amplitudes and frequencies were measured and so was the phase angle difference between the anemometer signal and the reference signal fed to the loudspeaker. He concluded that the excited TS waves matched stability theory results well in most respects and that the acoustic excitation merely generated a larger initial wave amplitude. For excitation levels larger than the residual tunnel disturbances, Shapiro concluded that the initial amplitude was constant ahead of Branch I of the neutral curve (that is, ahead of the point where TS wave amplification is predicted to occur), and that this amplitude matched the disturbance velocity amplitude of the sound wave. Inasmuch as the TS waves are supposed to decay ahead of Branch I, the constant amplitude condition is not consistent with flat plate stability theory. The conclusion is also contradicted by his experimentally determined amplification rate curves, for these show wave growth ahead of Branch I.

There is a problem here concerning the absence of upstream TS wave amplitude decay. In Shapiro's experiments the boundary layer ahead of Branch I was

in an adverse pressure gradient region. Boundary layers are less stable under such conditions and an absence of wave decay would not be an unusual feature. The TS wave amplitude behavior could therefore, in a vague sense, be considered to match the theory (but without a detailed analysis of the effects of the pressure gradient the extent of the compliance with theory cannot be accurately assessed). But one also has to face Shapiro's other contention that the TS velocity fluctuation amplitude matched the sound disturbance amplitude ahead of Branch I. The important question is: In the absence of an adverse pressure gradient, would the TS wave amplitude still have matched the sound field amplitude along the plate? Shapiro's answer would appear to be yes because he stated that the TS amplitude remained constant simply because the excitation remained constant as the wave progressed down the plate. Such behavior does not match stability theory in most respects but instead represents a significant departure. The contentions are contradictory.

The problem stems from the fact that with the sound field present a standing wave pattern with periodic spatial oscillations was always observed along the plate. Shapiro did not identify the cause of the wave pattern, but it is reasonable to believe, and supporting evidence will be offered, that the pattern was simply the result of the interference between the traveling sound and TS waves. Waves having the same frequency but different speeds produce a standing wave pattern when traveling together as long as their directions are not orthogonal. In fact, the concept of standing waves is usually introduced in textbooks by considering the case of waves with the same frequency traveling in the opposite direction. To obtain TS wave amplitude growth rates Shapiro faired curves through the oscillatory pattern. This is a natural thing to do and it is likely that some of the ambiguity resulted from the difficulty in the subjective fairing process. It will be shown below that the fairing procedure is not correct. Upstream of Branch I a faired result represents one quantity and somewhere downstream of the Branch it represents another, and the two quantities do not join smoothly. Thus trying to fair smoothly no doubt was a frustrating task. When the amplitude of the TS wave is less than that of the sound wave, fairing does not give the TS wave strength. Consequently, in the upstream boundary layer region where the TS wave amplitude is still small, a reevaluation of the amplitude data is in order. As was previously indicated, there is a particular interest in the upstream region for it is not well understood just how acoustic waves are ingested by the boundary layer in the production and possible modification of TS waves. The purpose of this report is to present and compare with theory the amplification rates, phase velocities, and wave numbers of the Tollmien-Schlichting instability waves as determined from a reexamination of data presented in Shapiro's report.

In the present report the acoustic and TS waves are represented by a mathematical model of traveling waves. The speed of the acoustic waves were taken as the speed of sound plus (or minus, depending on the wave direction) the free-stream speed of the fluid, and the amplitude distribution was adjusted to match Shapiro's free-stream acoustic data. The amplitude and wave number of the TS wave were considered as unknowns, and when the acoustic and TS waves were summed, these two parameters were adjusted so that the total signal reasonably matched the data. The amplitude data were used to determine the TS wave amplitude behavior and the phase angle data were used to determine how the wave number varied. The wave speed was obtained from the frequency and wave number information.

Stability experiments in which acoustic excitation is used require

considerable development work if they are to be done carefully. Shapiro did a lot of development work in his investigation and it is not likely that there will be a rash of such experiments. His results are interesting and have already been cited in the literature. For example, Murdock (ref. 4) has compared his computational findings with Shapiro's experimental results. And a significant portion of the review article by Leehey (ref. 5) was devoted to Shapiro's work. The initial one-to-one ratio of the TS-to-sound wave amplitude was cited and TS wave amplitude growth rate curves were displayed. It is likely that Shapiro's report will continue to be frequently cited by stability and transition researchers, and the primary objective of the present effort was to recover more appropriate TS wave amplitude information from the data.

The report is quite large for such a modest objective. It is inflated by such things as additional background information, discussion of aspects of wave interference, and a presentation of basic elements of sound propagation in ducts. These take up 60% of the report! The section on elements of duct acoustics is relegated to an appendix and is occasionally referred to in the section in which Shapiro's tunnel sound field is modeled. By and large this appendix may be useful only to those who have to work with tunnel acoustics for the first time. The final 20% of the report describes the precise details of the information extraction procedure and the resulting TS wave properties.

ADDITIONAL BACKGROUND

Standing Waves and Data Fairing

To show that it is reasonable to believe that the periodic standing wave pattern is due to acoustic-TS wave superposition, the measured wavelength can be compared with the expected wavelength for the interference phenomenon. The wavelength of the spatial oscillations in Shapiro's rms amplitude data was approximately 2 cm. The wavelength of the interference pattern can be estimated by considering the sum of two sinusoidal waves traveling in the x direction and having the same radian frequency ω but different wave speeds, c_1 and c_2. The respective wave numbers, defined by $k = \omega/c$, would therefore differ. Considering both waves to have unit amplitudes and using the trigonometric identity for the sum of two sine waves, the traveling wave sum is

$$\sin(k_1 x-\omega t) + \sin(k_2 x-\omega t) = 2 \cos \frac{k_1 - k_2}{2} x \quad \cos(\frac{k_1 + k_2}{2} x \quad -\omega t) \qquad (1)$$

The rms value of such a signal is easily shown to be the standing wave given by $\sqrt{2}\,|\cos Kx|$, where $K = (k_1 - k_2)/2$. Here the absolute value has been written instead of $\sqrt{\cos^2 Kx}$. The wavelength for a sinusoidal function is $2\pi/k$, and for the absolute valued function the wavelength is halved. Therefore, the wavelength of the resulting pattern is π/K. This quantity may be written in terms of the frequency f and the wave speeds as $c_1 c_2/[f(c_2 - c_1)]$. In the experiment $f = 500$ Hz. The free-stream velocity was $U_\infty = 29$ m/sec, and a reasonable estimate for the TS wave speed is $c_1 = U_\infty/3$. The velocity of the acoustic wave is $c_2 = U_\infty + a$, where $a = 344$ m/sec is the speed of sound in stationary air. Using these quantities the estimated wavelength is 1.98 cm, a value which is quite close to the observed value. This is rather convincing evidence that the data are showing the acoustic-TS wave interference pattern. The present work was initiated after examining Shapiro's report and discovering, through wavelength amplitude comparison, the cause of the standing wave pattern.

The effect of the data fairing procedure can be demonstrated by generalizing the above results to include non-unit amplitudes. Letting the variable amplitudes of the sound and TS waves be $A_s(x)$ and $A_{ts}(x)$, respectively, the rms signal $\tilde{s}(x)$ level can be shown to be

$$\tilde{s}(x) = \sqrt{\tfrac{1}{2}[A_s^2(x) + A_{ts}^2(x) + 2A_s(x)A_{ts}(x)\cos\theta]} \qquad (2)$$

where θ is the phase angle given by

$$\theta = (k_{ts} - k_s)\, x + \phi_{ts} - \phi_s \qquad (3)$$

The ϕ values are the initial phase angles at $x = 0$. The signal $\tilde{s}$ thus undergoes sinusoidal-like spatial oscillations, and in a data fairing procedure a curve would be plotted through the oscillations such that it would fall halfway between the local peaks and valleys. In Shapiro's experiment the peaks and valleys were close together and the amplitudes generally changed very little between a peak and a valley in the upstream region. Consequently A_s and A_{ts} may be treated as locally constant between adjacent peaks and valleys, and since the $\cos\theta$ varies from +1 to -1, adjacent local maximum and minimum values of $\tilde{s}$ reduce to, respectively,

$$\tilde{s}_{max} = \frac{A_s + A_{ts}}{\sqrt{2}} \tag{4}$$

and

$$\tilde{s}_{min} = \begin{cases} \dfrac{A_s - A_{ts}}{\sqrt{2}} & , \ A_{ts} \leq A_s \\ \dfrac{A_{ts} - A_s}{\sqrt{2}} & , \ A_{ts} > A_s \end{cases} \tag{5}$$

Fairing amounts to averaging s_{max} and s_{min} and hence

$$\tilde{s}_{faired} = \begin{cases} \dfrac{A_s}{\sqrt{2}} & , \ A_{ts} \leq A_s \\ \dfrac{A_{ts}}{\sqrt{2}} & , \ A_{ts} > A_s \end{cases} \tag{6}$$

Equation (6) shows that a fairing of the rms signal gives the rms value of the acoustic wave or the TS wave, depending on which of the two has the greater amplitude. By fairing the data Shapiro was hoping to obtain TS wave growth information, but eq. (6) shows that this procedure would be valid only in the downstream region where the TS wave had been sufficiently amplified so that its amplitude exceeded the acoustic level. In the important upstream region where the TS wave amplitude was small, the fairing procedure was therefore improper. Fairing should have produced a level which matched the stream acoustic level. This is precisely what Shapiro found! The acoustic level was relatively constant in the upstream region, and one of Shapiro's conclusions was that the TS wave amplitude was constant there. Shapiro also varied the acoustic level to see the effect on the TS level, and he also concluded that the initial TS wave amplitude and the exciting acoustic velocity were proportional to one another, with a proportionality factor equal to one. This finding confirms the impropriety of the fairing technique upstream. Equations (4) and (5) show that in the upstream region

$$A_{ts} = \frac{\sqrt{2}}{2} (\tilde{s}_{max} - \tilde{s}_{min}) \tag{7}$$

Thus a better procedure for determining $A_{ts}(x)$ would have been to have faired a curve through the maxima and another through the minima and used these faired values in eq. (7). In terms of rms values, a procedure for determining TS wave results would be

$$\tilde{A}_{ts} = \begin{cases} \dfrac{\tilde{s}_{max} - \tilde{s}_{min}}{2} & , \ A_{ts} \leq A_s \\ \dfrac{\tilde{s}_{max} + \tilde{s}_{min}}{2} & , \ A_{ts} > A_s \end{cases}$$

Other Sound-Stability Investigations

Thomas and Lekoudis (ref. 6) were the first to publish the finding that the observed standing pattern in the Shapiro experiment was a wave superposition phenomenon. In their study they considered the superposition of a constant amplitude acoustic wave and a TS wave in which the amplitude and wave number

were computed from stability theory (with the amplitude adjusted so that $A_{ts}/A_s = 1$ at the location of Shapiro's initial data station). The signal amplitude and phase were computed and compared with the data; the computed results did show the spatial oscillatory behavior. They concluded that the only active interaction between the acoustic and TS fields was the setting of the initial conditions for the TS wave by the sound wave. While this may indeed be the situation, their evidence does not support their conclusion and the case is yet to be made. Although it is not mentioned, their amplitude calculations show the normal TS wave decay and subsequent growth, but Shapiro's data show no wave decay. The departure of data from stability theory is the thing one looks for in acoustic-stability experiments, for departures provide the key to understanding the acoustic interactions. Thus it is essential that the amplitude departures be addressed before making conclusions. Concerning the phase angles the authors do state that the agreement with the data is poorer. The calculations show a mean phase angle growth with distance which is much greater than that shown in the data. Therefore both computed results show departures from the experimental findings. Shapiro discussed pressure gradient effects, and it will be shown later in this report that the absence of the TS wave decay may be due to the pressure gradient effects. It will also be shown later that the absence of a significant mean phase angle growth can likely be attributed to upstream propagating sound.

Standing wave patterns resulting from the superposition of acoustic and instability waves have been found in experiments with free shear layers and with attached boundary layers. A standing pattern along a flat plate is clearly visible in the acoustic instability experiment of Mechel and Schilz (refs. 7, 8). Results on a body of revolution with the acoustic radiation perpendicular to the stream have been presented by Vlasov, Ginevskiy, and Karavosov (ref. 9), and the data suggest acoustic-TS wave interference. The rms output from a hot-wire anemometer held fixed in the boundary layer while the frequency of the radiation was changed showed an oscillatory, albeit erratic, variation with frequency. An oscillatory behavior is consistent with the interference hypothesis because as the frequency is varied the phase angle changes (see eq. 3). A similar result from a flat-plate experiment is displayed in the report of Polyakov (ref. 2).

In the classic work of Schubauer and Skramstad (ref. 1), in which predictions of stability theory were experimentally confirmed for the first time, the authors emphasized in their conclusions the possible importance of sound to the transition process. In the experiment they did do some exploratory and revelatory work with loudspeaker acoustic excitation before arriving at their vibrating ribbon technique of exciting TS waves. With the loudspeaker axis nearly collinear with the leading edge of their flat plate they found that the location of transition could be moved all around simply by changing the frequency and amplitude of the sound. But in their quest for controlled excitation this technique was abandoned because the acoustic fields were always complicated ones. So, while emphasizing the importance of sound they were also the forerunners, in effect, of conceding the difficulty of performing acoustic-stability experiments. As will be reported later, a considerable portion of Shapiro's efforts was spent measuring and trying to control the sound field.

Acoustic difficulties indeed plague researchers. Wells (ref. 10) varied the free-stream turbulence level conditions while observing the transition

location on the wall of his low-speed tunnel. Subsequently it was reported by Spangler and Wells (ref. 11) that acoustic standing waves had been present in the experiment. These were reduced by venting the downstream end of the test section to the atmosphere, and it was reported that while no change in the transition locations occurred, there was a significant reduction in the measured free-stream disturbance levels. Transition experiments were then conducted in which an acoustic field was set up by a siren placed upstream of the nozzle entrance. Transition was detected with visual means using smoke. Four different fundamental frequencies were selected for the tests, but it was reported that the siren was imperfect and had several harmonics, some of which were as strong as the fundamental. The variation of transition Reynolds number with measured free-stream intensity was displayed for each of the four cases and marked differences did occur. No doubt standing waves still existed, and a troublesome aspect of the work is that the free-stream acoustic measurements were all taken at one location within the tunnel. Equations (2) and (3) show how the signal would change at a fixed distance when the frequency is varied. In eq. (3), since opposite-direction waves are considered, the sum rather than difference in wave numbers would be used. No tunnel dimensions are given; the authors force the reader to obtain the original reports to obtain such basic information.

Knapp and Roache (ref. 12) investigated transition and a few aspects of the TS waves on ogive nose cylinders aligned with the flow. Smoke was used for flow visualization and hot-wire data was also taken. A loudspeaker installed upstream of the nozzle provided acoustic excitation (reported to have a high first harmonic component). Tunnel dimensions are not given (this information is basic when acoustic fields are used and there is no excuse for not giving such simple facts); the reader must consult original documents to obtain this information and, presumably, information about the uniformity of the acoustic field. Spectral measurements were taken, with and without the sound, with a hot-wire fixed near the surface. Without the sound the spectra at various flow speeds showed a natural band of frequencies present (bandwidth of wave analyzer was not given). When the speaker frequency was set within the middle of this band a large peak at this frequency was reported to have occurred. As the speaker frequency was changed and the limits of the natural band approached, the amplitude of the wave analyzer output at the acoustic frequency was reported to decrease and more of the natural band to appear. No mention was made of occurrences of mean oscillations in the wire output as the frequency was changed, but any such occurrences may not have been considered particularly relevant to their study.

There have, of course, been many other experimental investigations of the subsonic noise-transition phenomena. Stability considerations were an important part of the research efforts, but the emphasis was more on the transition process than on a detailed study of the TS waves themselves such as in Shapiro's experiments. Two of the more recent investigations have been by Barinov, et al. (ref. 13) and Bohn and Mangiarotty (ref. 14). In both investigations it was found that the dominant frequencies of the disturbances leading to transition were in the range of unstable frequencies according to stability theory. The latter investigation was conducted as part of a laminar flow control technology program and much of the motivation for acoustic-stability studies has come from such programs. Some of the early work on this problem was described by Penninger and Reed (ref. 15). Many additional references may be found in the survey of Bushnell and Tuttle (ref. 16) and in the report of Hefner and Bushnell (ref. 17).

A very interesting experiment and review has been reported by Kachanov, Kozlov, and Levchenko (ref. 18) concerning the generation of TS waves. In their low-speed flat-plate experiment a vibrating ribbon was used to generate a vortex street upstream of the plate. Amplitude and phase angle disturbance measurements were made using a hot-wire. With the ribbon parallel to the plate and the vortex perturbations passing just slightly above the plate's boundary layer, no TS waves were generated in the boundary layer. When the perturbations were allowed to impinge directly on the leading edge, TS waves were generated. The plate was 1 cm thick and had a sharp leading edge with semielliptic contours and the hot-wire measurements were very detailed over a 10-15 mm region upstream and downstream of the leading edge. No TS waves were generated when the ribbon was rotated 90° so that it was stretched perpendicular to the plate. In this arrangement there were no v perturbations (plate in x-z plane) in the incoming disturbances and based on this fact and other observations they concluded that the v fluctuations at the leading edge play a significant role in TS wave generation. From a review of their own and other findings they further concluded that the same leading-edge v mechanism was responsible for TS wave generation in the cases of vortical, acoustical, and model vibratory disturbances. They also expressed their belief that downstream of the leading edge these types of disturbances did not feed energy into the TS waves.

The belief that a sound field is most important at the leading edge or that sound does not affect the TS wave development downstream from the leading edge region has also been expressed by some researchers in the theoretical domain. In the analytic study by Mungar (ref. 19) two equations were derived from the linearized Navier-Stokes equations. One governed the sound field and the other the fluctuating vorticity field. The latter was written in the form of an inhomogeneous Orr-Sommerfeld equation (the homogeneous version describes the TS wave behavior) which represented the generation by a sound field of fluctuating vorticity and its convected diffusion and amplification or decay by the boundary layer. For the two-dimensional case the acoustically induced vorticity source strength consisted of two terms, one proportional to the product of the acoustic pressure and the mean shear, and the other term proportional to the product of the acoustic pressure transverse derivative and the second derivative of the mean flow. Since both terms involved the transverse gradient of the mean flow, the vorticity production by a sound field only occurs in a boundary layer. The nondimensional wave number, $k\delta(x)$, appeared in one term and its reciprocal appeared in the other. Because of the $1/k\delta(x)$ term the acoustically induced vorticity source strength was considered to have the greatest concentration at the leading edge of a flat plate. Mungar also concluded that the vorticity field would have two components, one propagating at the acoustic speed and the other at the TS wave speed. These two components would give rise to an interference pattern and he cited the Schilz (ref. 8) experiment (Shapiro's report had not been published) as supporting evidence of this. (Mungar stated that the wavelength of the pattern would be proportional to the wave number difference, but it should be the reciprocal of the difference).

Miller and Callegari (ref. 20) examined the acoustic-stability problem by a numerical solution of the unsteady, compressible, two-dimensional, second order boundary layer equations (retaining terms of order $1/Re$ and $1/Re^2$). Inasmuch as compressible equations were used, sound waves with finite speeds could propagate through the flow. The investigation was centered, according to the authors, on the study of the amplification or damping of acoustical

disturbances propagated into the boundary layer (the Shapiro report was cited in their Introduction). The disturbance frequencies and the free-stream unit Reynolds number conditions were chosen, for the most part, to match those of the low-speed experiment of Spangler and Wells (ref. 11). The upstream velocity boundary condition was taken as the sum of the laminar Blasius profile and a temporal sinusoidal oscillation whose amplitude distribution across the layer was determined from a solution of the compressible analogue of the Orr-Sommerfeld stability equations (actually taken in the inviscid limit with the additional assumption of no temperature gradient in the mean flow--neutral stability conditions were selected). From a study of the behavior of the disturbance speeds and of the variation of the longitudinal velocity fluctuation disturbance amplitude with downstream distance, Miller and Callegari concluded that the downstream disturbances in the boundary layer were TS waves which essentially behaved according to linear stability theory. Thus, it was concluded, the response of a boundary layer to acoustic vibrations is similar to the response to other disturbances.

There are some curious and troublesome aspects of the results of Miller and Callegari. The most important of these is the lack of any discussion of TS-acoustic wave interference phenomenon. Such interference would be expected to occur, and the absence of discussion of the matter implies that their calculations did not show any wave interference. This signifies that perhaps something is wrong with their results. A closer examination shows that, in contrast to their statements, in some cases their results do not appear to be consistent with linear stability theory. In the paragraphs which follow, a disproportionately large portion of the present section will be devoted to discussion of some of the findings of Miller and Callegari. Readers may wish to skip this and may do so by jumping to the last review of the section, that of Murdock's paper (ref. 4), which begins on page 14.

As just mentioned, a troublesome aspect of the Miller and Callegari study is that, in contrast to their statements, in some cases their results do not appear to be consistent with stability theory. This issue will be considered first. Their first result is a figure which shows three amplitude-time histories at a given downstream distance and height in the boundary layer for the cases of disturbance frequencies of 27, 43, and 150 Hz, respectively. They all had equal upstream initial amplitudes, and the downstream signals are seen to be unequal. The figure shows that after about one cycle the oscillations became nearly sinusoidal. Without a detailed integration of boundary layer stability growth rates from the initial to final stations, it is not possible to accurately assess whether the results are actually in accordance with stability theory. For example, the 43 Hz signal amplitude nearly matches the upstream initial amplitude and the authors state that the signal appears to be neutrally stable. However, according to stability theory the station is well within the unstable region. In their next figure (fig. 4) it is possible to make such an assessment. For a given unit Reynolds number of 7.94×10^5 per meter (2.42×10^5 per ft), the temporal signal is displayed at the three downstream distances of 2.44 m (8 ft), 3.66 m (12 ft), and 4.88 m (16 ft) for the case of the 27 Hz disturbance. The signal amplitudes diminish with increase in distance, and this does not appear to be in accordance with stability theory. This is established with the aid of a flat plate boundary layer stability diagram of nondimensional frequency vs. displacement thickness shown in Obremski, Morkovin, and Landahl (ref. 21, fig. 10j). The displacement thickness Reynolds numbers at the three locations are, respectively, 2393, 2931, and 3385 (using $Re_{\delta^*} = 1.72 \sqrt{Re_x}$). To use the stability diagram of

reference 21, the nondimensional frequency defined by $2\pi f\nu/U_\infty^2$ must be determined. Assuming air at a temperature of 21.1° C (70° F), the kinematic viscosity may be taken as 1.47×10^{-5} m^2/sec (1.58×10^{-4} ft^2/sec) and the stream velocity and nondimensional frequency become, respectively, 11.68 m/sec (38.13 ft/sec) and 1.83×10^{-5}. For this frequency the unstable Reynolds number range may be estimated from ref. 21 to be from 1840 to 4150 (± 300? - determined from a small figure). Therefore, the three stations were all within the unstable region and the disturbance amplitude should have been increasing with increase in distance. The opposite trend was found by Miller and Callegari although they indicated that the results were satisfactory.

In their next case similar computations were performed for a 150 Hz signal and the results were displayed for downstream stations of 0.61 m (2 ft), 1.83 m (6 ft), and 3.05 m (10 ft). The amplitudes for the two most downstream stations were greatly diminished and this is consistent with the fact (using ref. 21) that the stations were downstream of the unstable region. In another positive check of their computations, Miller and Callegari compared amplitude vs. Reynolds number results with those of Murdock (refs. 22 and 23). In Murdock's investigation the unsteady, two-dimensional flow over a flat plate was studied, but the flow was considered incompressible. The initial velocity condition (at $Re_x = 10^5$) was taken as the sum of the Blasius profile and an Orr-Sommerfeld disturbance. Since the flow was incompressible the disturbance simulated conditions downstream of a vibrating ribbon (the ribbon is the usual way TS waves are generated in boundary layer experiments). His numerical results were in good agreement with stability theory. In the plot of amplitude vs. Reynolds number, Miller and Callegari's results were in fair agreement with Murdock's.

In a final test, Miller and Callegari made a rough determination of the neutral point for the case of a 25 Hz signal in a stream with a unit Reynolds number of 1.97×10^5 per meter (actually given in both the text and a figure as 0.6×10^5 per foot). This was done by plotting the signal output at a given instant of time against Re_{δ^*} and fairing curves through the positive and the negative peaks (actually, for a more accurate fairing two output curves taken at times such that they were nearly 180° out of phase were plotted). These faired curves showed that the signal amplitudes reached a minimum at a Reynolds number near the indicated theoretical neutral value of approximately 1130. A problem arises concerning the theoretical neutral point Reynolds number. Again taking the above value of kinematic viscosity for air, the resulting stream velocity is found to be 2.90 m/sec (9.50 ft/sec) and the nondimensional frequency parameter becomes 2.76×10^{-4}. From figure 10j of reference 21 one finds that for this frequency condition the flow is completely stable--there are no neutral conditions. So, something is wrong somewhere. There is another troublesome aspect of these results. The expected wavelength of a TS wave can be estimated by taking the wave speed to be $0.3U_\infty$ (a reasonable value). For a 25 Hz signal this wavelength is 3.5 cm (1.4 in). Using their given unit Reynolds number and their plot of signal amplitude vs. Re_{δ^*}, the average wavelength of Miller and Callegari's disturbance can be shown to be 61 cm (24 in), a length which is 17 times the expected wavelength of a TS wave. A sound wave would have a wavelength of nearly 14 m (45 ft).

Concerning the sound wave, the initial longitudinal velocity fluctuation profile (at Re_x values of 10^4 to 10^5) would not appear to be a very natural one. For plane waves propagating downstream the sound amplitude would be

rather uniform in the free-stream and would diminish to zero within its own acoustic boundary layer near the wall. But the initial condition used by Miller and Callegari has a disturbance profile similar to that of a TS wave. This profile has a maximum amplitude near $y/\delta = 0.2$, decays to zero amplitude in the outer portion of the boundary layer near $y/\delta = 0.7$, and finally increases again to a weak local maximum near $y = \delta$ before beginning a slow asymptotic decay towards zero well outside of the boundary layer. In a very crude sense, the very long wavelength sound wave is being driven by two out of phase pistons located near $y/\delta = 0.2$ and 0.7, and oscillating in an infinite baffle with, respectively, large and small amplitudes. It is important to know how such a nonuniform sound wave propagates through the boundary layer. It is reasonable to expect that the acoustic amplitude distribution would tend toward a uniform one outside the acoustic boundary layer and consequently the peak amplitude should diminish as signal spreading occurs with increase in downstream distance. Certainly the zero amplitude gap would begin to be filled. There is some evidence that this was happening; Miller and Callegari show disturbance profiles for an initial condition and one slightly downstream, and the latter shows that the amplitude in the gap is no longer zero. It would be of interest to know the relative amplitudes of the TS and sound waves just downstream of the initial station. Are they nearly equal? If so, there would be significant signal modulation due to the interference of the two waves because such modulation is greatest when the signals have equal strength. The wavelength of the interference pattern can be estimated to be (using eq. (1) with wavespeeds again taken as $c_{TS} = 1/3\ U_\infty$ and $c_s = a + U_\infty$) from 2 to 14 cm for the frequencies from 150 to 25 Hz. These wavelengths are quite close to the wavelengths of the TS waves themselves. If the waves are initially of equal strength, then it is easy to envision downstream conditions where the decaying sound wave amplitude could again equal the TS wave amplitude or where the amplitude could be dominated by or could dominate the TS wave amplitude. Certainly the sound wave would dominate the TS wave at the zero point near $y/\delta = 0.7$, but just above and below this point the situation could be reversed.

It is also possible that the peak near $y/\delta = 0.2$ could have been inside the acoustic boundary layer at the upstream boundary. If this were the case, the peak sound amplitude would undergo a decay due to viscous effects just downstream of the initial point. It will be shown later in the report that the ratio of the acoustic boundary layer thickness to the laminar boundary layer thickness can be taken as $0.175\ \sqrt{U_\infty/fx}$, and hence the ratio of the acoustic boundary layer thickness to the peak disturbance height can be estimated to be $0.875\ \sqrt{U_\infty/fx}$. The distance to the initial boundary station is not often specified by Miller and Callegari. For the figure in which the 27, 43, and 150 Hz signals were displayed, the nondimensional initial x value was given as 0.025. The reference length was not given, but if it is the same as it was for their test case in which the neutral Reynolds number point was determined, the value is 3.66 m (12 ft). This would give $x \simeq 9.14$ cm (3.6 in), which corresponds to $Re_x = 7.26 \times 10^4$. With this value for x, the ratios of acoustic boundary thickness to the initial peak disturbance height are 1.9, 1.5 and 0.81 for, respectively, the frequencies of 27, 43, and 150 Hz. Consequently, for these conditions perhaps only in the 150 Hz case would the peak disturbance have initially been outside of the acoustic boundary layer.

The situation holds the potential of interesting TS-acoustic wave interference phenomena. Significant interference would not occur if either wave were dominant. Only the sound field could dominate completely across

the boundary layer, but in this case all of the computed results would have to be explained in terms of sound wave rather than TS wave behavior. TS waves could dominate the interior portion of the boundary layer, but as mentioned above, there would always be a region in the outer half of the boundary layer where the TS wave has a zero amplitude (longitudinal velocity component) and would be dominated by the sound wave. Thus, there will always be outer regions where significant interference occurs when the boundary layer is TS-wave dominated. It appears that most of the results in the Miller and Callegari report were for locations rather near to the wall, but it is impossible to tell for sure because not enough information is given to untangle the dimensionless heights given (in some cases the usual Blasius variable was provided).

In terms of acoustic wavelengths, the longitudinal domain of the numerical calculations ranged from approximately 1.3λ for the 150 Hz case to 0.4λ for the 27 Hz study. Since the TS wavelength would be about 1/100 of the acoustic wavelength for the conditions of their study, it would seem plausible that plots of signal amplitude vs. distance for a given time should have clearly revealed the presence of the two signals as long as the amplitude of the sound wave was comparable to or greater than that of the TS wave. But the authors make no report of seeing two waves within the boundary layer. And, as discussed above, in the one figure shown to the reader of amplitude vs. distance, the wavelength is neither that of a TS nor a sound wave (approximately 20 times the former and 1/20 of the latter). The modeling procedure may in some manner have suppressed the dual wave behavior. Furthermore, Miller and Callegari reported initiating an investigation to determine a wave propagation speed inside the boundary layer. Had the computations shown the existence of the two waves traveling within the boundary layer it would seem unlikely that the authors would have tried to determine a single speed. (But a reasonable assumption would have been that both sound and TS waves were propagating, and propagating at significantly different speeds, and a search for a single speed at a given height within the boundary layer does seem a little strange). No information about their velocity determination procedure was given, but the result was displayed in the form of a curve of speed vs. height. Outside of the boundary layer the speed was found to match the speed of the sound wave, which would be about 30 U_∞, but inside the layer it dropped to about 4 U_∞ at $y/\delta \simeq 0.9$ and then decreased slowly to about 2 U_∞ at the wall (the graph has not been drawn correctly near the origin, so the proper magnitude of the speed is not clear). The fact that the speed inside the boundary layer was found to be of the order of the free-stream velocity was taken as evidence that the wave in the layer was a TS wave. Since the speed of unstable TS waves does not exceed 0.4 U_∞, and for the conditions given the particular wave speed can be estimated at 0.29 U_∞ using figure 13j of reference 21, a speed of two to four times the stream velocity should have been identified as unusual. An obvious explanation is that unusual results should be expected when a single speed is forced upon a two-speed situation. But it also raises the question of whether the model was in fact showing two-wave type behavior. If both types of waves were present, as long as the amplitude of the TS wave was significantly greater or less than that of the sound wave, it should have been possible to accurately determine the TS wave velocity by plotting amplitude vs. distance for different times and tracking the TS signal. Such a speed should not have been 2 U_∞ inside the layer and jumped to 30 U_∞ at the edge of the boundary layer. If the authors did use this wave-following technique, then it was a crazy hybrid sort of wave that they were following and something is

wrong with the modeling. Perhaps their code generated a BS wave (Bad Speed wave) rather than a TS wave. And what happened at the height where the TS wave amplitude should have gone to zero? Only the sound signal should have remained and its speed would still be at 30 U_∞, not 4 U_∞. There is another possible explanation for the unusual result, although it does not answer the problem just raised (the explanation of this problem could be that the speed determinations were only at a few heights in the boundary layer--none of which were at the TS zero point--and results faired). Miller and Callegari were apparently looking for single speeds, and a simple way of determining a wave speed, which would be accurate with only one wave present, would be to determine the time shift Δt between the sinusoidal time signatures taken from two stations a small distance Δx apart in the downstream direction. The wave velocity would simply be $\Delta x/\Delta t$ (a small Δx is used to make certain that the same particular time cycle is being tracked). A convenient feature of the signal to track is the time when the amplitude goes through zero. For a single wave the zero tracking procedure is valid, but when two waves with different speeds are present strange results can occur. One result is easily demonstrated by considering two traveling sinusoidal waves with equal amplitudes. Equation (1) is appropriate for this case, and it is easily shown that the signal travels with a constant phase velocity of $2\, c_1 c_2/(c_1 + c_2)$. If, as before, $c_1 = c_{ts} = U_\infty/3$ is the TS speed and $c_2 = c_s = a + U_\infty$ is the speed of the sound wave, the signal speed for low Mach number flow becomes $\simeq 2/3\, U_\infty$. Obviously, such a speed is neither TS nor sound speed. If the two wave amplitudes are not equal, then the result depends on their amplitude ratio and upon x.

To demonstrate results which can be obtained with the method, the signal speed was determined by tracking a zero crossing from a signal given by the sum of two traveling sinusoidal waves $A_{ts} \sin(k_{ts}\, x - wt) + A_s \sin(k_s\, x - wt)$. This was done for a number of different ratios of A_{ts}/A_s (10^{-4}, 10^{-3}, 10^{-2}, .1, .2, .3, .5, 1, 2, 10, 100). Conditions approximating those of the Miller and Callegari numerical computations were used. The frequency was 27 Hz, $a = 344$ m/sec, and $U_\infty = 10.06$ m/sec (33.00 ft/sec--the speed for the Miller and Callegari calculations was probably near 11.7 m/sec). The wave numbers were obtained using the TS and sound wave speeds given above. In trying to visualize the sum of the two signals it is helpful to keep in mind the fact that the speed of the sound wave is approximately 100 times greater than the TS wave speed and that its wavelength is correspondingly 100 times greater (13.10 m vs. 12.4 cm). The Miller and Callegari calculations were for $x = 3.66$ m (12 ft) and this distance was used here, along with other values. The 3.66 m distance results are not directly comparable to the Miller and Callegari computer results because the initial phase angles were no doubt different. At a given distance the time of the first zero crossing was determined. The stations were then moved slightly downstream and the time of the first zero crossing was again determined. The Δt time increment was then obtained from the corresponding time difference, and the velocity was calculated from $\Delta x/\Delta t$. Three different Δx downstream increments were used in this calculation; 0.15 cm (10.060 in), 0.61 cm (0.290 in), and 1.22 cm (0.480 in). The results showed that for $A_{ts}/A_s \leq 0.001$ the signal speed was within 10% of the sound wave speed (354 m/sec) and had little dependence on x or Δx. Likewise, for $A_{ts}/A_s \geq 10$, the speed was within 10% of the TS wave (3.35 m/sec) and varied little with x or Δx. With $A_{ts}/A_s = 1$ the speed agreed with the theoretical value of a constant 6.64 m/sec. For amplitude ratios between these conditions the results were greatly dependent

upon x. For $0.01 \leq A_{ts}/A_s < 1$, as x increased the speed changed from positive to negative values every half TS wavelength, and the influence of Δx was quite significant. For $1 < A_{ts}/A_s < 2$ the speed oscillated with increase in x, but it remained positive and less than the 6.64 m/sec value. But in these strange results there are very many x stations for which the speed variation with amplitude ratio could conceivably give a speed variation with height which would roughly match that found by Miller and Callegari. In the free-stream $A_{ts} << A_s$, and a signal speed of the sound wave would be found. If at x = 3.66 m (12 ft), for example, if the value of A_{ts}/A_s dropped to a value of 0.1 throughout most of the boundary layer, the determined signal speed would have been nearly 2 U_∞ within the region. The point of all of this is that if the authors happened to have used this method, the unusual speed results could be an indication that TS and sound waves were propagating in the boundary layer after all and the speeds were not of BS waves (but there remains the wavelength problem). Use of the compressible equations allows a more realistic simulation of the acoustic-stability problem, and additional work is needed.

The final study to be discussed is that of Murdock (ref. 4). The problem studied was the interaction of a plane sound wave with a Blasius boundary layer in incompressible flow. Because of the incompressibility the propagating nature of the sound wave was not present and the problem became one of sinusoidally oscillating flow over a flat plate. This could also be considered appropriate for the practical case of sound wavelength large compared to TS wavelength. The equations numerically solved were the parabolized vorticity equations which Murdock had previously used in the vibrating ribbon boundary layer stability study (refs. 22 and 23). In that study (which was briefly described earlier in the present report) these equations were found to satisfactorily describe TS wave behavior. For the sound interaction problem the boundary conditions were changed. The free-stream was taken as the sum of uniform flow plus a small oscillating perturbation. Two different upstream boundary conditions were used in the study and were obtained from the unsteady boundary layer solutions of Illingworth (ref. 24). For small $q = \omega x/U_\infty$ the solution for the x-component of the velocity was the sum of the Blasius profile and an unsteady flow which grew in thickness at the same rate as the Blasius boundary layer and was in phase with the free-stream oscillations. For $q > 1$ the unsteady component which was added to the Blasius profile did not grow in thickness with x and there was a phase shift across the region. This unsteady shear region is what is called the acoustic boundary layer in the present report. The upstream boundary conditions thus provide rather realistic conditions for the sound wave perturbations. For a given frequency, small q conditions are appropriate very near the leading edge, and $q > 1$ conditions are for regions away from the leading edge region. For most of the study Murdock used a nondimensional frequency parameter $\omega\nu/U_\infty^2$ value of 5.6×10^{-5} in order to match the conditions in Shapiro's experimental investigation.

Both boundary conditions were separately applied at different positions along the plate and TS waves were always generated at the boundary. Plots of the variation of the Fourier amplitude of the signal along the plate (which are equivalent to plots of $\sqrt{2}$ times the rms value of the signal) clearly showed the TS-sound wave interference patterns, and these were appropriately interpreted by Murdock to obtain the TS wave amplitude behavior. Murdock computed conditions down to the neutral point, and in all cases it was found that the TS wave amplitude decayed according to linear stability theory. He thus concluded

that there is no continuous flow of energy into the TS wave along the boundary layer. Since the computations showed no interaction between the sound field and the TS wave, the TS wave must be generated very locally at the leading edge region (or possibly, under different circumstances, locally at some downstream location).

Murdock also applied the small q condition at locations progressively closer to the leading edge while computing the ratio of the neutral point amplitude to the initial point amplitude (all at a constant Re_y value of 196). Computational costs limited the upstream location to a value of $Re_x = 1 \times 10^4$, and when he extrapolated his results to $Re_x = 0$ he concluded that the ratio of the neutral point amplitude at the height of the peak disturbance level in the boundary layer to the free-stream sound amplitude was 10^{-4} for the conditions studied. He noted that Shapiro's data showed a value of 0.4 for this ratio and considered the discrepancy to be due to pressure gradient effects or to the possibility that the experimental sound waves were not plane waves and thus effectively generated local disturbances. Murdock stated that his results suggest that localized disturbances can generate a larger TS wave than can a plane wave disturbance.

In summary, some of the experimental and theoretical work reviewed here suggests that in the acoustic-boundary layer interaction the most important region in the TS generation process is the leading edge region, at least for simple two-dimensional flows and waves. Furthermore, the theoretical studies show that once generated, the TS waves apparently travel unaffected by the sound field. Shapiro's work held out the possibility of experimentally verifying this aspect of the problem.

ASPECTS OF TOLLMIEN-SCHLICHTING AND ACOUSTIC WAVE INTERFERENCE

Boundary layer stability theory posits the existence of waves which undergo changes in amplitude and speed while traveling downstream in the laminar boundary layer. These TS waves are vorticity waves and they may travel in any direction, but in low speed (incompressible) flow it has been shown that waves traveling directly downstream, the two-dimensional waves, have the greatest growth rate. Because of this, and the fact that they are the simplest waves to analyze, the vast majority of flat plate boundary layer stability results are for the two-dimensional wave case. The principle results from stability theory have been experimentally verified. The two-dimensional results will be considered here.

According to the theory (see, for example, ref. 25), the wave phase velocity and amplitude amplification rate depend on the wave frequency, or the wave number, and the flow Reynolds number, usually based on a boundary layer thickness such as the displacement thickness. The results, suitably nondimensionalized, are usually displayed on stability diagrams, which most often consist of curves of constant amplification rates plotted on frequency or wave number vs. Reynolds number graphs. Phase speeds can also be drawn on such graphs. The constant amplification rate contours form loops which are open to the right on the diagrams. The contour of zero growth rate is termed the neutral curve and inside this curve waves are amplified and outside they are damped. Shapiro found that the TS waves were generated with the same frequency as that of the excitation sound field, and therefore the most convenient stability diagram to consider is a frequency-Reynolds number one. On such a diagram the TS wave would follow a known horizontal path. In the lower Reynolds number region the wave would be damped until reaching the so-called lower branch, or Branch I, of the neutral curve. Downstream of this point the wave would undergo amplification until the upper branch of the neutral curve was reached, and thereafter the wave would be damped. The lowest Reynolds number for which amplification is possible, when all frequencies are considered, is called the critical Reynolds number. However, because only one particular frequency, 500 Hz, is considered in the present report, the definition of the critical Reynolds number will be altered somewhat here. The critical Reynolds number will be taken as the Reynolds number at which a 500 Hz TS wave can begin to amplify (i.e., the Reynolds number of the intersection on the stability diagram of the 500 Hz line with the lower branch of the neutral curve). For the frequency and free-stream flow conditions of Shapiro's experiment, this value was $Re_{\delta^*} = 990$. The downstream Reynolds number at which damping begins is 1900. The corresponding distances are approximately 17 and 63 centimeters, respectively, from the leading edge of the plate. If the sound field generates TS waves but does not affect their subsequent growth, and if the flow field and boundary layer development match flat plate theory, than TS wave amplitudes would be expected to grow nearly sixty-fold in the 17 to 63 centimeter region and to decay elsewhere. In contrast to the wave amplitude, the wave speed is only a weak function of Reynolds number and would be expected to change by only 5% or so.

Another important feature predicted by stability theory is that at any station the rms streamwise velocity perturbations associated with the TS waves have a maximum amplitude in the lower portion of the boundary layer and go through a minimum in the outer half. Part of the reason for this is the fact that two-dimensional TS waves introduce vortical-like perturbations to the flow and, in a sense, may be likened to periodic counter-rotating transverse

eddies. These travel downstream with a speed of about one-third the free-stream velocity and their axes lie in the outer portion of the boundary layer near $y/\delta = 0.7$. At this height the vertical velocity perturbation is a maximum while the streamwise component is zero. The structure of the TS waves can be quite elongated in the streamwise direction. The minimum wavelength for unstable TS waves is about 6δ (the wavelengths of those of importance to the boundary layer transition problem are usually less than 30δ). The influence of the waves does extend into the free-stream, but not significantly above 2δ. Perhaps the most complete set of figures depicting the nature of TS waves is in a chapter in the textbook of Radbill and McCue (ref. 26). This book, while containing one of the most complete sets of flat plate boundary layer stability tables and figures, is an applied mathematics rather than fluid mechanics text, and it has not been widely referenced in the stability or transition literature.

The hot-wire anemometer responds, except at very low velocities, essentially to streamwise velocity fluctuations. Since the TS waves are periodic, the anemometer will therefore register sinusoidal signals everywhere in a TS wave field except at the null position in the outer region. Above and below the null position the signals will be 180° out of phase because of the vortical nature of the wave. This phenomenon was beautifully demonstrated in the now-classic stability experiment of Schubauer and Skramstad (ref. 1). There have been occasions, both in textbooks and the literature (refs. 27 and 28) where the location of this phase reversal has been inadvertently called the "critical layer," but this term refers to the height within the boundary layer where the local velocity matches the velocity of the TS wave. The term arose out of early inviscid stability analyses which predicted an infinite disturbance amplitude at this height. (Later analyses included viscous effects, and the precomputer asymptotic methods showed that a phase jump occurs at the critical layer (ref. 29); the equations show that a phase reversal occurs only during a part of the wave cycle. This reversal, by the way, does appear to be visible in figure 6.17 of the computer results of Radbill and McCue). The largest fluctuations do in fact occur in the vicinity of the critical layer, and the term has sometimes been used (misused) by experimentalists (especially in supersonic investigations) to mean the layer or region where maximum fluctuations are detected. In incompressible flow the critical layer and the region of maximum longitudinal velocity fluctuations is near the wall at $y/\delta \sim 0.2$. The height of the maximum, as well as the null, depends particularly on the Reynolds number (see figure 3 of Ross, et al., ref. 30). Shapiro kept the hot-wire probe well inside the boundary layer at the height of the maximum disturbance level while making the boundary layer measurements. This appears to be an accepted practice. He also measured the phase angle of the signal relative to the signal input to the upstream loudspeaker (no details were given as to how this angle was measured).

The sound field also introduced sinusoidal streamwise velocity fluctuations in the tunnel test section. The primary component of the acoustic field was a 500 Hz plane wave traveling downstream with a velocity of the speed of sound plus the stream velocity. There were also waves traveling in the upstream direction as a result of reflections from the end of the test section. Because of the relatively low frequency of the sound field, the refraction effects due to the velocity gradients in the boundary layer would not be expected to be significant. But while the flow boundary layer may have little effect on the sound waves, the flat plate itself, by virtue of the no-slip condition at the fall, produces the so-called acoustic boundary layer. It

will be shown later in the report that despite the anemometer being very close to the plate near the leading edge region, it was probably outside of the very thin acoustic boundary layer during the stability measurements. Consequently, the acoustic signal inside the flow boundary layer can be considered as essentially the same as that existing just outside of the layer.

The situation may be idealized and summarized as follows. Within the boundary layer there are two families of traveling waves, the acoustic waves traveling with constant speeds and relatively constant amplitudes, and the TS waves traveling with the same frequency as the acoustic waves but at a much slower velocity, and one which changes slowly with distance. The TS wave amplitude can change many-fold along the plate. The behavior of the superposed signals will now be examined using complex diagrams.

Shapiro presented boundary layer hot-wire anemometer data showing the signal amplitude and phase angle variation along the flat plate. Because both acoustic and Tollmien-Schlichting waves were present in the boundary layer, it was assumed in the present study that the anemometer output represented the superposition of signals from the acoustic and Tollmien-Schlichting waves. Since all of the signals are periodic with the same frequency, the relationship among the acoustic and TS wave amplitudes and phase angles can be easily understood if the signals are expressed in complex notation in polar form and represented on the complex plane. This will be done here. After reviewing complex representation of traveling waves, the complex diagram will be used to demonstrate the amplitude and phase angle behavior that should be expected in the acoustic-instability experiment.

A complex quantity can be expressed in polar form using Euler's equation $e^{i\theta} = \cos\theta + i \sin\theta$. A traveling sinusoidal wave with amplitude A, radian frequency ω, and speed c can therefore be represented by

$$\hat{s} = A\, e^{i(kx-\omega t+\phi)} = A\, [\cos(kx-\omega t+\phi) + i \sin (kx-\omega t+\phi)]$$

where $\hat{s}$ is the complex signal, $k = \omega/c$ is the wave number, and ϕ is the initial phase angle at $x = 0$ (circumflexed symbols indicate complex quantities). Since the real part of $\hat{s}$ is $A \cos(kx-\omega t+\phi)$, the usual form of a traveling sinusoidal wave, the standard convention is adopted that only the real part of $\hat{s}$ is considered to have physical significance. The complex signal $\hat{s}$ is represented on the complex plane with a line segment of length A having an angle of $kx-\omega t+\phi$ as shown in figure 1. The line segment will be referred to as a vector in this report. It is seen that at a given value of x the vector (in electrical theory this would be called a phasor) will rotate clockwise with increasing time at angular velocity $-\omega$ radians/sec. The projection on the real axis has the physical significance, and the rms value is $A\sqrt{2}/2$ At any instant of time, the vector rotates counterclockwise with increasing x at a rate of k radians per unit length.

Consider now the case of the sum of acoustic and TS traveling waves having the same frequency ω. The signal sum would of course have the same frequency and is

$$\hat{s} = [\, A_a\, e^{i(k_a x + \phi_a)} + A_{ts}\, e^{i(k_{ts} x + \phi_{ts})} \,]\, e^{-i\omega t}$$

Shapiro reported time-averaged values, and the rms value of $\hat{s}$ is simply

$$\tilde{\hat{s}} = \frac{\sqrt{2}}{2} \left[A_a e^{i(k_a x + \phi_a)} + A_{ts} e^{i(k_{ts} x + \phi_{ts})} \right] \tag{8}$$

The behavior of $\tilde{\hat{s}}$ can therefore be studied on the complex diagram by considering the sum of the two vectors in eq. (8). The vector representation and sum are shown in figure 2. The acoustic and TS vectors are displayed in figure 2(a), and the vector sum is shown in figure 2(b). To be representative of conditions upstream of the critical Reynolds number, the amplitude of the TS wave is shown as being smaller than the amplitude of the acoustic wave. The signal $\hat{s}$ may be expressed as $A(x)\, e^{i\theta(x)}$, where the amplitude A and phase angle θ are shown in the figure. $A(x)$ and $\theta(x)$ are the two quantities which were measured by Shapiro. The wave number of the TS wave is much larger than that of the acoustic wave, and the dotted circle in part (b) is to indicate that the TS vector spins rapidly about the tip of the relatively slowly rotating acoustic vector. The wave number ratio is the reciprocal of the wave speeds, and for a TS wave speed of $0.35\, U_\infty$, the wave number ratio is therefore $k_{ts}/k_a = (a + U_\infty)/0.35\, U_\infty$, where a is the speed of sound. Using values appropriate for the Shapiro experiment, ($a = 344$ m/sec, $U_\infty = 29$ m/sec), the wave number ratio is nearly 37, and consequently, for every revolution of the TS vector the acoustic vector rotates approximately 10°. From figure 2(b) it is clear that with increasing x the phase angle θ oscillates nearly sinusoidally about the slowly increasing phase angle of the acoustic vector. Also, the greater the TS wave amplitude the greater the phase angle oscillations. The phase angle behavior is verified in figure 2(c), which shows the computed angles for the case of $\phi_a = \phi_{ts} = 0$, $A_{ts} = 0.5\, A_a$, and wave number values appropriate to the Shapiro experiment. As shown by the dashed line, the signal phase angle oscillates about a linearly increasing value. Figure 2(b) also shows that the amplitude of the wave sum undergoes a cyclic oscillation with increase in x. This behavior is illustrated in figure 2(d), where the amplitude variation with x has been computed for the same conditions as in 2(c). The nondimensional logarithmic format is similar to that used by Shapiro.

Figure 2 shows how easy it is to understand the amplitude and phase angle behavior with the aid of the complex diagrams. From figure 2(b) it now becomes obvious, for example, that as long as the TS wave amplitude is less than the acoustic wave amplitude, the amplitude of the sum oscillates about the acoustic wave amplitude value. The average of the minimum and maximum values thus matches the acoustic wave amplitude, and this result was shown algebraically earlier. When the amplitude of the TS vector exceeds that of the acoustic vector, a simple polar sketch will show that the average matches the TS amplitude. The amplitude of the TS wave is of course not going to be constant as in the figure. The amplitude would be expected to diminish until the location of the critical Reynolds number is reached and then amplification should begin. In figure 2(b), instead of following the dotted circular path, or more properly, the circular-like path whose center is slowly swinging around the origin of the polar plot, the changing TS amplitude creates a spiral path whose center swings about the polar origin. This spiral, which will be referred to as the TS spiral, is inward when the wave is damped and outward when amplified. An interesting thing happens to the phase angle downstream of the critical Reynolds number. At some point the TS wave amplitude will exceed the acoustic amplitude, and when this happens the outward

TS spiral will encompass the polar origin on the next pass in its vicinity. As may be seen in figure 2(b), the phase angle will then exceed 90°, and in fact, will continue to increase beyond 360°. For every 360° TS vector rotation, the phase angle θ will be incremented by slightly over 360°. As the TS vector lengthens, the acoustic vector becomes smaller in comparison, and this results in a decrease in the eccentricity of the TS spiral about the polar origin. The reduced eccentricity decreases the oscillations in A and θ. When the TS wave nears its maximum amplitude the eccentricity is so small that the TS spiral is almost circular about the origin. As this happens θ increases nearly linearly with x and there is almost no oscillation in A. This feature will be evident in the acoustic-TS model of Shapiro's data.

As shown in figure 2(c), the mean of the phase angle oscillations increased linearly with distance. This was a consequence of there being only the single downstream propagating acoustic wave field. In Shapiro's experiment there was also a weak reflected upstream propagating acoustic field present, and with acoustic waves traveling in both directions it is easy to show the mean of the phase angle oscillations no longer increases linearly.

Upstream traveling waves are represented by clockwise rotating vectors on the complex diagram. The total acoustic signal, $\hat{A}_a(x)$, is now the sum of two counter-rotating vectors, and, as can be imagined, its amplitude as well as rate of rotation are no longer constant. Thus when the TS vector is added to $\hat{A}_a$ the center of the TS spiral moves in a nonuniform fashion. The effect of an upstream traveling sound wave is shown in figure 3. For simplicity, the wave numbers of the downstream and upstream traveling waves were taken as negatives of one another with $k_1 = -k_2 = 6$. The wave number of the TS wave was forty times greater at $k_{ts} = 240$.[2] The amplitudes of the downstream, upstream, and TS waves were respectively, $A_1 = 1$, $A_2 = 0.3$, and $A_{ts} = 0.5$. ϕ_{ts} was zero and $\phi_1 = \phi_2 = -90^{\circ}$. The initial phase angles of the sound waves were chosen so that a special situation existed between $x = 10$ and $x = 20$, the range where Shapiro presented detailed phase angle data. In figures 3(a) and 3(b) the two acoustic vectors and their sum are shown at $x = 10$ and $x = 20$, respectively. To minimize confusion the TS vector and spiral have not been included in these figures. Since A_1 rotates counterclockwise and A_2 clockwise, as x increases from 10 to 20 the amplitude of the acoustic vector A_a would pass through a minimum at $x = 15$ while undergoing its maximum rate of rotation. At the point of the maximum rotation rate the mean of the phase angle curve has its greatest slope, and this indeed occurs at $x = 15$ as may be seen in the phase angle plot in figure 3(c). The nonlinear behavior of the mean phase angle is clearly illustrated. The signal amplitude results are shown in figure 3(d), where the values have been nondimensionalized by the mean signal value near $x = 20$ (more precisely, by the signal value at $x = 20$ with $A_{ts} = 0$).

The acoustic phase angles at the leading edge of the flat plate, ϕ_1 and ϕ_2, depend on the geometry of the tunnel, the location of the plate within the test section, and in the case of ϕ_2, also on any phase shift that may occur in the downstream reflection process. The initial phase angles can obviously affect the results, and as an illustration of this the phase angle and amplitude results shown in figure 4 can be compared with those in figure 3. The only change in initial conditions from figure 3 to 4 is that ϕ_2 was changed from -90° to 90°. In the new situation the magnitude of $\hat{A}_a$ reaches a maximum at $x = 15$ where the rotation rate is a minimum. In figure 4 the mean phase angle changed from -17° to 17° between $x = 10$ and 20, while in figure 3 the corresponding angle change is -47° to 47°. Clearly the upstream traveling wave

affects the results and such a wave was included in the present model of Shapiro's data.

Recall that Thomas and Lekoudis (ref. 6), who only included downstream traveling sound waves in their calculations, found relatively poor agreement between their modeled phase angles and Shapiro's measured values. The computed phase angles had a linear mean growth which greatly exceeded that shown by the data. As demonstrated herein, the upstream sound waves may significantly alter the mean phase angle growth.

MODEL OF ACOUSTIC FIELD AND TS WAVES

The point which is being emphasized in the present report is that with acoustic excitation the induced laminar boundary layer TS waves are traveling in a field of acoustic waves. The signal sensed by a transducer is the superposition of the various waves, and in order to correctly interpret the measured signal one must have knowledge of the superposing wave fields. It is therefore very important in this situation to have, along with the data, a mathematical model of the acoustic field. The simplest acoustic field to model in a test section would be that of a plane wave traveling along the test section in the axial direction. This is the situation one would like to see when, such as in the experiment of Shapiro, a loudspeaker is placed far upstream of the entrance of the test section. But this desired plane wave condition is not easy to achieve or approximate in practice, and one can expect to find, in addition to the simple plane waves, a sound field rich in oblique waves bouncing from wall to wall. The reflecting waves set up standing wave patterns and these can greatly alter the sensed signal. Large spatial variations in signal strength can result from superposing or interfering waves of near equal strength. A sentence from the acoustic textbook of Kinsler and Frey (ref. 31), although not specifically written in connection with test sections, expresses the problem quite well: "The formation of these standing waves makes it difficult if not impossible to measure the pressure amplitude of the initially incident plane progressive waves when reflective walls are present." Since it is likely that a test section acoustic field will consist of standing waves caused by reflections, the estimate of the strength of any one wave cannot be made without considering and modeling, even in the crudest sense, the strengths of the principal waves involved. Inasmuch as the spatial variations in signal strength provide the evidence of the component wave amplitudes and phase relationships, simple one- or two-point measurements will not suffice to describe the acoustic field. It is easy to see that when using acoustic excitation the boundary layer transition investigator could (and probably does) spend considerable time just trying to investigate and control the sound field in his test section.

In the present study a very simple model of the test section acoustic field was adopted. It was based on a set of measurements presented by Shapiro which shows the variation of sound pressure level along the centerline of the test section (as will be discussed later, the measurements should be interpreted as longitudinal velocity fluctuation levels rather than sound pressure levels). Only three elements were included in the model to account for the variations in the data: a primary plane wave propagating down the test section in the axial direction, a much weaker upstream propagating plane wave which is the result of reflection of the primary wave from the test section exit, and random background noise (the fudge-factor element). Because of a need for additional data and for more information concerning the experimental conditions, it will become evident that there was an element of uncertainty in the present modeling exercise.

The topic of wave propagation inside ducts and channels is an important one in a number of disciplines and has received considerable attention. As an indication of the research activity in acoustics in this area, one can find under the heading "wave-guides, wave propagation in tubes and ducts" in the reference compilations of White and Teas (refs. 32 and 33) a listing of over 220 reports published (mostly) during the two-year period from 1977 to 1978. Of course, the transition researcher cannot switch to acoustic research and still accomplish his task, but it is imperative that some study of the subject

be made because of the importance of the modeling. For the benefit of those new to the subject, a brief review of sound propagation in ducts is given in the Appendix. The information for the review was taken from various textbooks and will serve little more than to introduce some terminology and concepts, but this section will occasionally be referenced later in the report. An extensive state-of-the-art survey of the subject, c. 1975, can be found in the article by Nayfeh, Kaiser, and Telionis (ref. 34). Some later articles may be found in references 35-39.

Acoustic Model of MIT Test Section

In the acoustic-boundary layer interaction model the sound field had to be accounted for, and in the present scheme the sound was assumed to be superimposed upon the TS waves traveling in the flat plate laminar boundary layer. For this purpose Shapiro's free-stream hot-wire anemometer data along the test section centerline were used. This was the only data available and had to be used, but aside from this important fact, this procedure requires some rationalization, for there are at least two assumptions implicit in the method. The first is that the sound and boundary layer do not affect each other in the mean (an energy transfer to the TS waves is allowed). By this it is meant that the sound field is not altered by the plate boundary layer as the sound traverses the layer, and that the sound does not affect the mean laminar flow. The second assumption is that Shapiro's free-stream centerline acoustic levels are the appropriate ones to use in the superposition. These two assumptions will be considered prior to discussing the acoustic model itself.

The assumption that the sound and laminar boundary layer do not interact with some net affect (aside from possible affects on TS waves--to be discussed shortly) is based on the fact that the sound field is weak and that the flow stations being considered are well away from the leading edge region. For these conditions ($\omega x/U_\infty > 1$) the results from Illingworth (ref. 24; see also Murdock's use of the results, ref. 4) are appropriate and these show that the flow can be represented by the superposition of a laminar boundary layer and a plane acoustic wave traveling over a flat plate. The acoustic field decays near the surface in its own boundary layer. The acoustic boundary layer, which does not grow with distance, is thus embedded within the flat plate laminar boundary layer. Outside of the acoustic boundary layer the fluctuation level matches that outside the layer and the plate boundary layer does not affect the acoustic field. It is assumed here that refraction effects are negligible, and this appears reasonable considering the low velocities and low frequencies involved. Furthermore, since the acoustic perturbations have zero mean, the acoustic field does not have a mean affect on the flow boundary layer (again, aside from affects on TS waves). So, there is no net affect on each other, and as long as positions outside of the acoustic boundary layer are considered the free-stream acoustic field can be taken as a superposing field.

The Illingworth analysis does not include TS wave behavior. If energy from the sound field was fed into the TS waves, the sound field inside the boundary layer could commensurately weaken along the plate. In such a case any acoustic measurements taken in the free-stream prior to plate insertion may not be the appropriate data to model because the signal weakening would not be present. It is the present author's opinion, however, that because of the low frequency involved, diffraction effects would operate to sustain the acoustic level within the boundary layer (the ratio of the acoustic wavelength to the length scale of the nonuniform region involved, the laminar boundary

layer thickness, ranged from 760 to 240 over the x stations of 7.5 to 75 cm covered in Shapiro's measurements). The free-stream acoustic measurements would thus still be the appropriate superposing acoustic field to model, at least from the standpoint of boundary layer effects.

There remains the task of showing that Shapiro's boundary layer measurements were taken outside of the acoustic boundary layer. Shapiro kept the hot-wire at the height within the boundary layer where the fluctuations were greatest. Stability theory predicts this height to typically be in the range of $y/\delta = 0.1 - 0.3$. Shapiro presented some disturbance amplitude profiles across the boundary layer, and the peak fluctuations levels occur in the range of $y/\delta = 0.15 - 0.17$. The acoustic boundary layer thickness may be taken as $\delta_a = 1.55\sqrt{2\nu/\omega}$ (see Attenuation section of Appendix) and the flow boundary layer thickness is $\delta = 5\sqrt{\nu x/U_\infty}$. The ratio of the two thicknesses may then be expressed as

$$\frac{\delta_a}{\delta} = 0.175\sqrt{\frac{U_\infty}{fx}}$$

For $f = 500$ Hz and $U_\infty = 29$ m/sec the ratio of the probe height to the acoustic boundary layer height may thus be estimated to have ranged from 1.0 to 3.5 as the probe's downstream station was varied from $x = 7.5$ cm to 75 cm. The effect of the acoustic boundary layer can therefore be neglected inasmuch as the wire was outside of this region.

The second assumption, concerning the suitability of Shapiro's free-stream acoustic measurements will now be considered. In the acoustic measurements of the test section noise field Shapiro did not specify the y, z position of his probe. It is the present writer's opinion that the measurements were taken along the centerline of the tunnel and without the flat plate present. If this was in fact the experimental situation, then the acoustic data may not be the most appropriate because the presence of the plate can change the acoustic field. The change occurs because of at least three factors: (1) the plate divides the test section into two channels and the acoustic modal behavior in the channels differ from that in the empty test section; (2) the reflection factor for the downstream open end of the test section does not equal the channel reflection factors; and (3) the different boundary conditions cause different evanescent noise fields. Furthermore, the plate was not mounted along the centerline, so the acoustics of the two channels would differ. Clearly the sound field along the centerline would not be the same as that existing just outside of the flat plate boundary layer, but the extent of the difference is not known. It will be conjectured shortly that the difference may not have been significant. The use of the free-stream acoustic data is thus far from ideal, but it is the only data available and the reader may judge the degree of the impropriety. These problems will be discussed in more detail after the MIT tunnel is described.

MIT tunnel and preliminary acoustic measurements. - The MIT facility was a low-speed open-circuit tunnel consisting of a settling chamber, contraction section, test section, diffuser and muffler, and blower. The settling chamber was about 2 3/4 m in length and was fitted with a honeycomb (soda straws) and screens to reduce the turbulence. The contraction section was approximately 1 3/4 m long and had a contraction ratio of 20 to 1. The test section was 38 cm × 38 cm and had a length of 2 m. The test section terminated in an open-duct configuration, and downstream the flow was an open jet for 2 m.

The test section and the open region were enclosed in what was called the blockhouse. The blockhouse was a structure 2 ¼ m high and 4 m long (depth not given), and the downstream wall held a collector nozzle for the entrance to the diffuser. The blockhouse was lined on the inside with acoustically absorbent material and was sealed so that no outside air could enter during tunnel runs. The tunnel was originally operated with a 4 m test section and no open region. For this closed-duct configuration the free-stream turbulence levels were around 0.05% of the free-stream velocity. In the open-duct configuration the disturbance level rose to 0.16%. The spectrum showed a broad peak at 2.5 Hz, and this was reported to be identical to the calculated Helmholtz resonance frequency of the blockhouse, with the test section and the diffuser constituting the resonator necks. When the measurements were filtered with a low frequency cutoff of 10 Hz, the turbulence reading was 0.04%.

Shapiro reported that early acoustic tests were performed with the test section in its original 4 m closed-duct configuration. The walls were hard and the acoustic excitation was white noise (flat spectrum) played through a loudspeaker placed in front of the settling chamber. A microphone was placed in the test section and rapid analyses were done with a real-time spectrum analyzer. Tests were done with and without flow, and there was very little qualitative change in the results, so subsequent tests were made with no flow. The report contains no information about the microphone or the microphone housing used when measurements were taken with flow. The author reported that the data showed tremendous peaks and nulls in the spectrum and in the spatial intensity of the test section noise field (up to 20 bB). The test section was changed to the open configuration and this improved the situation somewhat. The test section walls were then lined with a thick layer of fiberglass to reduce the transverse variations in the field. This worked very well at reducing these variations, but introduced a longitudinal attenuation of the order of 35 dB/meter. Finally, a smooth foam material with a moderate acoustic absorption coefficient was selected, and this reduced the longitudinal attenuation; the reader is not told what happened to the transverse distribution.

Tests were then conducted with a pure tone generated by the loudspeaker in front of the tunnel while the tunnel was running at test speed. The pure tone was later used in the boundary layer stability tests. A hot-wire anemometer, which is essentially sensitive to the longitudinal velocity fluctuations, was used to measure the acoustic velocity disturbance levels and these were converted to sound pressure levels using the plane progressive wave assumption $\tilde{p} = \rho\, c\, \tilde{u}$. A microphone was used to examine the transverse variations and to provide a check of the hot-wire calibration. A loud sound, over 100 dB, was necessary to overcome the wind noise on the microphone. The levels measured by the hot-wire and the microphone were reported to have agreed within ± 2 dB; no information about the transverse distribution is given. Measurements along the axis showed a standing wave pattern due to the reflection of incident sound from the open end of the test section. The reflection coefficient was estimated from the data to be 0.2. (Note: Inasmuch as the Mach number is low, 0.08, the effect of the flow can be neglected and the reflection coefficient can be estimated using eq. (29). This equation is for a circular duct, so the radius will be taken as the value which yields an area equivalent to the actual square duct area, i.e., $r = 0.38/\sqrt{\pi}$. The theory is for a flanged duct, which the test section is not. Because of the blockhouse walls the test section does not represent the unflanged case either, so it is not easy to assess the expected error. For a 500 Hz tone and a sound speed of 344 m/sec, the value of 2kr is 3.916. Equation (29) gives a value

of 0.26 for the reflection factor, a value which is close to the experimental one). To reduce the reflection factor Shapiro added an "acoustic impedance transformer" to the downstream end of the duct. "This consisted of tapered wedges extending each wall of the duct, so that the walls ended more gradually." This was reported to have reduced the reflection factor to 0.1. The resulting distribution of sound pressure level along the axis is presented as a figure in Shapiro's report, and this figure provided the basis for the noise model developed here.

The experiences with the hard and the absorbent walls would appear to indicate that with the white noise excitation the transverse and the evanescent modes (see Appendix) significantly contributed to the test section noise field. From eq. (42), the cutoff frequency in the test section for transverse modes is 453 Hz, and the white noise spectrum surely went well above this frequency. For the 500 Hz pure tone excitation case the only information available is the aforementioned longitudinal distribution figure (to be presented shortly). No spectral results are presented for the pure tone excitation case, and therefore it is not known just how pure the tone was. No description of the loudspeaker is given, but distortion and harmonics can occur when loudspeakers are driven to high levels, and in the literature review of the present paper, instances were cited where harmonic distortion was present. It does not appear that the hot-wire signal was filtered through a narrow bandpass filter centered at 500 Hz, so extraneous signals could be in the data. The free-stream turbulence extends beyond the 500 Hz frequency, but at the 100 dB sound levels the natural turbulence would not be significant unless the intense noise levels excited a mechanical response of the settling chamber honeycomb or damping screens. This lack of filtering in the free-stream measurements is unfortunate because the signal was fed through a narrow bandpass filter in the boundary layer stability phase of the experiment. It would have been nicer to have modeled a free-stream signal that had been conditioned in the same manner as the boundary layer signal.

Effects of plate. - As previously indicated, it appears that the free-stream acoustic measurements were made without the flat plate in the test section (present conjecture). The plate, mounted horizontally near the tunnel centerline, spanned the test section and its length, including a thin 15 cm splitter plate that was added to the end of the plate to prevent vortex shedding, was 183 cm. From an acoustic standpoint the plate would essentially divide the test section into two compartments and each would have its own modal characteristics. Because of local nonuniformities in the free-stream turbulence the plate was mounted 6.3 cm below the centerline. The modal conditions above and below the plate would therefore be different. The cutoff frequency for the lowest mode, the 1,0 mode [$m = 1$, $n = 0$, $w = 0.38$ m, $h = 0.253$ m - see eq. (42)], is 453 Hz and is determined by the width of the tunnel and is independent of the location of the plate. Without the plate there is a 0,1 mode at the 453 Hz frequency, but this mode is not present with the plate in place. The next higher cutoff frequency is 640 Hz (1,1 mode). With the plate the next higher cutoff frequency is 680 Hz (0,1 mode) above the plate and 905 Hz (0,2 mode) below ($h = 0.127$ m). With or without the plate only the first mode cutoff is below 500 Hz and therefore, in addition to the fundamental mode, only first mode propagation is possible. The pressure modal plane of the 1,0 mode lies along the axis and is parallel to the side walls. Data on the transverse distribution of sound pressure would have been desirable and interesting. The longitudinal location of the plate was not specified, but it is likely that the end of the splitter plate was near the end of the test section. Because the open-end impedance depends on the cross

section dimensions, the reflection coefficients in the regions above and below the plate would differ from each other and from the empty tunnel value (and when the reflected waves reached the leading edge the different amplitudes and phase angles--the phase angle also varies with the reflection process--would cause velocity perturbations in the normal to the flow, a phenomenon perhaps relevant to TS wave generation). Because of the acoustic transformer, eq. (29) cannot be used to estimate the reflection factor for conditions above the plate, but it may give a suitable indication of the percent change in factor due to the area reduction. Using radii determined in the manner shown previously, eq. (29) shows that a 30% increase in reflection factor might occur. If the actual reflection factor increased accordingly, the increase from 0.1 to 0.13 would not significantly increase the strength of the standing wave pattern in the channel above the plate.

The fundamental and 1,0 propagation modes have grazing incidence on the plate and the rigid plate would not be expected to significantly affect these modes. The 0,1 mode would be missing and would not contribute to the standing wave. The principal remaining unknown element is how the changed boundary conditions affected the evanescent fields. It will be assumed that there was little change.

Assessment of acoustic situation. - The acoustic situation is assessed as follows. Assuming the settling chamber to be square in cross section, there are 24 transverse modes with cutoff frequencies less than the 500 Hz tone from the loudspeaker. Since the loudspeaker certainly does not act as a perfect piston, it is likely that numerous oblique modes would be excited. What happens in the contraction region is a state-of-the-art problem. The entrance to the test section is probably far enough from the loudspeaker, so that a plane wave may be assumed to enter the test section. The 1,0 mode of propagation is possible in the test section and it is likely that this mode was excited. The 1,0 mode of propagation is a wave which travels parallel to the horizontal surface of the plate and reflects back and forth from the side walls. The boundary layer instability measurements were taken along the centerline of the plate and thus in the pressure modal plane of the first mode. It is very likely that many evanescent modes would be excited in order to meet the complicated entrance boundary conditions resulting from entering oblique waves which do not match the 1,0 modal conditions. In the test section the flow velocity is low, 29 m/sec and the gross effects on the sound field should not be too great. The boundary layer on the tunnel walls would probably be turbulent. At the rather low frequency of 500 Hz, the convective effects of the mean flow on the sound would probably dominate the refraction effects taking place inside the boundary layers. Because the wall material is not highly absorbent and because the boundary layers do not occupy much of the volume of the test section, it is likely that the fundamental mode suffered little attenuation. Attenuation of the sound field downstream of the test section entrance may reasonably be attributed to the natural decay of the evanescent modes and their partial absorption by the walls (the walls being more absorbent at nongrazing incidence). The 1,0 mode waves may suffer significant attenuation due to wall reflections; their angle of incidence is 25° from the normal to the wall, and a ray path will undergo approximately 11 reflections from the side walls over the downstream distance of two meters to the test section exit.

At the exit of the test section the fundamental plane-wave mode would undergo a complicated reflection process. The serrated walls (or whatever the shape of the acoustic transformer section) makes it difficult to envision

the nature of the reflection process of the fundamental and oblique modes. No doubt numerous evanescent waves are excited. As these die out only the fundamental and 1,0 mode reflected waves remain. It is clear that the strength of the reflected fundamental wave would be greatly diminished. Because of the low Mach number of the flow, the decay rates of all of the upstream propagating waves would differ little from the downstream rates. The upstream propagating waves would be partially reflected in the entrance region of the test section, but because the impedance change is gradual the strength of the reflected waves would be quite small in comparison with the incoming sound waves from the speaker.

Mathematical model. - The mathematical model of the acoustic pressure and velocity levels along the test section centerline will now be presented. Because the free-stream data modeled likely represent the conditions in the empty tunnel and may not adequately describe the disturbance level just outside of the boundary layer when the plate is present, there is an admitted element of uncertainty in the modeling exercise.

The data available are hot-wire data and represent longitudinal velocity fluctuation levels (except at very low speeds, the hot-wire anemometer is much more sensitive to longitudinal fluctuations than transverse ones). Shapiro converted the velocity levels to pressure levels using the progressive plane wave equation $\tilde{p} = \rho c \tilde{u}$, but it must always be kept in mind that the data represent fluctuating velocities rather than pressures. This point is not merely of academic interest, for the issue immediately arises when considering the 1,0 mode. If only the acoustic pressures had to be modeled this mode could be ignored because the mode has a pressure node along the centerline. The present interest is in the velocities, however, and the fluctuating velocities, in the 1,0 mode are at a maximum along the axis. Since off-axis measurements were not presented, the only hope of determining the extent of the presence of the 1,0 mode is through examination of the standing wave patterns set up with the fundamental mode or with an upstream traveling 1,0 mode. Based on such an examination of the data, the decision was made to ignore the 1,0 mode in the model. The situation is not a clear-cut one, and discussion concerning this decision is deferred until after the complete model is presented.

The downstream traveling 500 Hz fundamental mode is considered to be propagating with a constant amplitude and a phase velocity of $c + U_\infty$, and this wave is represented by $u_1 e^{i(k_1 x - \omega t + \phi_1)}$, where the amplitude and initial phase angle are to be determined. This wave is considered to reflect as a plane wave traveling upstream with a constant amplitude and a phase velocity of $c - U_\infty$. The wave is represented by $u_2 e^{i(-k_2 x - \omega t + \phi_2)}$. The $-k_2 x$ is needed because the wave travels upstream. The upstream and downstream ends of the test section are taken as source regions of evanescent waves. These waves die out exponentially at rates which depend on their modal numbers. Mathematically these modes at each end of the test section will be lumped into decay law expressions, and for simplicity the same mathematical form for each of the two groups of disturbances will be used. The disturbance field from each end of the test section decays with distance from the ends and the decay functions given below vaguely represent this phenomenon. The real purpose of the functions is to provide a means of fitting a curve through some data points. If expressions describing all of the individual disturbances in time and space were available, the proper way of determining the mean-square value of the total signal would of course be to sum, square, and average the result over time. Obviously this cannot be done here, and instead the square of each of the decay expressions will be added to the mean-square value of the

sum of the two traveling waves. The square root of this sum is then taken as the rms value of the total disturbance field.

For the upstream source of evanescent waves the signal is assumed to decay according to $B_1/(x + a)^b$, where a, b, and B_1 are constants to be determined from the data; x is the distance from the location of the leading edge of the plate. The location of the plate was not given in the report. Also, the origin for the x axis in the free-stream sound pressure level figure was not specified as coinciding with the leading edge location, but it is reasonable to assume that it was. The decay law describing the signal from the downstream disturbances is taken as $B_2/(\ell-x + a)^b$ where B_2 is to be determined and ℓ is rather arbitrarily taken as 170 cm, the guessed distance from the leading edge to the end of the test section. There is nothing particularly special about the form of the decay functions chosen other than the fact that they were tried initially and found to be satisfactory.

The mean-square value of the two traveling waves is one-half of the sum of the squares of the real and imaginary parts. If u_{fs} represents the total fluctuating velocity signal in the free-stream along the tunnel axis, then according to the above recipe,

$$\overline{u_{fs}^2} = \tfrac{1}{2}\left\{[u_1\sin(k_1x-\omega t+\phi_1) + u_2\sin(-k_2x-\omega t+\phi_2)]^2 + [u_1\cos(k_1x-\omega t+\phi_1) + u_2\cos(-k_2x-\omega t+\phi_2)]^2\right\} + \left[\frac{B_1}{(x+a)^b}\right]^2 + \left[\frac{B_2}{(170-x+a)^b}\right]^2 \tag{9}$$

Letting $R_2 = u_2/u_1$ be the reflection factor and $\Delta\phi_{12} = \phi_1-\phi_2$, eq. (9) can be simplified to

$$\overline{u_{fs}^2} = u_1^2\left\{\tfrac{1}{2}(1+R_2^2) + R_2\cos[(k_1+k_2)x + \Delta\phi_{12}]\right\} + \left[\frac{B_1/u_1}{(x+a)^b}\right]^2 + \left[\frac{R_2\,B_2/u_2}{(170-x+a)^b}\right]^2 \tag{10}$$

The strength of the evanescent waves at the entrance to the test section may be expected to depend on u_1 and that of the evanescent waves at the exit to depend on u_2. To simplify matters B_1/u_1 will be equated to B_2/u_2, and with this ratio denoted by D, eq. (10) becomes

$$\overline{u_{fs}^2} = u_1^2\left\{\tfrac{1}{2}(1+R_2^2) + R_2\cos[(k_1+k_2)x + \Delta\phi_{12}]\right\} + D^2\left[\frac{1}{(x+a)^{2b}} + \frac{R_2^2}{(170-x+a)^{2b}}\right] \tag{11}$$

The value of x is to be in units of centimeters. The rms fluctuating velocity

signal is thus $\tilde{u}_{fs} = \sqrt{\overline{u_{fs}^2}}$. The unknowns, which are essentially determined by trial-and-error, are u_1, R_2, $\Delta\phi_{12}$, A, a, and b. The reflection factor R_2 is expected to be about 0.1. R_2, u_1, A, a, and b are used to adjust the amplitude of the signal. The upstream and downstream traveling plane waves produce a standing wave pattern, and the periodicity is determined by $k_1 + k_2$, a sum which is known. The phase angle difference, $\Delta\phi_{12}$, shifts the oscillatory pattern upstream or downstream and is rather easily determined from the data. This factor depends upon the length of the test section, the values of c and U_∞, the phase shift which occurs during the reflection process, and the location of origin of the x axis.

A desk-top computer with a CRT screen and a multi-color plotter were used in the data fitting task. The figure containing the data in Shapiro's report was photographed, and an enlargement was placed on the plotter and the data points digitized so that they could be displayed on the CRT screen. In much of the data fitting work the data and computed curve were plotted on the screen, since plotting on this device was much faster than on the hard plotter. Besides being used for the final plot, the hard plotter was also occasionally used in the data fitting work because the plots were larger, and also by using different line colors and types a convenient record could be kept of the effect of changing various model parameters.

Shapiro obtained the sound pressure levels from the hot-wire data by using the relation $\tilde{p} = \rho c\tilde{u}$. As is discussed in the Appendix, this formula is only valid for plane waves and is not strictly correct when a standing-wave field is present (if one of the progressive waves involved in the production of the standing wave is much stronger than the remaining components, the error incurred in using the relation is reduced). To match Shapiro's data his procedure was followed and therefore $\tilde{p}$ was also taken as $\rho c\tilde{u}_{fs}$. Figure 5 shows the comparison of the data with the resultant model. Of particular importance is the range from 10 to 60 cm, and the agreement is good here. The periodicity agrees well with the two-wave model. The values of the constants are as follows: $u_1 = 3.337 \times 10^{-3}$ m/sec, $R_2 = 0.1$, D = 1.4, a = 9, b = 0.32 and $\Delta\phi_{12} = -58^o$. The speed of sound was taken as 344 m/sec, $U_\infty = 29$ m/sec, $\rho c = 416.24$ (kg/m^2-sec), and the frequency was 500 Hz. The sound pressure level in decibels is computed from 20 log $p/\tilde{p}_{ref}$, where p_{ref} is the standard value of 2×10^{-5} N/m^2. The sound pressure level formula reduces to 20 log $\tilde{p}$ + 93.9794.

Figure 6 shows the variation of the acoustic velocity and pressure along the tunnel axis according to the present model. The velocity was determined using equation (11). As discussed in the review, the pressure and velocity in a standing wave are 180° apart in phase (they are in phase in a plane progressive wave), so the pressure was determined by changing the sign of the cosine term in eq. (11) and multiplying the results by ρc. Presumably the sound pressure levels in the figure should compare favorably with microphone measurements of the pressure. Shapiro did not present the results of his microphone measurements inside the test section, but as mentioned earlier, he did state that they were in agreement, ± 2 dB, with the hot-wire results. When the pressures in figure 6 are compared with the hot-wire "pressures" of figure 5, the values are within 1.5 dB of each other. It is possible that far fewer axial stations were surveyed with the microphone than with the hot-wire, and hence the microphone data would appear as scatter about the hot-wire data instead of revealing a 180° phase shift.

The 1,0 mode issue. - The deferred matter of the presence of the 1,0 mode will now be considered. Actually, with the plate absent both the 1,0 and 0,1

modes can propagate (both have the same cutoff frequency). But since these modes have the same x-component wave number, for the sake of brevity only the 1,0 mode will be referred to here. As previously stated, evidence for the extent of presence of the 1,0 mode must be sought in the standing waves it would set up along the tunnel axis. Equation (43) shows how the wavelength of the standing wave is related to the wave numbers of the modes involved. For a square duct, eq. (41) gives

$$k_{x_{m,n}} = \frac{\pi}{h} \sqrt{\frac{4f^2 h^2}{c^2} - (m^2 + n^2)} \tag{12}$$

where $h = 0.38$ m here. The amplitude of the oscillations in the standing wave depends on the relative strength of the two waves involved; the greater the disparity, the smaller the amplitude. Four wave families are involved here, the 0,0 (fundamental) mode and its reflection, and the 1,0 mode with its reflection (actually, an upstream 1,0 mode would also likely be created in the reflection of the fundamental mode since, as is mentioned in the Appendix, modes are coupled in complicated reflection processes). The downstream 0,0 mode is expected to have the greatest strength. Its reflection is weak, but may be comparable in strength to the downstream 1,0 mode waves. In the hierarchy of wave amplitudes these two waves might be expected to occupy the second and third positions, but it is not clear in which order. Accordingly, the two standing waves which should be the most prominent would be those produced by the fundamental and its reflection and by the fundamental and the downstream propagating 1,0 mode. Equation (43) and (12) were used to compute the wavelengths of the possible standing waves (the effects of the flow were properly ignored) and the results are displayed in Table I.

TABLE I. - LONGITUDINAL WAVELENGTHS OF INTERFERENCE PATTERNS PRODUCED IN 38 CM × 38 CM DUCT BY 500 Hz MODES TRAVELING IN THE SAME AND OPPOSITE DIRECTIONS

Interfering modes	Wavelength, cm	
	Same direction	Opposite direction
0,0 - 0,0		34
0,0 - 1,0	120	48
1,0 - 1,0		81

The two standing waves of special interest, the 0,0 - 0,0 and the same-direction 0,0 - 1,0, have wavelengths of 34 and 120 centimeters, respectively. Figure 5 clearly shows the 0,0 - 0,0 standing wave, and this phenomenon was included in the model. The data may also be showing a 120 cm wave. A peak at 5 cm occurs, and one at 125 cm would be consistent with an extrapolation of the data. Thus the 1,0 mode may be present with an amplitude exceeding that of the 0,0 reflected wave. But the evidence here rests primarily on the fact that the last two data points show a rising signal strength instead of falling as would occur if the 1,0 mode was insignificantly present. Also, the existing data do not show a symmetry about the half-wavelength point of 65 cm. Without

additional data the issue is moot. There does not appear to be evidence of 48 cm or 81 cm waves present, the remaining two possibilities in Table I.

In order to counter the feeling that it may generally be safe to neglect the transverse modes, the reader is invited to examine figure 7. This figure is from Shapiro and shows the variation of the sound pressure (read velocity) level along the axis for the case of 1000 Hz excitation. Most of the data in Shapiro's report were for the 500 Hz case, but 1000 Hz was also used in the investigation. For 1000 Hz, the 1,1 and 2,0 (and 0,2) modes are also possible (cutoff frequencies of 640 Hz and 905 Hz, respectively). The relevant standing wave wavelengths are given in Table II.

TABLE II. - LONGITUDINAL WAVELENGTHS OF INTERFERENCE PATTERNS PRODUCED IN 38 CM × 38 CM DUCT BY 1000 Hz MODES TRAVELING THE SAME AND OPPOSITE DIRECTIONS

Interfering modes	Wavelength, cm	
	Same direction	Opposite direction
0,0 - 0,0		17
0,0 - 1,0	318	18
0,0 - 1,1	148	19
0,0 - 2,0	60	24
1,0 - 1,0		19
1,0 - 1,1	279	21
1,0 - 2,0	74	26
1,1 - 1,1		22
1,1 - 2,0	100	29
2,0 - 2,0		40

Unlike the 500 Hz case, some of the wavelengths for different mode interactions are nearly equal and this makes it even more difficult to make unambiguous conclusions. The data show a short wavelength, 19-22 cm, standing wave of relatively small amplitude superimposed on a much larger wavelength, 45-70 cm, standing wave having a much larger amplitude. The short wavelength wave is characteristic of many of the opposing-direction wave mode interactions. Because of the higher frequency, smaller reflection coefficients for the waves reflected from the open end of the tunnel should be expected, at least for the fundamental mode. Only the same-direction 0,0 - 2,0 interaction has a wavelength comparable to the long-wavelength, large amplitude pattern shown in the figure. It is of interest to note that the 2,1 mode, not shown in the table, has a no-flow cutoff frequency of 1012 Hz and a 1009 Hz frequency in the downstream direction if flow is included. The 1009 Hz is within 1% of the stated excitation frequency, and unless the signal generator was one of great precision, there is a distinct possibility that the excitation frequency slightly exceeded the cutoff frequency for the 2,1 mode. As indicated in the duct acoustics

review, when a nonrigid duct is excited with a frequency just greater than some cutoff frequency, it is possible that this mode will have a large amplitude. Table III contains the computed no-flow standing wave wavelengths for a 1015 Hz signal. The only interactions with a 2,1 mode that give a wavelength comparable to the long-wavelength pattern in figure 7 are the 2,0 - 2,1 opposing-direction and 1,1 - 2,1 same-direction interactions (for a 1020 Hz signal, these wavelengths change, respectively, to 58 and 52 cm). Without additional data it is not possible to be confident of just what modes created the large amplitude, long wavelength standing wave pattern.

TABLE III. - LONGITUDINAL WAVELENGTHS OF INTERFERENCE PATTERNS PRODUCED IN 38 CM × 38 CM DUCT BY 1015 Hz MODES TRAVELING THE SAME AND OPPOSITE DIRECTIONS

Interfering modes	Wavelength, cm	
	Same direction	Opposite direction
0,0 - 0,0		17
0,0 - 1,0	323	18
0,0 - 1,1	153	19
0,0 - 2,0	62	23
0,0 - 2,1	37	32
1,0 - 1,0		19
1,0 - 1,1	285	20
1,0 - 2,0	77	25
1,0 - 2,1	41	35
1,1 - 1,1		22
1,1 - 2,0	105	28
1,1 - 2,1	48	40
2,0 - 2,0		37
2,0 - 2,1	90	64
2,1 - 2,1		225

A very important distinction exists between the 500 Hz and 1000 Hz cases. The presence of the plate does not affect which modes may propagate in the 500 Hz case but it does so for the 1000 Hz situation. With the plate present, the first few modes and cutoff frequencies for the channel above the plate are as follows: 1,0 - 453 Hz; 0,1 - 680 Hz; 1,1 - 817 Hz; 2,0 - 905 Hz; and 2,1 - 1132 Hz. Below the plate the modes and frequencies are 1,0 - 453 Hz, 2,0 - 905 Hz, and 0,1 - 1354 Hz. The 2,1 mode, which may have been present without the plate, certainly does not propagate with the plate present. In addition, the 1000 Hz signal is not very close to the cutoff frequency of the nearest

propagating mode and therefore no mode would be strongly excited. It is thus possible that in the 1000 Hz case the sound field could be significantly altered with the plate present. Offsetting the rigid plate would also affect the attenuation rates of modes which involve reflection from the plate. This is so because in addition to changing the angle of incidence of these modes (recall eq. (40)), it also changes the number of times an oblique ray path meets the absorbent tunnel wall. The present writer is content to stay with the 500 Hz case.

Modeling of Tollmien-Schlichting Waves

The longitudinal velocity perturbations produced by Tollmien-Schlichting waves can be represented by sinusoidal traveling waves whose speed and amplitude growth rate depend upon the frequency of the wave and the local boundary layer conditions. For a flat plate the boundary layer dependency is characterized by a Reynolds number, often the Reynolds number based upon the local boundary layer displacement thickness $Re_{\delta*}$. Shapiro observed that the TS waves were induced with the same frequency as that of the excitation sound field, and this observation will be incorporated in the TS wave model. The TS waves will accordingly be modeled as downstream traveling sinusoidal waves whose wave number and longitudinal velocity fluctuation amplitude vary with x, and hence with $Re_{\delta*}$, and whose frequency is constant at 500 Hz. Mathematically, at a given distance from the plate, the TS wave will be represented as $u_3\, e^{i(k_3x-\omega t+\phi_3)}$, where the subscript 3 is used inasmuch as this is the third traveling wave in the total model. The complete model, which embodies the fundamental assumption that the fluctuations in the boundary layer result from the superposition of the free-stream disturbances and the TS waves, comprises the three traveling waves and the two terms representing the evanescent waves, all summed as in the free-stream model. The mean-square value of the velocity fluctuations in the boundary layer, $\overline{u_{BL}^2}$, is thus taken as

$$\overline{u_{BL}^2} = \tfrac{1}{2}\left\{\left[u_1\sin(k_1x-\omega t+\phi_1) + u_2\sin(-k_2x-\omega t+\phi_2) + u_3\sin(k_3x-\omega t+\phi_3)\right]^2 + \left[u_1\cos(k_1x-\omega t+\phi_1) + u_2\cos(-k_2x-\omega t+\phi_2) + u_3\cos(k_3x-\omega t+\phi_3)\right]^2\right\} + \left[\frac{B_1}{(x+a)^b}\right]^2 + \left[\frac{B_2}{(170-x+a)^b}\right]^2 \tag{13}$$

The unknown quantities are u_3, k_3, ϕ_3, and ϕ_1. Once ϕ_1 is determined, ϕ_2 is computed from $\phi_2 = \phi_1 - \Delta\phi_{12}$ since it is now known that $\Delta\phi_{12}$ is -58°. Letting $R_3 \equiv u_3/u_1$, $\Delta\phi_{23} = \phi_2 - \phi_3$, and $\Delta\phi_{13} = \phi_1 - \phi_3$, eq. (13) may be simplified to

$$\overline{u_{BL}^2} = u_1^2\left\{\tfrac{1}{2}(1+R_2^2+R_3^2) + R_2\cos[(k_1+k_2)x + \Delta\phi_{12}] + R_3\cos[(k_1-k_3)x + \Delta\phi_{13}] + R_2R_3\cos[(-k_2-k_3)x + \Delta\phi_{23}]\right\} + D^2\left[\frac{1}{(x+a)^{2b}} + \frac{R_2^2}{(170-x+a)^{2b}}\right]$$

Calculations were actually performed using equation (13) because it was also necessary to determine the phase angle θ obtained from

$$\theta = \tan^{-1} \frac{\Sigma \text{ sine terms}}{\Sigma \text{ cosine terms}}$$

and the summations are explicitly contained in eq. (13).

Shapiro presented data showing the variation with x of the rms velocity fluctuation level and the phase angle θ as obtained from the hot-wire measurements in the boundary layer. In the present model u_3 and k_3 were varied with x so as to make $\tilde{u}_{BL}$ reasonably match the hot-wire data. From the variation of u_3 with x the growth rates of the TS waves could be determined, and from $k_3(x)$ the behavior of the TS phase velocity could be obtained. The procedures for doing this, which are trial-and-error, are given in the next section.

Within the boundary layer TS waves traveling obliquely across the plate exist as well as two-dimensional waves traveling directly down the plate. Boundary layer instability theory predicts that the two-dimensional waves have the greatest growth rate, and therefore these waves should dominate the TS wave field in the region away from the leading edge of the plate. The present single TS wave model can be expected to be more appropriate for the downstream region where one type of wave predominates. The upstream region would likely encompass the area from the leading edge to some distance downstream of the critical Reynolds number station, the station where the flow is unstable and TS wave amplification can begin. Unfortunately, this upstream region is also the one of greatest interest in the acoustic excitation problem.

Tollmien-Schlichting Wave Amplification Rates and Phase Speeds

The quantities $u_3(x)$ and $k_3(x)$ were determined using a trial-and-error procedure. Amplitude data were used to determine $u_3(x)$ and the phase angle data were used to obtain ϕ_1, ϕ_3, and $k_3(x)$. The desk-top computer and plotter were again indispensable in the procedure. As before, the Shapiro report figures were photographed, enlarged, printed, and then copies were made using an office copier. In matching the model to the data the model parameters were varied and the computed results were compared with the data by either plotting the results directly on the enlarged data plots or else on the CRT screen together with data points which had been read from the enlarged plots using the digitizing capability of the computer/plotter system. The CRT was primarily used in the initial phase of the modeling because of the greater plotting speed. As will be explained, once $u_3(x)$ and $k_3(x)$ were obtained, the TS wave growth rates could be determined from a differentiation of $u_3(x)$ (actually of $\ln u_3$) and the phase speeds calculated from the reciprocal of $k_3(x)$.

Procedure for TS wave amplitude determination. - Since the amplitude data were plotted against Re_{δ^*} and the phase angle against x, a relationship between x and Re_{δ^*} was needed. For a flat plate the Blasius velocity profile is appropriate, and for such a profile $Re_{\delta^*} = 1.72 \sqrt{Re_x}$. For the data considered here the nondimensional frequency $\omega\nu/U^2$ was given as 5.6×10^{-5}. The relation between x and Re_{δ^*} for these tests can therefore be expressed as

$$x = \frac{5.6 \times 10^{-5}}{(1.72)^2} \frac{U_\infty}{\omega} Re_{\delta^*}^2 .$$

With $U_\infty = 29$ m/sec and $f = 500$ Hz, the equation reduces to x [cm] = $1.747 \times 10^{-5} \, Re_{\delta^*}^2$ and this was the relation used in the present work. Letting A represent a rms signal level, Shapiro plotted the boundary layer oscillation amplitude data in the form of $\ln A/A_o$ vs Re_{δ^*}. In boundary layer stability theory A_o is taken as the TS wave amplitude at the critical Reynolds number location. Since Shapiro believed that his experimentally determined values of A were a measure of the TS wave amplitude, it would be natural to take as A_o the value of A at the critical Reynolds number. The problem is that A exhibited the spatial modulations of a 2-cm wavelength standing wave pattern, and it would seem rather capricious to select a value of A at some particular value of Re_{δ^*}. Recall, however, that Shapiro treated the data by fairing a curve through the spatial oscillations. By doing so he concluded that the TS wave amplitude was "approximately constant" ahead of the neutral point and took A_o as "this constant level." So A_o was rather nebulously defined. As discussed in the Introduction, the standing wave produced by the TS and acoustic waves is such that as long as the TS wave amplitude is less than that of the acoustic wave, a fairing of the data should produce a curve which matches the acoustic field strength. The acoustic field strength, at least in the absence of the plate, varied by about 25% over the range of x being considered. With no further guidance, A_o was taken as the value of the free-stream acoustic field strength at the location of the critical Reynolds number. The critical Reynolds number for a 500 Hz TS wave traveling in a flat plate boundary layer is 990, a value which corresponds to $x = 17.1$ cm. Accordingly, in the model A/A_o was represented by $\tilde{u}_{BL}/\tilde{u}_{BL_o}$, where $\tilde{u}_{BL_o}$ was evaluated using eq. (13) with $x = 17.1$ and $u_3 = 0$.

Some of the lower Reynolds number $\ln A/A_o$ data have been replotted in figure 8 in the form of A/A_o vs. Re_{δ^*}. The Reynolds number range in the figure corresponds to a distance of 7 to 25 cm from the leading edge. The data show a standing wave pattern having a wavelength of approximately 2 cm. This wavelength is close to what would be expected (using eq. (43)) if a 500 Hz TS wave traveled downstream with a typical phase speed of $1/3 \, U_\infty$ and interfered with either the downstream or upstream traveling fundamental acoustic wave. The figure thus presents rather convincing evidence that the standing wave is the result of the superposition of the TS and acoustic wave fields.

The dashed curve in the figure corresponds to the modeled level of the free-stream acoustic field strength. According to the model the data should oscillate about this curve in the upstream stable region where the TS wave amplitude is small, and the data do appear to exhibit this behavior. The line $A/A_o = 1$ has also been drawn on the figure. This line intersects the dashed curve at the Reynolds number of 990, showing that A_o has been modeled correctly. The line also shows the subjective element in the present modeling effort. Not much imagination would be needed to conclude that the data may be oscillating about the line $A/A_o = 1$. Statistical tests could be applied for more conclusive results, but this was not done in any of the modeling work.

The data also show a rapidly increasing average signal level downstream of the critical Reynolds number. Again recall from the Introduction that the average amplitude of two sinusoidal signals equals the amplitude of the larger signal. The increasing signal level is thus consistent with the expected growth of the TS waves upon entering the unstable region. The data show that

somewhere in the Reynolds number range of 900 to 1000 the TS wave amplitude has exceeded the amplitude of the acoustic signal. A troublesome feature of the figure is that in the upstream supposedly stable region, where a diminution of the oscillations with increasing Reynolds number would be expected to occur, the data show the opposite trend. This problem will be addressed later.

Because $u_3(x)$ was expected to vary over a considerable range and not be representable by a simple function, the decision was made to express u_3 by a cubic spline. The cubic spline (ref. 40) is a piecewise continuous cubic polynominal which can be made to pass through any number of points while having continuous first and second derivatives. With spline representation u_3 would therefore be a smooth curve whose amplitude could conveniently be controlled by adjusting the points, or nodes as they are often called, through which the spline passed. Forty nodal points were distributed along the abscissa and covered the $Re_{\delta*}$ range of 600 to 2070. Points were clustered in regions where greatest control was needed; the closest points were a Reynolds number of 25 apart. The ordinate value of the nodes were then shifted as necessary to make $\tilde{u}_{BL}/\tilde{u}_{BL_o}$ match the behavior of the A/A_o growth curve data. Actually, there was one other factor considered while doing the matching, and this was the TS wave amplitude growth rate.

Once $u_3(x)$ was determined, the TS wave amplitude growth curve, $\ln u_3/u_{3_o}$ vs. $Re_{\delta*}$, could be obtained, where u_{3_o} is the TS wave amplitude at the critical Reynolds number. The growth rate is the derivative of $\ln u_3/u_{3_o}$ with respect to $Re_{\delta*}$. The differentiation process makes readily apparent any oscillations in the curve and thus inherently magnifies any scatter in the experimental growth curve data. The modeling process, on the other hand, is inherently a smoothing one, but judgement is required in the data matching and differences in judgement again become quite apparent under the differentiation operation. Furthermore, with the spline fit, the differentiated results were obviously sensitive to small shifts in the nodal points which were closest together. So while the ordinates of the nodal points were shifted up and down to match the model to the A/A_o data, a close eye was kept on the resulting growth rate curve to make sure that it did not suffer excessive gyrations.

The derivatives needed for the growth rate curves were computed numerically. A five-point linear smoothing differentiation formula was used to help reduce the oscillations (ref. 41). The Reynolds number spacing between the points was 20. The growth rate curves were plotted with the aid of a cubic spline.

The amplitude of the A/A_o data was used to model the amplitude of the TS waves, and the wavelengths in the standing wave pattern could have been examined for the modeling of the TS wave number behavior, $k_3(x)$. This procedure was not followed because over the range of 7 to 18 centimeters from the leading edge Shapiro presented detailed phase angle data which appeared to be more suitable to the wave number determination task. In a separate figure Shapiro presented somewhat less detailed phase angle data covering the distance from 15 to 75 cm. As will be seen later, over this range the phase angle data provide a very sensitive indication of TS wave number behavior. This is indeed fortunate because beyond a distance of about 35 cm Shapiro's A/A_o data show no oscillatory pattern and it would be impossible to determine wave number information from the amplitude data.

Procedure for determination of phase speed and wave number. - The TS wave phase speed $c_3(x)$, rather than the wave number, was the quantity which was directly adjusted to make the periodicity of the model match that of the periodicity of the phase angle data. Since $kc = \omega$, either quantity could have been used. Furthermore, because the phase speed was not expected to vary much along the plate, a simple piecewise continuous first degree polynominal representation was chosen rather than the spline fit. (As will be discussed later, for large x the periodicity was not considered but rather the value of $c_3(x)$ was adjusted so that the mean phase angle growth matched that of the data).

For comparison with theory the phase velocity and wave number needed to be suitably nondimensionalized. In stability theory the phase speed is nondimensionalized by the free-stream velocity and the wave number by a boundary layer thickness, which was taken here as the displacement thickness. The equation $k = \omega/c$ may be written as

$$k\delta^* = \frac{\omega\delta^*/U_\infty}{c/U_\infty} \tag{14}$$

and if dimensionless quantities are denoted with the superscript o, eq. (14) becomes

$$k^o = \frac{\omega^o}{c^o}$$

where

$$k^o = k\delta^*, \quad c^o = \frac{c}{U_\infty}, \quad \omega^o = \frac{\omega\delta^*}{U_\infty}$$

This quantity ω^o may further be expressed as

$$\omega^o = \frac{\omega\nu}{U_\infty^2} \, Re_{\delta^*}$$

and the quantity $\omega\nu/U_\infty^2$ is recognized as the nondimensional frequency which was given as 5.6×10^{-5}. The nondimensional wave number was therefore conveniently determined from

$$k^o = 5.6 \times 10^{-5} \, \frac{Re_{\delta^*}}{c^o}$$

Procedure for determination of ϕ_1 and ϕ_3. - The phase angle θ was measured, presumably, with respect to the signal fed to the loudspeaker. Since the leading edge of the plate was taken as $x = 0$, the quantity ϕ_1 would be the phase angle with respect to the loudspeaker signal of the downstream traveling fundamental acoustic mode wave at the plate's leading edge. But in fact the value of ϕ_1 in the model has no such correspondence with the actual phase of the wave at $x = 0$. Shapiro did not describe how θ was measured, but data taken in the test section alone would not be sufficient to determine the total phase angle. Because the initial measurement station was a few wavelengths away from the loudspeaker, the actual phase angle would have advanced by more than 360^o through the settling chamber, and in the test section some multiple of 360^o would have to be added to the measured angle to obtain the true angle. But there is no need to make such an absolute determination, for the primary interest is in the variation of θ along the

plate. In fact, the initial measurement could be taken as any convenient angle and thereafter departures from this value recorded. Regardless of whether θ was measured or adjusted, ϕ_1 should not be considered as physically significant. The $\Delta\phi$ values are the quantities with physical significance.

To see how the choice of ϕ_1 affects the model results figure 3 can be used. Here the downstream and upstream traveling fundamental mode waves may be considered as being represented in part (a). The label states that the situation depicted is for x=10, but for the present purposes this should be taken as x=0. Since the angle between ϕ_1 and ϕ_2 at $x = 0$ is fixed at $\Delta\phi_{12}$, changing ϕ_1 changes the angle of the vector sum by the same amount. As shown in part (c) of the figure, with small amplitude TS waves present, the angle θ of the total signal oscillates about the angle of the sum vector, which is represented by the dashed line. Therefore, increasing or decreasing ϕ_1 while holding $\Delta\phi_{12}$ constant causes the dashed curve, and consequently the whole pattern, to shift up or down, respectively, on the phase angle plot. Finding a suitable value of ϕ_1 was thus not a difficult task.

Changing the TS wave initial phase angle ϕ_3 shifts the oscillatory phase angle pattern to the right or left along the dashed curve. This is more readily seen in figure 2. Again, it is not difficult to select an appropriate value for ϕ_3. Since the phase angle data began at $x = 7.5$ cm rather than $x = 0$, ϕ_3 was chosen to make the model best match the phase angle data in the range of $x = 7.5$ to 10 cm. The value of ϕ_3 therefore depended strongly on the assumed TS wave phase velocity upstream of the 7.5 cm station. Over the range of $x = 0$ to 10 cm $c_3(x)$ was assumed to be constant. This was an appropriate but probably unrealistic assumption, so again, ϕ_3 has no physical significance.

Comparisons of measured and modeled values of A and θ. - With the phase velocity initially taken as $1/3\ U_\infty$, a rough variation of u_3 with x was obtained. Then, in an iterative fashion, refinements were made on c_3 and u_3, with consideration given to keeping the derivative of u_3 fairly smooth. The resulting values of the phase angles were: $\phi_1 = -55^\circ$, $\phi_2 = 3^\circ$, and $\phi_3 = 180^\circ$. There is a story, to be told later, concerning ϕ_3.

Figure 9 shows a comparison of the lower Reynolds number A/A_o data values with the modeled simulation. Considering the somewhat erratic behavior of the data, the fit of the model to the data is not too bad. Under the assumption that the stronger signal levels could be measured more accurately, there was a bias towards fitting the data peaks more closely than the valleys. For Reynolds numbers of less than 1000, the bias resulted in the model overestimating the data minima. This behavior needs further study. The cyclic property of the data is well matched for Reynolds numbers greater than about 850, but below this value there appears to be a phase difference between data and model. As will be shown shortly, there is a good match between the phase angle data and the modeled phase angles over this Reynolds number region, so this discrepancy between model and data also needs further study. Although not discernable in the figure, the numerical results from the model show that the TS wave amplitude exceeded the acoustic signal amplitude at a Reynolds number of 949, a value corresponding to $x = 15.73$ cm.

In figure 10 the $\ln A/A_o$ data and model values are shown over the complete Reynolds number range of the test. The data and axes are from an enlarged reproduction of Shapiro's report figure. The asterisks have been added to indicate the distance from the leading edge in decades, starting with

x = 10 cm. The model matches the data's oscillatory behavior out to a Reynolds number of about 1300 (x ≈ 30 cm); thereafter Shapiro increased the spacing between his measurements and could not follow the cyclic behavior. The data and model show the expected decrease in oscillation amplitude as the TS wave amplitude becomes quite large (the eccentricity of the TS spiral becomes small).

The measured and modeled phase angles are shown in figure 11. The arrow is the same symbol used by Shapiro to indicate that θ continues to increase with increasing x. Before going into the data-model comparison there is an apparent anomaly in the data which must be discussed. The problem is in the relation between the phase angle θ and the signal amplitude. Figure 2 is helpful in this matter. From figure 2(b) it is clear that, with increasing x, as A increases from a local minimum to a local maximum, θ goes through a local minimum while changing from one midpoint to the next. This behavior may be observed in parts (c) and (d) of the figure (examine, for example, the curves from x = 3 to 4). Shapiro's data, however, shows the opposite behavior. With increasing x, as the amplitude A goes from a minimum to a maximum the value of θ goes through a maximum while changing from one mid-value to the next. This may be clearly seen in figures 10 and 11. In figure 10, over the Reynolds number range of 870 to 900, for example, the amplitude goes from a valley to a peak, while in figure 11 the phase angle traverses a local maximum over the corresponding range of x = 13.2 to 14.2 cm. The modeled phase angle also follows this anomalous behavior because the model was manipulated; the phase angle of the TS wave has been increased by 180°. This is the aforementioned story in connection with ϕ_3. The amplitude results were plotted with $\phi_3 = 0$, while the phase angle results were plotted with $\phi_3 = 180^{\circ}$. In figure 12 the amplitude calculations have been replotted with $\phi_3 = 180^{\circ}$ to match the conditions of the phase angle figure, and the data and model results do appear to be 180° out of phase.

The present writer has no explanation of the data's amplitude-phase behavior. The 180° factor immediately suggests some kind of accidental polarity reversal in the experimental wiring hookups, but reversing an electrical wire's connection to an instrument or device would not produce the effect. The rms amplitudes would not be altered by such a reversal. The phase angle at the initial measuring station would be changed by 180°, but the subsequent downstream variation would be unaffected. There is also a possibility that Shapiro did not use the same distance-to-Reynolds number conversion as used here, but the conversion consistency was demonstrated earlier.

This data peculiarity presented a modeling dilemma, and the dilemma was bypassed using a hybrid matching procedure; the amplitude was modeled with $\phi_3 = 0$ and the phase angle with $\phi_3 = 180^{\circ}$. Either value of ϕ_3 could have been used consistently, but the data matching was simpler when the model and data oscillated in phase. The final results would probably differ little with either hybrid or consistent matching.

Returning to figure 11, it should be restated that the phase angle data were used to model the TS wave phase velocity only. While the amplitude of the phase angle oscillations does depend on the TS wave amplitude and could therefore have been used in the modeling of $u_3(x)$, this was not done. The fact that the amplitude of the phase angle oscillations in figure 11 has been modeled well attests to the fidelity with which the $u_3(x)$ modeled the A/A_o data. The phase velocity affects only the periodicity, and the sensitivity of the periodicity to the phase velocity is illustrated in figure 13. Here the phase angle behavior is shown for three different nondimensional phase

velocities, c_3/U_∞, of 0.33, 0.35, and 0.37. In each case the value of ϕ_3 was altered so that the curves all began at the same point. By comparing figures 13 and 11 it is clear that with the scatter in the data it would be difficult to narrow the choice of a phase velocity value to closer than 0.02.

As seen in figure 11, the periodicity has been modeled fairly well except for the last cycle of the data, which the model missed completely. The condition likely means that either (1) the modeled TS wave amplitude growth is slightly in error in having exceeded the acoustic field amplitude a little too soon, or (2) the extra cycle represents a slight experimental error. Concerning the first possibility, the model showed the TS wave amplitude exceeded the acoustic field amplitude at $x = 15.73$. The computed phase angle at this point was 56°, and on the complex-plane diagram the TS outward spiral would, within a short distance, encompass the origin. This in fact occurred, for just a half centimeter downstream the phase angle underwent a rapid increase beyond 180°. Had the modeled TS wave amplitude been a little smaller, the origin would not have been encompassed, and near this location the phase angle would have undergone a rapid swing to some negative angle close to -90°.

The model also shows that it would have been difficult to have experimentally detected a behavior similar to that exhibited by the model, and this raises the possibility that the data are in error. The computations show that the first time the phase angle exceeds 90° the angle remains in the second and third quadrants only over a short distance. If there are no data stations in this region, and if the next station happens to be where the phase angle is in the fourth quadrant, then the angle could be interpreted as being between 0° and -90° instead of 270° and 360°. In the particular circumstances here, the model shows that the phase angle was only in the second quadrant from $x = 16.04$ to $x = 16.25$, and was in the third quadrant from 16.25 to 16.34. The nearest data points appear to be at $x = 15.78$ and 16.45, and consequently there may have been no data stations where the phase angle was between 90° and 270°. If 360° were to be subtracted from the computed angles greater than 270°, a resulting plot would closely follow the last four data points in figure 11.

Even if the data station spacings were adequate to catch the phase angle's traverse of the second and third quadrants, the model shows that it would be no easy task to measure the angle accurately. The resultant amplitude of the signal for the three waves considered in the model is very small in this region (the TS spiral is passing very near the origin on the complex-plane diagram). Under such conditions the experimenter would likely encounter signal-to-noise problems. According to the present model, when the phase angle first reached 180° the ratio of the signal component from the three waves to the total signal (which included the evanescent terms) was only 0.17. Thus the signal would have been buried in the noise. The noise is considered here to have a random phase angle behavior. In any event, while the model-data discrepancy in figure 11 looks bad, it should not be considered as a serious one.

The phase angle data and model results covering the remaining $x = 16$ to $x = 75$ range are shown in figure 14. The figure is again an enlargement of the Shapiro figure with the model results superimposed. Shapiro plotted the data in two groups, with each group having a separate linear growth removed. For a constant TS phase velocity the phase angle should oscillate

about a linear growth curve. In the modeling the indicated growth rates were also removed. In the first data group the spacing between data stations beyond $x = 37$ cm was too large to follow the oscillating behavior. In the data overlap region it appears that the data points in the first group represent local phase angle minima points, but Shapiro did not state what criterion he used for the large-spacing data points. Based on the model and the data in the $x = 32$ to 35 range it would appear reasonable to assume that the oscillations were so small that there was no need for taking data at close intervals. Yet the data in the second group clearly show oscillations over the $x = 50$ to 55 range where, because the TS wave strength is greatest, the oscillations should be smallest. The lack of agreement between model and data of the amplitude of the phase angle oscillations over the $x = 51$ to 70 range is puzzling.

As before, the TS wave phase speed behavior could be determined by modeling the periodicity of the oscillations in the phase angle data whenever the data oscillations were presented. The periodicity is reasonably matched by the model, but, in fact, the periodicity was not the criterion used in the modeling of the data in figure 14. The quantity used in the modeling was the mean growth rate (this procedure could not, of course, have been used for the data of figure 11). The phase speed was varied so that the mean behavior of the model reasonably matched the mean behavior of the phase angle data. If this is done well and if the model has incorporated the primary physical phenomena involved, than the periodicity should naturally fall in place. That the mean behavior of the phase angle is quite sensitive to the TS wave phase speed is shown in figure 15. It is immediately apparent that the phase speed over the last 25 cm is 0.34. The slope of the mean of the data strongly depends on the phase speed. A phase speed difference of 0.02 would clearly be discernible over a distance of 2 cm. Such was not the case for the region upstream of $x = 16$ cm.

The mean behavior of the data in figure 14 has been modeled well except in the regions of $x = 36$ to 40 and 43 to 48. If the model had been tailored to follow the data in these regions, two spikes in the phase speed (5% changes) would have occurred, but the decision was made to smooth.

TS wave amplitude growth and growth rate results. - The resulting TS wave amplitude growth curve, in the form of $\ln u_3/u_{3_o}$, is displayed in figure 16. As is expected, beyond a Reynolds number of about 1000 the shape of the curve is the same as that of a curve faired through the A/A_o data. In the lower Reynolds number range the growth curve behaves more akin to a curve faired through consecutive $(A/A_{o_{max}} - A/A_{o_{min}})/2$ points. The growth curve does not truly match this behavior because the model overestimated the low Reynolds number data minima. Numerical differentiation of the displayed growth curve produced the growth rate curve shown in figure 17.

In figure 17 the modeled growth rate curve is compared with that obtained by Shapiro and with amplification rates from flat plate stability theory.*

*The author gratefully acknowledges the help of Dr. Mujeeb Malik, Systems and Applied Sciences Corporation, for providing the stability code and setting up the input procedure for the determination of stability results with the present frequency. The code is described in reference 42, and unless a specific reference is given, all results labeled as Theory come from this code.

The amplification rates are spatial rates obtained from a temporal analysis using Gaster's transformation (refs., 43 and 44) whereby the spatial rate equals the negative of the imaginary part of the eigenfrequency divided by the group velocity. Due to numerical limitations only the positive theoretical amplification rates are shown; the parabolic shape of the curve of course extends into the negative region. Shapiro's curve is reported to represent an average of three data runs; the bars, also taken from Shapiro, indicate the approximate deviation of the data. Shapiro obtained amplification rates by differentiation of his growth curves, but because of his fairing procedure the low Reynolds number results must be in error. (Readers are also invited to try their hand at fairing the growth data shown back in figure 8. If this data is typical, a fairing taken between the dashed and solid lines does not seem unreasonable up to a Reynolds number of about 950, and the resulting "growth rate" would appear to differ significantly from Shapiro's). As explained in the Introduction, fairings through the low- and high-Reynolds number data should in fact not join smoothly. To force them to do so would require some compromising. Because of the fairing technique, Shapiro's results would perhaps be expected to be in better agreement with the present results for Reynolds numbers greater than a 1000 or so. Such are the vagaries of fairing, differentiating, and using fifth-hand reproductions and enlargements of original figures.

There are two striking differences between the presently derived experimental amplification rates and the theoretical values. The maximum rates appear to have been truncated (the curve displays a post-eruption Mt. St. Helens profile) and positive amplification rates occur upstream of the critical Reynolds number. Shapiro attributed most of the amplification rate behavior to pressure gradient effects, and this appears to be a reasonable explanation. In fact the present results may be reflecting the pressure gradient effects to a greater degree than shown in Shapiro's findings.

Pressure gradients affect stability in two important ways; they change the critical Reynolds number and they alter the amplification rates. An adverse gradient lowers the critical Reynolds number and increases the amplification rates while a favorable gradient produces the opposite effects. In the experiment the largest gradients were the result of the leading edge conditions. Recall that this region was semi-elliptical in shape, with a 6:1 axis ratio, and extended back 3.81 cm. Based on numerical studies this shape was chosen as one suitably satisfying the conflicting needs of short length and small pressure gradients. Shapiro's plate had pressure orifices located at what appears to be 5.08 cm (2 in) intervals beginning at about 5 cm from the leading edge, with an additional orifice near $x = 2.5$ cm. The measured pressure distributions were displayed in two separate figures. In one figure the variation of pressure with length was shown and in the second the variation with $Re_{\delta*}$ was exhibited.

Shapiro reported that surface pressure calculations were performed by M. Davis using a program by J. Milgram. The theoretical results were not shown, but they can be inferred from the curves presented by Davis in reference 45. Using the computer program of Milgram, Davis presented pressure coefficient distributions for various flat plate leading edge shapes, including those with elliptical leading edges (the axis ratios were 2, 4, and 8, but the results for 6, needed here, can be easily estimated). Shapiro presented his pressure coefficient results using an unspecified reference pressure, so a direct comparison with Davis' numbers cannot be made, but from the shape of the distribution curves it is clear that the measured pressure distribution differs markedly from the theoretical result. Based on the theoretical findings,

the pressure on Shapiro's plate would be expected to reach a minimum at $x \approx 0.95$ cm, to recover to about half the pressure minimum by $x \approx 2.5$ cm, and by $x = 5$ cm the pressure gradient would be extremely small. The data, however, show that at $x \approx 2.5$, the location of the first orifice, the pressure is falling with a very steep gradient. The pressure minimum occurs in the vicinity of the second orifice at $x \approx 5$ cm. The pressure then recovers to a local maximum near $x = 20$ and then slowly falls to a second local minimum in the vicinity of $x = 60$. If the computational results are correct, then there must have been problems with the plate's geometry and perhaps with some pressure gradients in the free-stream. If this is the situation then it is a most encouraging one, for it leaves hope that perhaps a similar experiment could someday be conducted with a much improved pressure distribution condition. As will be demonstrated below, the TS wave behavior in Shapiro's experiment appears to have been markedly influenced by the pressure gradients.

First, it should be mentioned that there is a discrepancy between the distance and Reynolds number pressure distribution figures. The minimum pressure, which occurs near the second orifice, is plotted on the Reynolds number figure with a value approximately 2.2 times more negative than its value on the distance figure. This data point is important because it determines the location of the maximum adverse pressure gradient. If the value nearer zero is correct then the maximum adverse pressure gradient occurs in the region between the third and fourth orifice. If the more negative value is correct then the maximum adverse pressure gradient occurs, and is nearly constant, over the region from the second to the fourth orifice. In terms of Reynolds numbers, in the former case the most adverse pressure gradient extends, approximately, over the 740 to 920 range, and in the latter, over the 580 to 920 range. As shown in figure 17, the presently derived amplification rate curve begins a rapid increase near $Re_{\delta^*} = 750$, and this behavior is consistent with the pressure data if the minimum pressure point which is nearer to zero is accepted as the correct value.

The general behavior of the amplification rate curve does exhibit, at least qualitatively, a considerable correlation with the pressure gradients along the plate. This may be judged by examining the curve and the following qualitative description of the pressure gradients. The gradients and approximate Reynolds number range over which they occur are as follows; the numbers in parentheses times the dynamic pressure, $\frac{1}{2} \rho_\infty U_\infty^2$, provide a rough indication of the magnitude of the gradient per centimeter: very favorable (-8.7×10^{-3}), 370-530; very unfavorable ($1.7 \times 10^{-3} - 3 \times 10^{-3}$), 530-920; transition from unfavorable to favorable, 920-1190; moderately favorable (-3.3×10^{-4}), 1190-1500; slightly unfavorable, 1500-1600; moderately favorable, 1600-1770; transition from favorable to unfavorable, 1770-2000; moderately unfavorable (2.4×10^{-4}), 2000-2300. The complete low Reynolds number region ($Re_{\delta^*} < 1060$) for which TS wave data are available is under an adverse pressure gradient. The "premature" positive growth rate is consistent with the pressure gradient effect and consequently little, if any, quantitative information can be obtained about the sound-instability problem. An unfortunate circumstance indeed.

There is a puzzling aspect of the TS wave behavior which should be reported. This concerns the critical Reynolds number. The effects of pressure gradients on boundary layer stability have been the subject of much theoretical study. The report by Obremski, et al. (ref. 21) contains the stability characteristics of two families of laminar boundary layer profiles: (1) the Falkner-Skan family, a one-parameter self-similar set of profiles, and (2) the Obremski

family, a nonsimilar three-parameter set of profiles. Numerical solutions of the stability equations were obtained, and the results were displayed in tables and stability diagrams. The Falkner-Skan family may be characterized by the so-called Hartree parameter β (see, for example, ref. 25). For $-0.199 \leq \beta \leq 0$, β relates to retarded flows, and in particular, to flows downstream of corners. In the inviscid case, the surface flow downstream of a corner is described by $U_\infty \propto x^{\beta/(2-\beta)}$. Negative values of β thus describe retarded flows, and in the inviscid case, since $dp/dx = -\rho U\, dU/dx$, negative values of β also characterize adverse pressure gradients. In the Falkner-Skan laminar boundary layer solutions the velocity gradient is zero at the wall for $\beta \approx -0.199$, and consequently this value of β gives the flow separation condition. Shapiro stated that an approximate value of β for the adverse pressure region was -0.03. (No details given; Leehey, who was Shapiro's supervisor, gives the value as -0.05 in ref. 5). Based on an examination of the stability diagrams for various values of β in the Obremski report, the present writer found the following β-critical Reynolds number pairs for the nondimensional frequency of 5.6×10^{-5}: 0.05, 1160; 0.0, 980; -0.05, 840; -0.10, 720; and, -0.14, 640. Interpolating these values gives a critical Reynolds number of 900 for $\beta = -0.03$. This Reynolds number is well downstream of wave growth in Shapiro's experiment. Rapid growth begins at $Re_{\delta^*} \approx 750$, and if this represented the critical Reynolds number value, the corresponding value of β would be about -0.085. Inasmuch as some growth actually occurs upstream of $Re_{\delta^*} = 750$, the 750 value should not strictly be taken as the critical Reynolds number. This value could perhaps be considered as the critical Reynolds number if the relative slow growth in the upstream region were the result of sound feeding energy into the TS waves and not from an instability mechanism. One of the purposes of the experimental investigation was to determine how the sound field affected TS wave development, but as stated above, the pressure gradients have clouded the issue.

The variation along the plate of the ratio of the amplitude of the longitudinal velocity fluctuation level associated with the TS wave to that of the acoustic field at the leading edge has been plotted in figure 18. The modeled low Reynolds number results are shown in the figure, and, as always in this study, the TS wave amplitude at any station is to be considered as the maximum value across the boundary layer of $u(y)/U(y)$ (which generally occurs near $y/\delta \sim 0.2$). The figure shows that the TS level continuously increases and that at the earliest data station the TS amplitude has already reached about 25% of the initial acoustic level. This value is very much larger than the theoretical estimate by Murdock (ref. 4) of 0.01% at the critical Reynolds number location (see the discussion in Additional Background section). Because of unknown pressure gradient effects the theoretical value can not be adequately assessed, although very large gradient-induced growth rates would have had to occurred upstream of $Re_{\delta^*} = 650$. Since all flat plate models will always have pressure gradients present in the leading edge region, it may well be incumbent on the theoretician studying the acoustic-instability problem to trace the wave growth through the pressure fields; with present technology the experimenter cannot probe this upstream region.

It should be noted that Shapiro also reported growth rate results for the natural, unexcited case. One of the actual growth curves was shown, and while there are some oscillations present, their magnitude is small and a fairing procedure would produce little error (according to Leehey, ref. 5, this data was obtained with the 500 Hz narrow bandpass filter in place). For the data shown it appears that amplification occurred in the 750 to 850 Reynolds number range, and continued at a lower amplification rate out to

about $Re_{\delta^*} = 1000$. Thereafter a large increase in amplification began. Shapiro's amplification rate curve, averaged over three data runs, shows an amplification rate beginning near zero and increasing roughly linearly with Reynolds number up to a value of 1600 where the rates matched those of the excited case. Beyond 1600 the growth rates for both cases were in good agreement. The low initial growth rate for the unexcited case was attributed to their being TS waves of comparable initial amplitudes propagating in many directions in the lower Reynolds number regions. The oblique waves have lower growth rates than two-dimensional waves and the measured growth rate would reflect the lower average value. Further downstream the two-dimensional waves would dominate independent of the source of excitation, and the measured growth rates should converge for all cases. Estimated values of the critical Reynolds number, now used in its proper sense (all frequencies considered), read from figures in reference 21 are: $\beta = 0.05$, $Re_{\delta^*} = 860$; 0.0, 515 (correct value is 520); -0.05, 315; -0.1, 198; and -0.14, 136. A β of -0.03 has a critical Reynolds number of about 780 and this is close to where a small amount of amplification occurred. For $Re_{\delta^*} < 750$ it is difficult to assess from the data what was happening in the boundary layer.

A testing of the above hypothesis that the measured low growth rates are due to oblique waves could perhaps be done with an interesting acoustic excitation experiment. Growth rates could be measured and compared for the cases of acoustic excitation at frequencies below and just above the cutoff frequency of the tunnel's first mode. The fundamental plane acoustic wave is likely to dominate the acoustic field at both frequencies, but for the higher frequency case there could be a substantial oblique wave component at some known angle. If the two-dimensional and oblique waves set up respective two-dimensional and oblique TS waves, and if the initial TS wave amplitudes are proportional to the strength of their respective acoustic exciters, then the measured growth rates at the lower Reynolds numbers should be perceptively different in the two test runs. A nicer experiment would be one in a tunnel with a moveable side wall. Frequency and mean flow conditions could be held constant, and by moving the wall in and out the tunnel's first mode could be cut off and on.

In this and in any stability experiment in which acoustic excitation is used, the boundary layer probe should not be held at one longitudinal station while the frequency is changed. This is obvious now, but the point bears emphasis. Clearly, the rms output of a stationary probe will show cyclic oscillations as the frequency (and hence wave number) of the acoustic field is allowed to change.

A final thought before leaving the amplitude section. The matching of the model amplitude to those of the data has been done here in a subjective manner, and this fact probably has been emphasized enough. But while the matching of model to data has generally been good, there always existed a suspicion in the writer's mind that the match was in fact quite poor and that the trend of the data was entirely missed. To show how such suspicions can arise, consider figure 19 (a). In this figure the TS wave has been modeled with a constant amplitude; $R_3 = u_3/u_1 = 0.9$. For Reynolds numbers of less than 950, one could perhaps be convinced that this modeling is just as valid as the one which was actually used. Consider the following argument. The data's first local minimum and maximum points are not matched well, but neither were they in the original model. The second data minimum has a good match. The second data maximum appears to have been truncated due to some experimental error, and except for the error the match would have been a good one also. The third data minimum has a truncation problem as well. The rest of the data is matched well

except for the fifth minimum, and this minimum has obviously undergone an erroneous truncation. This plausible model gives a low-Reynolds number TS wave growth rate of zero! Quite a different trend from the original modeling result. What is to be done? Fortunately the corresponding phase angle data are also available for comparison and this is done in figure 21 (b). The resulting phase angles do not match the data well at all. At the smaller distances the amplitude of the phase angle oscillations is much too large. This shows that the $R_3 = 0.9$ modeled TS wave amplitudes at the smaller Reynolds numbers are in fact too big. This exercise did allay some fears. (But what about that first data minimum and those truncations and that 180^o phase shift?)

Phase velocity and wave number results. - A comparison of the nondimensional phase velocities derived from the model with theoretical values are shown in figure 20. For convenience, the variation with Reynolds number is shown in figure part (a) and with distance in part (b). The phase velocity representation by piecewise continuous first degree polynomials is clearly evident in part (a). For $x \leq 14$ cm, a double values result is given, and this was due, as explained earlier, to the difficulty in modeling the velocities in this region. For $x \geq 17$, the modeled speeds are within 2% of the theoretical speeds for two-dimensional TS waves. This is striking evidence that the principal phenomenon modeled was TS wave propagation. The theoretical results from reference 26 were obtained by interpolating with a cubic spline the tabulated values in tables which contained results near the nondimensional frequency of 5.6×10^{-5}. These values were then plotted in figure 20 using a cubic spline interpolation. The wave number results shown in figure 21 reflect the phase velocity findings since the wave number involves the reciprocal of the phase velocity. The difference between the flat plate theory and the experimentally derived results for the lower Reynolds number region, $Re_{\delta^*} < 980$ and $x < 17$ cm, will be ascribed to the influence of the adverse pressure gradient. Adverse pressure gradients cause an increase in the laminar boundary layer displacement thickness (see, for example, Table 5.1 of reference 46 for formulas appropriate for Falkner-Skan flows). From the stability diagrams shown by Obremski, Morkovin, and Landahl (ref. 21) for adverse pressure gradient flows, it can be seen that increasing δ^* above the flat plate values will increase the phase speed of a given frequency disturbance in the unstable region.

CONCLUDING REMARKS

The primary purpose of the present study is the reevaluation of the hot-wire anemometer amplitude data contained in the 1977 subsonic flat plate acoustic boundary layer instability investigation report of P. J. Shapiro entitled, "The Influence of Sound Upon Laminar Boundary Layer Instability." As shown here, the low-Reynolds number boundary layer disturbance data were misinterpreted and the present effort was made to improve the corresponding disturbance growth rate curves. The data show a standing wave pattern along the plate and it is known that this can be satisfactorily explained as being due to the superposition of the free-stream sound waves and the laminar boundary layer instability Tollmien-Schlichting (TS) waves. To extract the TS wave amplitude and phase velocity information the data were modeled as the sum of acoustic waves and a wave representing the TS wave. Using the free-stream disturbance data, the sound field was modeled by a primary downstream traveling sound wave, a weak reflected upstream traveling wave, and nonpropagating "noise" terms representing possible decaying evanescent sound fields at each end of the test section. The amplitude and phase velocity of the TS wave were then adjusted so that the total signal reasonably matched the amplitude and phase angle from hot-wire data along the laminar boundary layer on the plate.

Except for the region upstream of the rapid increase in boundary layer disturbance growth, the resulting phase velocity variation of the third wave was within 2% of the theoretical two-dimensional TS phase speed, thus showing that the third wave indeed represented a TS wave. In the upstream region the speeds were about 10% higher than the flat plate values, but the increase is qualitatively consistent with the adverse pressure gradient existing in this region. The TS wave amplitude at the earliest measurement station was 0.25 times the sound field amplitude near the leading edge. Shapiro's TS growth rate curves showed growth ahead of the theoretical flat plate stability neutral point, and the revised rates show growth occurring even further upstream. It appears that the premature growth is due to the adverse pressure gradient created by the shape of the plate. One of the purposes of Shapiro's investigation was to determine if the sound could be affecting TS wave growth along the plate, but the pressure gradient has prevented such a determination. Comparison of the measured pressure distribution with published theoretical distributions for plate leading edge shapes similar to Shapiro's shows considerable disagreement. Obviously, it would be desirable to reduce the pressure gradients in future experiments.

Acoustic excitation experiments are important to the boundary layer transition problem because sound pervades the aircraft and wind tunnel flow environment. But these experiments are difficult ones to satisfactorily conduct because of the problem of establishing a controlled acoustic field. Some of the basic elements of sound propagation in ducts have been reviewed in the present report. Sound field measurements are an important part of tunnel experiments which are affected by sound. Shapiro's test section sound measurements may have been taken with the flat plate removed. Since the presence of the plate would be expected to alter the field somewhat, the modeled sound field may not have been the most appropriate. However, the resulting error introduced in the modeled TS wave amplitude would probably be small.

Some of the experimental and theoretical acoustic-stability literature was

reviewed in the report. There seems to be a growing consensus that the acoustic-boundary layer interaction in the leading edge region is the source of the TS waves, at least for two-dimensional flows, and that away from the leading edge there is no significant interaction between the sound and TS waves. Additional experiments along the line of Shapiro's are needed for experimental verification of the latter contention. Finite amplitude TS wave behavior in two-dimensional flow can now be studied numerically. But since all wind tunnel model flat plates have leading edge regions with pressure gradients, it will be difficult to obtain meaningful comparisons between theoretical and experimental TS wave amplitudes unless some assessment of the gradient effect is made.

APPENDIX

ELEMENTS OF SOUND PROPAGATION IN DUCTS

In duct acoustics one deals with wave propagation inside enclosures which have changing dimensions and directions, and often, as in the present case, contain flow. In constant area ducts there is attenuation of the sound field, with most of the energy losses usually occurring at the walls due to absorption during reflections. Even if the walls are quite rigid, viscous losses occur in the so-called acoustic boundary layer which results from the no-slip condition at the surface. Abrupt changes in the duct cross-sectional area produce reflections and hence alters the transmitted energy along the duct. With gradual contractions or enlargements the sound energy can be concentrated or diffused and thus amplification as well as attenuation of sound levels can occur. If temperature gradients are present the sound field is altered by refraction effects. Likewise, if a flow field exists the velocity gradients can produce refraction effects. If the duct contains a nozzle and if appreciable changes in velocity occur, this change and the attendant changes in density and temperature can appreciably affect the sound field. At the higher speeds the wall turbulent boundary layer itself can significantly add to the noise level. Clearly, duct acoustics challenges both the theoretician and the noise controller. With the interest in noise abatement, it is no wonder that the literature is extensive.

The basic discussion topics will be restricted to those relevant to the test section which Shapiro used. The tunnel was at the Massachusetts Institute of Technology, and the facility will herein be referred to as the MIT tunnel. The test section had straight walls, was open at the downstream end, and had a low flow velocity ($M \sim 0.08$). From modeling, analysis, and discussion viewpoints, these are convenient features. Rigid walls were originally used, but the resulting sound field had unacceptably large spatial variations. The nonuniformity was reduced by lining the walls with an acoustically absorbent material. The relevant discussion topics will therefore be: plane progressive waves, standing waves, reflections from an open-ended duct, traveling waves undergoing side-wall reflections (transverse modes), attenuations, and the effects of flow. The last two subjects, attenuation and flow effects, are so complex that they will necessarily be discussed in a more qualitative fashion.

Plane Progressive Waves

Plane waves are generated in practice by two means. The first is by using a sound source and working in its so-called far-field region. At large distances from a source the waves are essentially spherical waves, but if the working region is small the amplitude decay with distance due to spherical spreading can be neglected and the waves can be considered locally as plane waves. This method was mentioned earlier in connection with placing a loudspeaker well upstream of the test section. The second method consists of placing the source in a rigid tube and generating waves in the frequency range where the wavelength is long in comparison with the tube diameter. It will be shown later that only the plane wave mode can be sustained in such a case.

For the case of a medium with no flow, one form of the plane wave equation is

$$\frac{\partial^2 \varepsilon}{\partial t^2} = c^2 \frac{\partial^2 \varepsilon}{\partial x^2}$$

where ε is the particle displacement from equilibrium position along the x-axis and x is the equilibrium coordinate of a particle of the medium. Similar equations exist for other acoustic variables (ref. 31, p. 113) such as particle velocity u, acoustic or excess pressure p ($p = P-P_o$, where P is the instantaneous pressure and P_o the equilibrium pressure in the medium), condensation σ (the fractional change in density defined by $\sigma = (\rho-\rho_o)/\rho_o$), and velocity potential (defined such that the particle velocity is the negative of the gradient of the velocity potential). Once the solution for ε has been obtained, the behavior of the other acoustic variables can be obtained from

$$p = -\rho_o c^2 \frac{\partial \varepsilon}{\partial x} \quad , \quad u = \frac{\partial \varepsilon}{\partial t} \quad , \quad \sigma = -\frac{\partial \varepsilon}{\partial x} \tag{15}$$

The most general solution of the wave equation is (d'Alembert's solution)

$$\varepsilon = f_1(x-ct) + f_2(x+ct)$$

where f_1 and f_2 are completely arbitrary functions of the arguments $(x-ct)$ and $(x+ct)$ and represent independent traveling waves moving with speed c in the positive and negative directions, respectively. The sinusoidal wave is a particular solution of the wave equation and is, of course, of special importance. Sources of many waves vibrate periodically, but the primary importance of the sinusoidal function in wave theory is that they are the simplest of periodic functions and all functions which occur in practice can be represented by Fourier's theorem as a sum or integral of sinusoidal functions.

For a plane progressive sinusoidal wave in an infinite medium with no reflections, the complex particle displacement is

$$\hat{\varepsilon} = \hat{A}\, e^{i(kx-\omega t)}$$

where the initial phase angle has been absorbed by the complex amplitude $\hat{A}$, i.e., $\hat{A} = A\, e^{i\phi}$. The other acoustic variables are, using eq. 15,

$$\hat{p} = -i\rho_o\, c\, \omega\, \hat{\varepsilon} \tag{16}$$

$$\hat{u} = -i\, \omega\, \hat{\varepsilon} \tag{17}$$

$$\hat{\sigma} = -i\, k\, \hat{\varepsilon}$$

Because the density term in the formulas to be used will always mean the equilibrium density, henceforth the subscript on density will be omitted. For plane waves traveling in the positive x direction the acoustic pressure, particle velocity, and condensation are in phase with each other and differ from the displacement by 90^o of phase angle. From equations (16) and (17) it is seen that for plane progressive waves

$$\hat{p} = \rho\, c\, \hat{u} \tag{18}$$

and hence the rms value of the fluctuating pressure is proportional to that of the fluctuating velocity. For the plane progressive wave situation, equation (18) allows both pressures and velocities to be determined from measurements using either microphones or hot-wire anemometers.

Standing Waves

In the more general one-dimensional case boundaries are present and wave reflections occur. With a reflecting surface present the solution of the plane wave equation consists of the sum of incident and reflected waves. The solution in complex form is thus

$$\hat{\varepsilon} = \hat{A}\, e^{i(kx-\omega t)} + \hat{B}\, e^{-i(kx+\omega t)}$$

Letting

$$\hat{\varepsilon}_+ = \hat{A}\, e^{i(kx-\omega t)}$$

and

$$\hat{\varepsilon}_- = \hat{B}\, e^{-i(kx+\omega t)}$$

denote the progressive waves traveling in the positive and negative directions, respectively, then

$$\hat{\varepsilon} = \hat{\varepsilon}_+ + \hat{\varepsilon}_-$$

and the other important acoustic variables are

$$\hat{p} = -i\rho c\omega\, (\hat{\varepsilon}_+ - \hat{\varepsilon}_-)$$

$$\hat{u} = -i\omega\, (\hat{\varepsilon}_+ + \hat{\varepsilon}_-)$$

$$\hat{v} = -ik\, (\hat{\varepsilon}_+ - \hat{\varepsilon}_-)$$

Of particular interest here are the rms values of the acoustic pressure and particle velocity. The rms value of a wave signal of the form $\hat{s} = \hat{A}\, e^{i(kx-\omega t)}$ is the square root of the average of the real part of the expression squared, and it is easy to show that this value is simply $\sqrt{\tfrac{1}{2}\,\hat{s}\,\hat{s}^*}$, where the asterisk denotes the complex conjugate (i.e., the value of $\hat{s}$ with i replaced by $-i$). Using the fact that the conjugate of a sum or product of two values is the sum or product of the conjugate of the values, the rms values of the acoustic, pressure and particle velocity are quickly found to be

$$\tilde{p} = \rho c\omega A \sqrt{\tfrac{1}{2}[1+R^2-2R\cos(2kx+\phi_A-\phi_B)]} \qquad (19)$$

$$\tilde{u} = \omega A \sqrt{\tfrac{1}{2}[1+R^2+2R\cos(2kx+\phi_A-\phi_B)]} \qquad (20)$$

where $R = B/A$ and use has been made of the identity $2\cos\theta = e^{i\theta} + e^{-i\theta}$. Equations (19) and (20) show that the rms values of the fluctuating pressures and velocities vary cyclically with a wavelength which is half that of the component waves. Furthermore, since $\cos(\theta+\pi) = -\cos\theta$, equation (20) may be written as

$$\hat{u} = \omega A \sqrt{\tfrac{1}{2}[1+R^2-2R\cos(2kx+\phi_A-\phi_B+\pi)]} \qquad (21)$$

and comparison of equations (19) and (21) reveals that $\tilde{p}$ and $\tilde{u}$ are 180^{o} out of phase. Hence at a location where the acoustic pressure is a maximum the fluctuating velocity is a minimum, and vice versa. Measurements at more than one station are needed to show the presence of a standing wave, and thus, in contrast to the progressive wave case, it is not possible to determine both fluctuating pressures and velocities with a single measurement using a microphone or hot-wire anemometer. The plane wave assumption is often made in acoustic measurements, and justifiably so, but the plane wave relation $\tilde{p} = \rho c \tilde{u}$ is strictly valid for progressive waves. Inside enclosures standing waves are usually present, and the plane wave pressure-velocity relation must be used with caution (it is not unusual to see the relation used with no apparent regard for the standing wave problem). An appropriate example for stability and transition researchers of the difference in behavior of $\tilde{p}$ and $\tilde{u}$ when a standing wave is present may be found in the classic stability investigation of Schubauer and Skramstad (ref. 1). They made acoustic measurements along the test section centerline using a conventional microphone and a ribbon microphone. The latter responds to velocity fluctuations, and their data show a single large maximum in acoustic pressure occurring at the location where the fluctuating velocity is a minimum. They interpreted this result as showing the presence of a low-frequency standing acoustic wave in the test section.

Reflections From An Open-Ended Duct

The strength of a reflected plane wave depends upon the nature of the reflecting medium and the amplitude, frequency, and angle of incidence of the incident wave. In the present section interest is focused on plane waves normally incident upon a reflecting medium, and because the test section in Shapiro's experiment was open ended, the real concern is with waves reflected from the open end of a duct. This is a complicated problem but solutions do exist.

In analyzing reflections, acousticians frequently work with quantities called impedances. Different impedances have been defined for different purposes, and the terminology is not quite standard. In a general sense, impedance is ratio of the force, due to acoustic pressures, to the particle velocity. When working with electro-mechanical radiation devices, the interest is often in the acoustic forces on the device, and the ratio of the force to velocity is termed the mechanical or radiation impedance $\hat{Z}_r$. The specific acoustic impedance, $\hat{z}$, is defined as the ratio of acoustic pressure to particle velocity. It can be considered specific impedance because it is the force-to-velocity ratio per unit area. The acoustic impedance $\hat{Z}$ is defined as the ratio of acoustic pressure to volume velocity, where, for a duct with cross-sectional area S, the volume velocity $\hat{V}$ is $\hat{u}\,S$. The acoustic impedance is thus the specific acoustic impedance divided by the area. The terminology is confusing, for one might expect the specific acoustic impedance to be the acoustic impedance per unit area, but it is just the opposite; acoustic impedance is the specific acoustic impedance per unit area. The relationship among the quantities is $\hat{Z}_r = \hat{z}S = \hat{Z}S^2$. The term impedance arises from the analogy of volume velocity to electric current and acoustic pressure or force to voltage, and of course the ratio of voltage to current is called the impedance (the reciprocal of impedance, admittance, is also used in acoustic work). As may be seen from eqs. (16) and (17) the specific acoustic impedance, $\hat{p}/\hat{u}$, of a plane progressive wave is ρc, a real quantity. The product ρc occurs so frequently that it has been given the name of characteristic impedance, a quantity which is characteristic

of the medium and independent of acoustic wave type or condition. So many impedances certainly provide an impediment. Impedance is intuitively an appealing quantity in reflection analyses, for generally, the greater the difference in impedance at a reflection boundary, the greater the intensity of the reflected wave (after all, no reflected wave would be expected at a junction if there were no change in resistance or impedance across it). At reflecting surfaces the pressure and volume velocity are continuous and therefore so is the acoustic impedance. The continuity of acoustic impedance provides the boundary condition which allows the transmissions and reflections to be analyzed.

Consider next what happens at a junction where the acoustic impedance changes. A plane wave is assumed to be normally incident at the junction. A reflected wave occurs and for the analysis let the incident and reflected plane waves be represented, respectively, by

$$\hat{p}_i = \hat{A}\, e^{i(kx-\omega t)}$$

$$\hat{p}_r = \hat{B}\, e^{-i(kx+\omega t)}$$

These equations are appropriate because frequency is conserved in the interaction. For plane progressive waves the particle velocity is $\hat{p}/\rho c$ and for a duct of cross-sectional area S, the volume velocity, $\hat{V}$, is $S\,\hat{p}/\rho c$. The volume velocities of the incident and reflected waves are therefore

$$\hat{V}_i = \frac{\hat{p}_i}{\rho c/S}$$

$$\hat{V}_r = \frac{-\hat{p}_r}{\rho c/S}$$

where, for the reflected wave, the particle velocity is negative for a positive pressure.

From the definition, the expression for the acoustic impedance is

$$\hat{Z} = \frac{\hat{p}_i + \hat{p}_r}{\hat{V}_i + \hat{V}_r}$$

It is clear from the preceding study of two standing waves that $\hat{Z}$ will vary from point to point. In terms of pressure, $\hat{Z}$ becomes

$$\hat{Z} = \frac{\rho c}{S}\,\frac{\hat{p}_i + \hat{p}_r}{\hat{p}_i - \hat{p}_r}$$

or

$$\hat{Z} = \frac{\rho c}{S}\,\frac{\hat{A}\, e^{ikx} + \hat{B}\, e^{-ikx}}{\hat{A}\, e^{ikx} - \hat{B}\, e^{-ikx}}$$

Without loss of generality, the origin of the coordinate system may be located where the change in impedance occurs. Denote the acoustic impedance

here by $\hat{Z}_o$, and at $x = 0$,

$$\hat{Z}_o = \frac{\rho c}{S} \frac{\hat{A} + \hat{B}}{\hat{A} - \hat{B}}$$

which gives

$$\frac{\hat{B}}{\hat{A}} = \frac{\hat{Z}_o - \frac{\rho c}{S}}{\hat{Z}_o + \frac{\rho c}{S}} \tag{22}$$

Equation (22) will be applied to the open-end duct problem, but before doing this it is instructive to apply it to two typical examples. Consider first the case of a constant area duct in which the impedance change is due to a fluid change (e.g., air and water in a vertical duct). In addition to the reflected wave there is a transmitted wave. In the transmitting medium only the transmitted wave is present and hence the acoustic impedance is that for a plane progressive wave. It should be pointed out that while $\rho c/S$ in equation (22) is the acoustic impedance of a plane progressive wave, it is not the acoustic impedance in the medium where the incident and reflected waves propagate precisely because there are two waves present. Using subscripts 1 and 2 to denote, respectively, the properties in the incident and transmitting media, equation (22) shows that

$$\frac{\hat{B}}{\hat{A}} = \frac{\rho_2 c_2 - \rho_1 c_1}{\rho_2 c_2 + \rho_1 c_1} \tag{23}$$

Equation (23) shows that $\hat{B}/\hat{A}$ depends only on the characteristic impedances of the two fluids. If $\rho_2 c_2 >> \rho_1 c_1$, $\hat{B}/\hat{A} = 1$ and thus the amplitude of the reflected waves equal that of the incident wave and there is no phase angle change. When the characteristic impedances match there is no reflected wave. When $\rho_2 c_2 << \rho_1 c_1$, the wave amplitude ratio becomes $\hat{B}/\hat{A} = -1 = 1\, e^{i\pi}$, and it is seen that the amplitudes of the two waves are again equal but there is a 180^o phase angle difference.

For the second example, consider the case of a single fluid in a pipe which has an abrupt area change. In this situation equation (22) gives, with $\hat{Z}_o = \rho c/S_2$,

$$\frac{\hat{B}}{\hat{A}} = \frac{S_1 - S_2}{S_1 + S_2} \tag{24}$$

If $S_1 = S_2$ there is, of course, no reflected wave. If $S_1 >> S_2$, the case of a pipe almost completely capped, the expected result occurs, namely, $\hat{B}/\hat{A} = 1$. If $S_1 << S_2$, $\hat{B}/\hat{A} = -1$ and again the equal amplitude 180^o phase shift situation exists. The $S_1 << S_2$ situation is equivalent to an open-end condition, and this is essentially the condition of Shapiro's test section. This result states that the wave is totally reflected and that no energy leaves the end of the duct. This result is essentially valid only for the low-frequency case when the wavelength of the incident wave is much greater than the diameters or perimeters of the ducts involved. Some textbooks do not make this clear. It has been assumed here that the plane waves remain as plane waves at the

location where the acoustic impedance change occurs, and this is a valid assumption for the long wavelength case. When the wavelength is comparable to the duct cross section dimensions, diffraction effects occur; the wavefronts become distorted and the acoustic pressure is not uniform across the duct. The inadequacy of the preceding results for high frequencies is rather dramatic. For the case of wavelengths which are small in comparison to the duct diameter, the method of geometric or ray acoustics is appropriate. In this method signals are considered to propagate along ray paths and the wave strengths are determined from energy conservation along ray tubes. If there are no mean density gradients or physical obstructions, the ray paths are straight lines. Thus, for very high frequencies and $S_2 >> S_1$ (or just $S_2 > S_1$), all ray paths lead directly into the second medium and there is no change in the ray tubes. The effective area of the wave remains at S_1 and there is no change in wave strength and no reflected waves are generated. This result is just opposite of the previous conclusion concerning this case (i.e., for $S_2 >> S_1$ no energy leaves, all is reflected). So again, equations (23) and $(24)^2$ are appropriate for the case where the wavelength is much greater than the duct diameter.

Equation (22), however, is still of use if an appropriate acoustic impedance for an open duct can be determined. This is accomplished by adopting the solution from a classical problem in acoustics, the radiation of sound from a piston in an infinite baffle (i.e., from a piston moving in and out of a wall or a flanged pipe). The radiation impedance is known for such a case, and this result can be used here because in an open-ended duct the air at the open end may be considered, for long wavelengths, to be a piston of zero mass, radiating some of the energy into the open and reflecting some back. The long wavelength condition is involved because for this case the air does retain plane wave motion with a uniform pressure distribution, and the piston calculations show that for long wavelengths the pressure on the face of the piston is uniform and that the piston area radiates as a whole (ref. 47, pp. 386-387). For a short wavelength case, as will be shown shortly, the piston results do agree with what would be expected from geometric acoustics. Thus for the short and long wavelength conditions the piston model is an appropriate one; for intermediate wavelengths the situation is less clear, but the model is probably not a bad one.

One of the approaches to solving the piston problem is to replace the piston area with an array of simple sources, where the sources are considered to represent differential areas of the piston surface. A monopole is a pulsating sphere, and a simple source is monopole whose radius is small compared with the pulsating signal wavelength. The sources are assumed to oscillate in phase and with the same frequency with which the piston would vibrate. The acoustic pressure at any point in the medium is the superposition of the acoustic pressures from all of the simple sources. The problem thus becomes one of evaluating an integral. The signals from the sources are spherical waves. (Spherical waves have not been discussed here, but they usually are the subject of a chapter in most acoustic textbooks).

The resulting superposition or interference pattern shows that at low frequencies (wavelengths considerably greater than the piston radius) the acoustic pressure is uniform in all directions in front of the piston. At higher frequencies cancellations and reinforcements produce an acoustic pressure field which is more intense along the axis of the piston. At very high frequencies nearly all of the energy is beamed in the axial direction, a result consistent with ray acoustics. When the acqustic pressures on the face of the

piston are integrated to determine the net force on the piston, the result is

$$\hat{F} = \rho c\, S\, V_o\, e^{i\omega t} \left[1 - \frac{2J_1(2kr)}{2kr} + i\, \frac{2K_1(2kr)}{2kr} \right]$$

where V_o is the amplitude of the piston velocity, r is the radius of the piston, S the area, and J_1 and K_1 are Bessel functions of the first and second kind, respectively. The radiation impedance, the ratio of force to velocity, is

$$\hat{Z}_r = \rho\, c\, S \left[1 - \frac{2J_1(2kr)}{2kr} + i\, \frac{2K_1(2kr)}{2kr} \right] \tag{25}$$

This result holds for circular ducts and rectangular ducts if the sides are nearly equal in length (see ref. 47, p. 384 and 393). Recalling that the acoustic impedance is $\hat{Z}_r/S^2$, one can thus obtain from equation (25) the value of the acoustic impedance which we can substitute into equation (22); namely;

$$\hat{Z}_o = \frac{\rho c}{S} \left[1 - \frac{2J_1(2kr)}{2kr} + i\, \frac{2K_1(2kr)}{2kr} \right] \tag{26}$$

The real and imaginary terms in the brackets are sometimes called, respectively, the radiation resistance, R, and radiation reactance, X, and are tabulated in some texts (e.g., ref. 31, table IV and ref. 47, table IX). Substituting equation (26) into (22) gives the desired result for an open tube

$$\frac{\hat{B}}{\hat{A}} = \frac{R_r(2kr)-1 + iX_r(2kr)}{R_r(2kr)+1 + iX_r(2kr)}$$

The magnitude and phase angle of $\hat{B}/\hat{A}$ are therefore

$$\frac{B}{A} = \sqrt{\frac{(R_r-1)^2 + X_r^2}{(R_r+1)^2 + X_r^2}} \tag{27}$$

and

$$\phi = \tan^{-1} \frac{2X_r}{R_r^2 - 1 + X_r^2} \tag{28}$$

The present author has found that B/A is described within $\pm$ .04 by

$$\frac{B}{A} = \begin{cases} 1 & 0 \le w < 0.3 \\ e^{-\frac{w-0.3}{2.7}} & 0.3 \le w < 9 \\ e^{-\frac{w}{4}} & 9 \le w \end{cases} \tag{29}$$

where $w = 2kr$. For large and small values of w, R_r and X_r behave as (ref. 31):

$$\begin{aligned} R_r(w) &\approx 1, \quad X_r(w) = \frac{4}{\pi w}\ ;\ w >> 1 \\ R_r(w) &\approx \frac{w^2}{8}, \quad X_r(w) = \frac{4w}{3\pi}\ ;\ w < 1 \end{aligned} \tag{30}$$

Substituting equations (30) into equations (27) and (28) shows that for the long wavelength case (small w) $B/A \to 1$ and $\phi \to 180^{\circ}$, and this corresponds to the result obtained from equation (24). For the short wavelength case $B/A \to 0$ and this corresponds to the geometric acoustic result. Kinsler and Frey (ref. 31, p. 183) show that the radiated power for the high frequency case is the same as the plane-wave power that would be radiated by piston into a tube of radius r. This is consistent with the idea that the ray paths emerge axially out of the tube with no change in ray-tube area.

The preceding results are for a duct or pipe whose open end is flush with a wall or has a large flange on the end. For an unflanged pipe there is an even greater impedance mismatch at the open end due to the larger solid angle of radiation; the radiated power is less and the amplitude of the reflected wave is greater. Some impedance curves for the unflanged case are presented by Morse and Ingard (ref. 47, p. 472). Kinsler and Frey (ref. 31, p. 200) state that for $2kr << 1$, both theory and experiment show that for the unflanged pipe

$$\hat{Z} = \frac{\rho c}{S} \left(\frac{k^2 r^2}{4} + 0.6\, ikr \right)$$

Transverse Modes

The discussion is now broadened to include waves which undergo reflections from the side walls as they propagate down a rigid-walled duct with rectangular cross section. The discussion will bring out the concepts of transverse modes and cutoff frequencies. Consider first the case of waves whose reflections involve only two walls, that is, waves whose wave normals lie in the x-y plane, where x is the distance along the length of the duct. Let h (the height) be the separation distance between the reflecting walls. The wave equation in this case is

$$\frac{\partial^2 p}{\partial x^2} + \frac{\partial^2 p}{\partial y^2} = \frac{1}{c^2} \frac{\partial^2 p}{\partial t^2} \tag{31}$$

The solution should represent a traveling wave in the x direction and, because of complete reflections at the rigid walls, a standing wave in the y direction. The solution is thus expressed as

$$\hat{p} = \hat{A}\, f(y)\, e^{i(k_x x - \omega t)} \tag{32}$$

The boundary condition on the acoustic pressure is that the gradient normal to a wall is zero. This condition comes from Euler's equation, which for small velocity fluctuations is

$$\rho \frac{\partial \vec{v}}{\partial t} + \nabla p = 0$$

where $\vec{v}$ is the velocity perturbation, and the fact that the normal component of velocity vanishes at the wall. Substituting eq. (32) into eq. (31) and applying the boundary conditions yields the solution to equation (31)

$$\hat{p} = \hat{B} \cos(k_y y)\, e^{i(k_x x - \omega t)} \tag{33}$$

where

$$k_y = \left[\left(\frac{\omega}{c} \right)^2 - k_x^2 \right]^{1/2} \tag{34}$$

and

$$k_y = \frac{n\pi}{h}, \quad n = 0, 1, 2, \ldots \tag{35}$$

This solution can be decomposed into two progressive plane waves

$$\hat{p} = \frac{\hat{B}}{2} \left[e^{i(k_x x - k_y y - \omega t)} + e^{i(k_x x + k_y y - \omega t)} \right] \tag{36}$$

Each of these waves represents a plane wave and the surfaces of equal phase are given by

$$k_x x \pm k_y y = \omega t$$

or

$$\frac{k_x}{k} x \pm \frac{k_y}{k} y = \frac{\omega}{k} t \tag{37}$$

where, from equation 34,

$$k = \frac{\omega}{c} = (k_x^2 + k_y^2)^{\frac{1}{2}}$$

The normal form for an equation of a plane with distance d from the origin is

$$n_x x + n_y y = d \tag{38}$$

where n_x and n_y are the direction cosines of the normal to the plane. Comparison of equations (37) and (38) shows that k_x/k and k_y/k are the direction cosines of the component progressive plane waves. The velocity of propagation of the surfaces of equal phase is obtained by differentiating the right-hand side of eqs. (37) and (38) with respect to time, giving

$$\frac{d(d)}{dt} = \frac{\omega}{k} = c$$

The velocity of the component progressive waves is the sound velocity, as one would expect. The angle of the direction of propagation of the wave normals with the y-axis is given by $\pm \cos^{-1} k_y/k$ and hence one term of eq. (36) may be considered as the incident wave and the other as the reflected wave. It should be noted that it is $\vec{k} = k_x \vec{i} + k_y \vec{j}$, not the wave velocity c, that is the mathematical quantity having a vector character which specifies the direction in which a wave is propagating.

Equation (35) is the characteristic equation of the duct. The various values of n defines the modes of the duct and the discrete y wave-number spectrum. Equations (33) and (35) show that the mode number, n, corresponds to the number of pressure nodal planes existing between the two reflecting walls. For $n = 0$ there are no nodes and this corresponds to the axial plane wave case. Besides the necessity of meeting the boundary conditions, the characteristic equation can also be considered to arise out of a wave interference condition. Since $k_y = k \cos\theta$, where θ is the angle of the wave normal from the y axis, eq. (35) may be written as

$$\cos\theta = \frac{n\pi}{hk} = \frac{n\lambda}{2h} \tag{39}$$

This shows that for a given free-space wave number k, only certain directions of propagation are possible and these depend on n. A physical significance of eq. (39) is that waves obeying this relationship constructively interfere with multiple reflections. Equation (39) is the condition that the path length of an element of a wavefront be an integral number of wavelengths, λ, after two reflections (thus giving constructive interference). This may be seen with the aid of figure 22. The figure shows a portion of a wavefront and a phase path from A to B involving two reflections. It can be shown that the path length is $2h\cos\theta$, and equating this to $n\lambda$ gives eq. (39). The characteristic equation is therefore, as one would expect, a coherence condition for multiple reflected wave fields.

From equations (34) and (35)

$$k_x = \pm \left[k^2 - \left(\frac{n\pi}{h}\right)^2\right]^{\frac{1}{2}}$$

For a particular non-axial mode, if $k < \frac{n\pi}{h}$ the value of k_x becomes imaginary and hence $\hat{p}$ becomes

$$\hat{p} = \hat{B} \cos\left(\frac{n\pi y}{h}\right) e^{\pm k_x x} e^{i\omega t}$$

This wave disturbance is no longer periodic in x but decreases exponentially. These waves, which quickly die out, are sometimes called evanescent waves. Such terms are needed to satisfy boundary conditions and it is near the boundaries of irregular regions that evanescent waves are found. For $k \geq n\pi/h$ the value of k_x is real and the disturbance is a true propagating sound field. In terms of frequency, the condition is $\omega \geq n\pi c/h$, and the cutoff frequency is defined as

$$\omega_c = \frac{n\pi c}{h}$$

For a given mode, the frequency must be greater than ω_c in order for that transverse mode to propagate. In terms of wavelength, the condition for a transverse mode is $\lambda < 2h/n$ and hence for $\lambda > 2h$, no sustaining oblique waves can exist. This is the basis for an earlier statement that one method of generating plane waves was to use a low-frequency source in a rigid tube. For the low-frequency case of $\lambda > 2h$, all oblique waves die out leaving only an axially propagating plane wave, the zeroth or fundamental mode. The fundamental mode can always propagate unattenuated, and the discussion below is for $n \geq 1$.

For a given mode, the angle of propagation of the sound waves for various frequencies can be expressed in terms of the cutoff frequency as

$$\theta = \cos^{-1}\frac{n\pi c}{\omega h} = \cos^{-1}\frac{\omega_c}{\omega} \tag{40}$$

As the frequency, ω, is increased from 0, no transverse modes are set up until

$\omega = \omega_c$ for the first mode. At $\omega = \omega_c = \pi c/h$, $\theta = 0$ and the situation is that of plane waves bouncing back and forth at normal incidence to the walls. As the frequency is increased the direction of propagation moves toward the axis of the duct as shown in figure 23. For all frequencies between the cutoff frequency of the first mode and that of the second mode, only first mode propagation can exist (the zeroth mode can always exist). At the cutoff frequency for the second mode, a transverse resonance can set in, and as ω increases the direction of propagation of the second mode waves become increasingly axial. As long as the frequency is less than the cutoff frequency for the third mode, only first and second mode sound waves propagate, and the maximum value of θ is limited to $\cos^{-1}(\omega_{c_1}/\omega_{c_3})$, where the subscripts c_1 and c_3 refer, respectively, to the first and third mode cutoff frequencies.

The phase velocity is the velocity of the phase pattern in a given direction. It is the velocity with which a point of intersection of the wave front with a given axis travels. Letting c_{ph} be the phase velocity in the direction of the channel,

$$c_{ph} = \frac{\omega}{k_x} = \frac{\omega}{k \sin\theta} = \frac{c}{\sin\theta}$$

and it is seen that the phase velocity varies from ∞ at the cutoff frequency (the wavefronts are parallel to the walls) to c at the high frequencies, where the wavefronts are nearly perpendicular to the duct axis. Thus, for frequencies below $\pi c/h$ only the fundamental mode propagates without attenuation and it propagates at speed c. As ω is increased above $\pi c/h$ the first higher mode also propagates with zero attenuation, though at a phase velocity higher than c. As ω is further increased successively higher modes can be transmitted along the duct, and the phase velocity of each decreases, coming closer to the constant value c of the fundamental mode.

The group velocity, $\vec{c}_g$, is the velocity in which energy is transported and is determined from

$$c_{g_j} = \frac{\partial\omega}{\partial k_j}$$

In the present case, the energy transport is in the x direction and its velocity is given by

$$c_{g_x} = \frac{\partial\omega}{\partial k_x} = k_x \frac{c^2}{\omega} = c \sin\theta$$

Thus, c_{g_x} is zero at a cutoff frequency, an expected result since the wave paths are normal to the walls, and there is no energy flux in the x direction, and $c_{g_x} \approx c$ at the higher velocities where the wave paths are nearly axial.

The preceding results can be generalized to the case where all four walls of the duct are involved in the reflection process. The solution to the three-dimensional wave equation becomes

$$\hat{p} = \hat{B} \cos(k_y y) \cos(k_z z) e^{i(k_x x - \omega t)}$$

and there are now two characteristic equations

$$k_y = \frac{n\pi}{h} \qquad n = 0, 1, 2, \ldots$$

$$k_z = \frac{m\pi}{w} \qquad m = 0, 1, 2, \ldots$$

where w is the width of the duct, that is, the wall separation distance in the z direction. Furthermore,

$$k_x = \left[\left(\frac{\omega}{c}\right)^2 - (k_z^2 + k_y^2)\right]^{\frac{1}{2}}$$

or

$$k_x = \left[\left(\frac{\omega}{c}\right)^2 - \left(\frac{m\pi}{w}\right)^2 - \left(\frac{n\pi}{h}\right)^2\right]^{\frac{1}{2}} \tag{41}$$

k_x will be real only when

$$\frac{\omega^2}{c^2} \geq \left(\frac{m\pi}{w}\right)^2 + \left(\frac{n\pi}{h}\right)^2$$

and hence the cutoff frequency is given by

$$\omega_c = c\pi \left[\left(\frac{m}{w}\right)^2 + \left(\frac{n}{h}\right)^2\right]^{\frac{1}{2}} \tag{42}$$

As expected, the cutoff frequency depends on the dimensions h, w of the duct cross section and on the indices m, n of the particular mode. There are n nodal surfaces (where p is zero) parallel to the y walls and m parallel to the z walls. The previous discussion concerning wave angles and phase speeds is relevant and can be generalized (e.g., the angle of incidence is

$$\cos^{-1} \frac{\pi c}{w} \left[\left(\frac{m}{w}\right)^2 + \left(\frac{n}{h}\right)^2\right]^{\frac{1}{2}}$$

The solutions are orthogonal and complete and hence any arbitrary wave can be represented by a unique superposition of these solutions. Near locations where the boundary conditions change, evanescent waves can be expected to exist and be an important part of the solution, but away from these regions only the unattenuated wave modes remain significant.

If the sound source in a duct with rigid walls is a rigid piston oscillating with frequency ω, then only the fundamental mode is excited (plane waves propagating axially). If the piston is not perfectly rigid and the oscillation velocity is a function of y and z, some of the higher modes at this frequency will be excited.

For a simple source (a pulsating sphere) in a rigid duct the sound field is of course modified because the radiated energy is channeled along the duct instead of radiating in all directions. For high frequencies and for positions close to the source, the behavior of the sound field is similar to that in free space. For wavelengths of the same size as the duct, the radiated pressure

is appreciably different from the free-space conditions, even in regions close to the source. As in the case of the piston source, the solution is expressed in terms of the duct modes and the y, z location of the source. The radiation resistance (the real part, the term responsible for radiated power, of the radiation impedance) of the source depends upon the frequency and its proximity to a cutoff frequency. In a rectangular duct the calculations (ref. 47) show that as the frequency increases past a cutoff frequency the resistance takes a sudden jump and then follows a subsequent and slower decay. The minima which each decay reaches before reaching the next cutoff (more appropriately, cut-on) frequency increase with increasing frequency inasmuch as the steps get closer together. At the higher frequencies the averaged values approaches the resistance behavior of a simple source in free space, a quantity which varies as the square of the frequency.

The previous discussion concerning reflections from open and closed ends of ducts and from locations where abrupt area changes occurred was restricted to the fundamental mode. The reflection of transverse modes from such boundaries is a complicated process because the reflected and transmitted waves may contain modes other than those of the incident ones. If the duct is semi-infinite and terminated at $x=0$ with a plane wall of uniform acoustic impedance, the modes will not mix on reflection; if an nth mode wave is sent from $-\infty$, an nth mode wave will be reflected back (ref. 47, p. 523). But if the impedance is a function of position on the wall, or if there is some other nonuniform obstruction at $x = 0$, a single mode sent from $-\infty$ will be reflected as several modes. The problem of reflections of transverse modes from the open end of a duct does not appear to have been examined in textbooks. One is thus bereft of guidance on this particular problem. The textbook of Morse and Ingard (ref. 47) may be consulted for information on other types of reflections of transverse modes.

Other Standing Waves

Equations (19) and (20) describe the rms values of the acoustic pressure and velocity in a standing wave produced by two progressive plane waves of the same frequency traveling in the opposite direction. The equations are obviously applicable to the standing wave along the axis of a duct produced by a fundamental mode wave and its reflection. The wave numbers in this case are equal in magnitude and opposite in sign. The interest here is in a generalization of these equations. With the transverse waves, standing waves in the transverse directions are set up due to the fact that waves of the same frequency have wave number components of the opposite sign in the transverse directions. It is important to note that if transverse modes propagate in both the upstream and downstream directions, then, like the fundamental mode case, standing wave patterns are created along the duct. As discussed at the beginning of the report, it is not necessary for waves to travel in opposite directions to produce standing waves. The necessary conditions for a standing wave pattern are that the constituent wave families have the same frequency and travel in nonorthogonal directions. If the waves travel in the same direction they must have different wave numbers, i.e., different phase speeds. The interest here is in the standing wave patterns set up along a duct by upstream and downstream traveling fundamental and transverse mode waves of a given frequency. For a given frequency, eq. (41) shows that the wave number component in the x direction, k_x, depends on the modal numbers and that, in general, each mode has its own value of k_x. Because of the differing wave numbers, each pair of modes, including downstream-downstream pairs and downstream-upstream pairs, may be considered to set up standing waves along the duct. Of course the

amplitudes of these standing waves would depend on the amplitudes of the individual modes involved and on the y, z coordinates (e.g., there would be no standing wave along a mode's nodal plane). The results also depend upon which acoustic variable is being considered. Since pressure is a scalar quantity and velocity is vectorial, the standing wave patterns for each will differ. Thus microphones and hot-wire anemometers will not show identical patterns.

Later there will be a need for an expression giving the wavelength of the standing waves. This is easily obtained. Suppose a signal $\hat{s}$ is composed of two traveling waves, with

$$\hat{s} = A\, e^{i(\alpha x - \omega t + \phi_A)} + B\, e^{i(\beta x + \omega t + \phi_B)}$$

The rms value of the signal is $\tilde{s} = \sqrt{\tfrac{1}{2}\, \hat{s}\, \hat{s}^*}$, and hence, with $R = B/A$ and $\Delta\phi_{AB} = \phi_A - \phi_B$,

$$\tilde{s} = A\sqrt{\tfrac{1}{2}\,(1 + R^2) + R\cos[(\alpha-\beta)x + \Delta\phi_{AB}]}$$

This equation is a slight generalization of eqs. (19) and (20). Since the wavelength is 2π divided by the wave number, the wavelength of the pattern is $\lambda = 2\pi/(\alpha-\beta)$. Letting $\alpha = k_{x_1}$ be the wave number component in the x direction for a downstream propagating mode, and $\beta = \pm k_{x_2}$ be the component for a different downstream (+) or an upstream (-) propagating mode, the wavelength becomes

$$\lambda = \begin{cases} \dfrac{2\pi}{k_{x_1} - k_{x_2}} & \text{waves traveling in same direction} \\ \dfrac{2\pi}{k_{x_1} + k_{x_2}} & \text{waves traveling in opposite directions} \end{cases} \qquad (43)$$

Obviously waves traveling in the opposite direction produce standing waves with shorter wave lengths. Again, the k_x's can be from either the oblique or fundamental modes; they need only be from fields of the same frequency. If the waves reflected from the open end of a duct are weak, then it is entirely possible that the strongest standing waves in the duct could be due to the waves traveling in the downstream direction.

Attenuation

The subject of attenuation is a difficult one, and, like the problem of the reflection of transverse modes, very little quantitative information will be presented. Up to this point, the sound waves have been considered to be with no losses and the reflecting walls have been considered as perfectly rigid. Sound is absorbed by air and of course losses occur at real reflecting surfaces. Losses in the medium may be divided into three basic types, viscous losses, heat conduction losses, and losses associated with molecular exchanges of energy. The viscous and heat conduction losses are often referred to as the classical types of sound absorption in fluids because they were analyzed in the

mid 1800's. The absorption of acoustic energy is associated with the fact that the pressure and density changes are truly not in phase, even for a plane progressive wave. Following Kinsler and Frey (ref. 31, p. 219), the time lag of the density change relative to the pressure change depend upon a characteristic or relaxation time required for (1) viscous stresses associated with relative fluid motion to tend to equalize the fluid velocities, (2) heat conduction to occur between high pressure (high temperature) and low pressure (low temperature) regions in the fluid, or (3) molecular energy changes among the different modes of internal energy (energies of molecular translation, rotation, and vibration) to occur. The phase lag between the pressure and condensation result in net work done on the fluid and a corresponding loss in acoustic energy. The attenuation coefficients for the classical forms of dissipation have been shown to be proportional to the square of the frequency. Molecular absorption in air is a maximum in the lower ultrasonic and audible frequency range, and is appreciably affected by the relative humidity. In air, it is likely that in most problems molecular attenuation will be the dominant mode of attenuation. In general, classical attenuation can be taken as a lower limit to the attenuation, and in non-dry air in the audible frequency range, molecular attenuation accounts for 90%-99% of the losses. Over the short distances involved inside wind tunnels, sound absorption in the free-stream can be neglected.

Even in the case of rigid walls there are losses at the walls in the acoustic boundary layer. The acoustic boundary layer, like the usual flow boundary layer, is the result of the no-slip condition at the wall and viscous effects. A number of authors (refs. 31, 40, 48 and 49) state that thickness of the acoustic boundary layer is given by $\sqrt{2\nu/\omega}$, where ν is the kinematic viscosity; Meyer and Neumann (ref. 48, p. 106) state that the velocity amplitude distribution is given by

$$\frac{\hat{u}(y)}{u_\infty} = 1 - e^{-y\sqrt{i\omega/\nu}}$$

where u_∞ is the particle velocity amplitude well outside of the boundary region. Taking the real part of this equation gives

$$\frac{u}{u_\infty} = 1 - e^{-y\sqrt{\omega/2\nu}} \cos y\sqrt{\omega/2\nu}$$

Although the result is for the case of no mean flow, for small amplitudes the relation also describes the perturbation introduced to the flow when the flow is present (ref. 4). The velocity fluctuation amplitude, unlike in the flow boundary layer, does not approach the free field conditions monotonically, but undergoes a damped oscillation. The wavelength of the oscillations is $2\pi\sqrt{2\nu/\omega}$, and the peak amplitude overshoots the far field amplitude by about 7% at $y \approx 2.4\sqrt{2\nu/\omega}$. u/U_∞ first reaches 0.995 at about $y \approx 1.55\sqrt{2\nu/\omega}$ and hence when comparisons are made with flow boundary layer thicknesses (where the thickness is sometimes taken to be the location whose u/U_∞ is 0.995) the acoustic boundary layer thickness should be taken as $\delta_a = 1.55\sqrt{2\nu/\omega}$. The losses that occur in the viscous boundary layer because of friction and heat conduction attenuate sound waves in ducts. It has been found (e.g., ref. 31, p. 241) that in tubes the attenuation constant, that is, the value of α in the amplitude decay $e^{-\alpha x}$, is proportional to $\sqrt{\omega/r}$, where r is the tube radius. This attenuation is usually important only in small tubes at high frequencies (e.g., the attenuation is only 0.2 dB/m for a 1 kHz sound field in a 5-cm radius tube - ref. 48, p. 111). For most wind tunnel situations the acoustic boundary layer losses would not be significant.

While the losses due to the acoustic boundary layer may be small, significant losses are likely to occur at the walls due to the fact the walls are not perfectly rigid and energy is transmitted into them. The reflection of sound waves from solid surfaces can be a rather complicated matter and there is no simple method of analysis available. Complications arise partly because solids have the ability to sustain shear stresses and therefore can propagate shear or transverse waves in addition to compression or longitudinal waves, and the internal elastic structure of various solids differ. In addition, many walls are built-up structures having laminations and cavities. Surfaces which are constructed to absorb sound energy are usually porous surfaces, and in these cases not only is there elastic compression of the solid but there is also fluid moving back and forth in the voids.

In unbounded solids there are only two types of sound waves which can be propagated: (1) Compressional, or longitudinal waves, in which particles move in the direction of propagation. These waves have the highest propagation speed. (2) Shear or transverse waves, in which the particles oscillate in the transverse direction. The speed of these waves is slower than the compression wave speed, and the ratio of the two speeds depends only on Poisson's ratio. In ducts it is often the case that the thickness of solid walls is small in comparison with the wavelength of the compression wave. In this situation the wall or plate can have a great many propagating waveforms (ref. 48). Extension waves are those having a symmetric mode in which particles on the upper and lower surfaces move in phase. The particle motion is predominantly longitudinal but an additional transverse component due to contraction of the transverse dimension will also be present (Poisson's ratio is thus important). The phase speeds can be much smaller than the compression wave speed in an unbounded medium. The speed depends on the wavelength as the wavelength approaches the thickness of the plate. Flexural waves propagate in an antisymmetric mode. The particle motion is predominantly transverse, but some longitudinal motion occurs due to rotation of the cross section about the transverse axis. The wave speed generally increases with frequency. Surface waves, called Rayleigh waves, can be propagated on the surface of solids whose dimensions are large in comparison with λ. The oscillations have longitudinal and transverse components and are restricted to a surface layer of about λ thickness. The speed is somewhat lower than the speed of shear waves. A plate acts in a fashion as a wave-guide. The extension and flexural waves may be considered as zeroth or fundamental mode propagation. As the product of frequency and plate thickness increases various symmetric and antisymmetric modes cut on. These propagate along the plate with phase speeds which, with increasing frequency-thickness product, approach that of the Rayleigh waves.

Sound in a porous material is damped by viscous motion. The acoustic properties of porous materials are characterized to a large extent by its flow resistance, a quantity which can be determined by a fluid flow experiment. Acoustic attenuation generally increases with flow resistance and decreases with increasing frequency (ref. 48).

Kinsler and Frey (ref. 31) divide the sound reflection process into three categories, depending on the waves transmitted into the solid. Thus, waves transmitted into solids may be: (1) refracted so that it propagates effectively at right angles to the surface, (2) refracted in a manner similar to a fluid-fluid boundary, and (3) refracted into longitudinal waves traveling in one direction and shear waves traveling at a lower velocity in a different direction. Type (1) refraction occurs for the so-called "normally reacting" or "locally acting" surfaces. In such materials the motion of various parts of the surface are not strongly coupled, and the motion normal to the surface

of one portion can be considered dependent only on the acoustic pressure incident on that portion and independent of the motion of any other part of the area. A honeycomb structure is an example of such a material (the velocity of compression waves through the fluid in the capillary pores oriented at right angles to the surface is much higher than that at right angles to this direction from pore to pore through the solid material of the structure). Many highly absorbing materials used in buildings appear to behave as locally reacting surfaces. Such interactions are rather easy to analyze because the waves are propagating normally into the surface. The interaction is completely characterized by the specific acoustic impedance, $\hat{z}_n/\rho_1 c_1$, where $\hat{z}_n = \hat{p}/\hat{u}_n$ and $\hat{u}_n$ is the normal component of the particle velocity at the surface and $\rho_1 c_1$ are properties of the fluid. Since the normal component of the particle velocity is involved, the angle of incidence, θ, also enters into the result. $\hat{z}_n$ may be frequency dependent and complex with $\hat{u}_n$ not in phase with the pressure; $\hat{z}_n = v_n + i\, x_m$. For most solids $v_n > \rho_1 c_1$ and one finds that there is some angle where the absorption is a maximum. For grazing incidence there is complete reflection. Often the angle of incidence for maximum absorption is closer to the grazing angle than normal incidence.

Type (2) reflection is typical of a sea water and sand bottom reflection since the saturated sand behaves more like a fluid than a solid in its inability to transmit shear waves. In these interactions the angle of incidence equals the angle of reflection and Snell's law holds. If $c_1 > c_2$ there is a critical angle (measured from the normal) beyond which no acoustic energy is transmitted into the second medium. Morse and Ingard (ref. 47) refer to this type reaction as one from a surface of extended reaction. In this situation the behavior of the surface at one point depends on the behavior at neighboring points. Instead of $\hat{z}_n$, the effective impedance of the surface is $z = \rho_2 c_2/\cos\theta_p$, where θ_p is the angle of penetration of wave in the second medium, which depends on the angle of incidence of the wave in the first medium (via Snell's law). Thus the degree to which the surface yield to the incident wave depends on the distribution of the incident wave; the surface is aware of the wave shape, so it is one of extended reaction.

Meyer and Neumann (ref. 48, p. 53) present a short discussion of the type (3), or elastic solid surface reflection. They discuss the case of a longitudinal wave propagating in a solid striking a solid-air boundary at oblique incidence. A transverse as well as a longitudinal wave are reflected, and therefore at the boundary a mode conversion takes place (the extent of the conversion depends on the angle of incidence and Poisson's ratio). There are incident angles for which complete mode conversion occurs. For a transverse mode reflecting at the interface, the degree of mode conversion depends upon the angle of incidence and Poisson's ratio and also the angle of the plane of polarization of the transverse wave. Morse and Ingard (ref. 47, chapt. 10) discuss the coupling of wave motion of plates and that of the surrounding medium.

Morse and Ingard have also examined some aspects of the problem of sound propagation in ducts with nonrigid walls. Their analysis was restricted to the case of locally reacting walls which were characterized by a specific acoustic admittance $\beta = \rho c/\hat{z} = \xi - i\sigma$, where, as before, the specific acoustic impedance is $\hat{p}/\hat{u}_n$ and $\hat{u}_n$ is the normal fluctuating velocity component. Thermal and viscous fluid effects could be included in an approximate manner by ascribing to the duct walls an additional specific admittance which varied with or depended upon the type of acoustic modal propagation in the duct. If the value of β due to the wall itself was not very small, then the additional admittances could usually be neglected, but if the walls were quite rigid, these

additional admittances could become the largest part of the effective wall admittance (but still negligible for the cases of interest here). If the impedance of the duct surface is purely reactive ($\xi = 0$), the phase velocities of all modes including the fundamental, are altered. In the rigid wall case only the oblique modes were dispersive (phase velocity in x direction depended upon frequency), and with nonrigid walls the fundamental mode is dispersive as well. If β has a real part as well, that is, if the conductance ξ is nonzero, then in addition to the phase velocity changes there is also an attenuation of all modes. This situation makes the distinction between no attenuation above cutoff frequencies and no transmission below it become less clear. If, however, $\xi<<1$, the attenuation above cutoff is slight and below cutoff is great.

A particular case of sound propagation in a duct was considered in which the walls perpendicular to the y axis had specific acoustic admittances which differed from the two walls perpendicular to the z axis. An approximate solution was obtained for the practical case in which the walls were rigid enough so that $|\beta|$ was small in comparison with the ratio between the wavelength of the sound in the duct and the perimeter of the duct. For the propagating modes, the attenuation factor was found to be the weighted mean $(\varepsilon_m \xi_y/h) + (\varepsilon_n \xi_z/w)$ of the specific conductances of the walls, divided by the sine of the angle of incidence, $\sin\theta_{mn} = \sqrt{1 - (m\pi/kw)^2 - (n\pi/kh)^2}$, where $\varepsilon_m = 1$ when $m = 0$ and $\varepsilon_m = 2$ when $m > 0$. Since $m = 0$ corresponds to the fundamental mode, it is seen that the attenuation effects are felt only half as much for this mode. For the other modes, except for those in which the waves travels parallel to one pair of walls and hence one of the ε's is 1, the numerator is the same. The denominator is a maximum, equaling 1, for the fundamental mode and therefore this mode is attenuated least. For the oblique modes the attenuation factor decreases with increasing frequency because of the denominator approaching one as the frequency increases, but because of the numerator these modes will have twice the attenuation as the fundamental. Near the cutoff frequency $\theta_{mn} \to 0$ and the attenuation factor becomes very large.

When the nonrigid duct is fitted with a rigid oscillating piston which drives the air with a uniform amplitude $U(y,z) = U_o$, one finds that higher modes are excited to some extent. This behavior is in contrast to that in a rigid duct where only the fundamental mode is excited by a perfect piston. When the driving frequency happens to be just greater than some cutoff frequency, the results indicate that this mode will have a large amplitude (but the attenuation is large as well). Morse and Ingard (ref. 47) warn that measurements made in such a duct, if interpreted on the assumption that only the fundamental mode is present, will appear to produce erroneous results, since both the phase velocity and attenuation constants of these higher modes may differ, by fairly large factors, from those of the fundamental.

The authors (ref. 47) also considered the case of walls with large admittances and presented a figure (p. 510) showing some results typical of a square duct with fairly "soft" walls (with acoustic impedance similar to a number of sound-absorbent materials). In the figure are plots of the variation with frequency parameter h/λ ($h/\lambda \leq 2$) of attenuation coefficients and phase velocities for the fundamental (0, 0)-mode and a higher (1, 1)-mode wave. With increasing frequency the attenuation coefficient for the principal wave rises from zero to a maximum and then exhibits a monotonic decay. The coefficient of the (1, 1) wave shows a rapid drop from its cutoff value. It reaches a

minimum on par with the maximum value of the (0, 0) wave, and rises slightly and levels off. The phase velocity of the principle wave rises from about 0.8c at very low frequencies to a value very close to c. The phase velocity of the (1, 1) wave drops very rapidly from the cutoff condition to a value near c. It then begins to rise with frequency, obtaining a value of approximately 1.2c at $h/\lambda = 2$.

Near the end of their discussion of sound propagation in ducts with yielding walls, the authors (ref. 47) state that it is obvious that the behavior of sound waves, even the principal wave, is quite complicated when the admittance ratio of the walls is not small compared with unity. They further state that if one adds to this the fact that many porous acoustic materials have impedances that vary considerably with change in frequency, it becomes apparent that very few sweeping generalities can be made concerning the behavior of sound in ducts with highly absorbent walls. The present writer is staying out of the broom closet.

Effects of Flow

The effects of flow is the last topic for discussion in this review. The subject will be disposed of in a rather brief manner because it is so complex that few elementary aspects can be synthesized for presentation here. Most textbooks do not include discussions of flow effects (Morse and Ingard, ref. 47, have a chapter on the subject; Meyer and Neumann, ref. 48, also have a chapter, but it is very brief). A review of the literature is really needed here, but this is beyond the scope of the present study. Essentially every phenomenon which has been discussed so far, from plane progressive and standing waves to reflection and attenuation, is affected by flow in a duct.

The reflection of plane progressive waves from the open end of a duct provides an interesting introduction to the discussion of the effects of flow. For the case of no flow, as discussed earlier, the reflection factor R, the ratio of the reflected to the incident wave amplitudes, decreased from a value of one at very low frequencies to a value of zero for very high frequencies. With flow in the direction of the open end, measurements (refs. 50-- these data are shown without credit in the Meyer and Neumann textbook, and ref. 51) reveal the reflection factor can be greater than one over a range of low frequencies. At higher frequencies the reflections factors increase with increase in flow Mach number. In ducts with sudden (step) enlargements reflection factors are found to increase with increase in Mach number (refs. 36 and 52). The fact that reflection factors greater than one occur does not mean that more energy was reflected than was sent down the duct. Obviously the flow field is involved, and in fact, the mathematical relations which express the conservation of energy have the flow velocity as one of the factors. When this is taken into account the data show that indeed energy is lost from the end of the tube in the reflection process. For waves propagating in a direction parallel to the flow direction, the energy intensity I is given by (ref. 48).

$$I = \frac{p^2}{\rho c} (1 \pm M)^2 \qquad (44)$$

where M is the flow Mach number the + is used when the sound is propagating in the direction of the flow and the - when in the opposite direction. Thus, if a downstream propagating wave were to undergo a 100% reflection in a duct, the ratio of the reflected to incident amplitudes would be $(1 + M)/(1 - M)$, a quantity which is greater than one. If plotted in the form of $R\,(1 - M)/(1 + M)$ vs. frequency, the data at all Mach numbers lie

below 1.0 and, after reaching a peak value, decrease with increasing frequency. At all frequencies the data, when plotted in this form, decrease with increase in Mach number, showing that more energy is being lost in the reflection process as the Mach number is increased.

The phase velocity for waves traveling in the direction of the flow is $c + U$, where U is the flow velocity, and $c - U$ when traveling against the flow. The respective wave numbers then become $k^+ = k/(1 + M)$ and $k^- = k/(1 - M)$, where k is the wave number in the absence of flow. One of the consequences of this is that the nodal spacing in a standing wave produced by incident and reflected waves is reduced by a factor of $(1 - M^2)$. In the case of real fluids the dissipation rates will also be altered by the convective effect. If α is the attenuation rate, the loss per unit length in a stationary medium, the attenuation rate with flow becomes $\alpha/(1 \pm M)$. The convective effects on attenuation can also be observed for flow and sound passing over absorbent walls; the attenuation is least when the sound travels in the direction of the flow (as will be discussed shortly, refraction effects can alter this behavior).

The transverse modes are also affected by flow. For the rigid wall case with inviscid flow (no boundary layers) the cutoff frequencies are changed by the factor $\sqrt{1 \mp M^2}$ (ref. 34), where the minus sign is for downstream propagation. In duct flow one has to contend with the flow boundary layers on the walls as well as the mean flow. In some cases the boundary layer has been treated as an additional admittance to the wall. A most important effect of the boundary layer on the sound propagation is due to refraction resulting from the gradients in the flow. The boundary layers refract the sound waves toward the wall for downstream propagation and away from the wall for upstream propagation. The effects are stronger at higher frequencies and higher Mach numbers. The resulting acoustic pressure field across the duct can become quite nonuniform, and it becomes difficult to interpret the pressure distribution in terms of individual modes. At high frequencies the wave propagation can be analyzed using geometric acoustics and certain energy invariants. It is generally found that the rays are bent more sharply towards the center of the duct in upstream propagation than toward the wall in downstream propagation (e.g., ref. 38 - in ref. 53 geometric acoustics was used to analyze the refraction of wind tunnel aerodynamic noise through boundary layers in supersonic flow). It may be noted that if the upstream and downstream ray tube areas are equal, the geometric acoustic method yields eq. (44).

For ducts with nonrigid walls the situation is of course more complex. Morse and Ingard analyzed the case of uniform flow (no boundary layers) in a duct with walls having small surface admittances. The attenuation coefficient was found to vary as $1/(1 \pm M)^2$. The effect of boundary layers on attenuation is most pronounced when the duct walls are of sound absorbent materials. At low frequencies, where the refraction is less, the convective effect dominates and the attenuation is less in the downstream direction. At high frequencies the refraction effect is dominant, and the channeling of energy towards the wall in downstream propagation results in greater losses for downstream propagation than for upstream propagation. The convection and refraction thus have the opposite effects on attenuation. Data showing this may be found in the textbook of Meyer and Neumann and the review article by Nayfeh, Kaiser, and Telionis (ref. 34). For the fundamental mode, increasing the boundary layer thickness leads to an increase in the attenuation in downstream propagation and a decrease in upstream propagation. However, exceptions

to this trend have been noted in the higher modes (ref. 34). And while the expectation is that the fundamental mode is the least attenuated, calculations show that this need not be so (ref. 34). A fine place to begin on all of these matters is the review article by Nayfeh, Kaiser, and Telionis (ref. 34). It should be noted that at high speeds the boundary layers themselves can become a significant contributor to the duct sound field if they are turbulent. And finally, acoustic measurements become much more difficult to make when flow is present.

REFERENCES

1. Schubauer, G. B.; and Skramstad, H. K.: Laminar-Boundary Layer Oscillations and Transition on a Flat Plate. NACA Rep. 909, 1948.

2. Polyakov, N. F.: The Influence of the Low Free-stream Perturbations on the Condition of Laminar Boundary Layer. Archiwum Mechaniki Stosowanej, vol. 31, no. 3, 1979, pp. 327-338.

3. Shapiro, Paul J.: The Influence of Sound Upon Laminar Boundary Layer Instability. Acoustics and Vibration Laboratory Report No. 83458-83560-1, Massachusetts Institute of Technology, Sept. 1977. (Available from DTIC as AD A046 057.)

4. Murdock, J. W.: The Generation of a Tollmien-Schlichting Wave by a Sound Wave. Proc. R. Soc. Lon. A, vol. 372, 1980, pp. 517-534.

5. Leehey, Patrick: Influence of Environment in Laminar Boundary Layer Control. In Viscous Flow Drag Reduction, ed. by Gary R. Hough, vol. 72 of Progress in Astronautics and Aeronautics Series, 1980, pp. 4-16.

6. Thomas, Andrew S. W.; and Lekoudis, Spyridon G.: Sound and Tollmien-Schlichting Waves in a Blasius Boundary Layer. Physics of Fluids, vol. 21, no. 11, Nov. 1978, pp. 2112-2113.

7. Mechel, F.; and Schilz, W.: Untersuchungen zür akustischen Beeinflussung der Strömungsgrenzschicht in Luft. Acustica, vol. 14, no. 6, 1964, pp. 325-331.

8. Schilz, W.: Experimentelle Untersuchungen zür akustischen Beeinflussung der Strömungsgrenzschicht in Luft. Acustica, vol. 14, no. 4, 1965/66, pp. 208-223.

9. Vlasov, Ye. V.; Ginevskiy, A. S.; and Karavosov, R. K.: Response of Unstable Laminar Boundary Layer to Acoustic Excitation. Fluid Mechanics, vol. 7, no. 1, Jan.-Feb., 1978, pp. 116-124.

10. Wells, C. Sinclair, Jr.: Effects of Free-stream Turbulence on Boundary Layer Transition. AIAA J., vol. 5, no. 1, Jan. 1967, pp. 172-174.

11. Spangler, J. G.; and Wells, C. S., Jr.: Effects of Free-stream Disturbances on Boundary-Layer Transition. AIAA J., vol. 6, no. 3, Mar. 1968, pp. 543-545.

12. Knapp, C. F.; and Roache, P. J.: A Combined Visual and Hot-Wire Anemometer Investigation of Boundary Layer Transition. AIAA J., vol. 6, no. 1, Jan. 1968, pp. 29-36.

13. Barinov, V. A.; Gedymin, V. A.; Lebedev, O. V.; and Printsev, B. K.: Effect of Acoustical Disturbances on Pulsating Characteristics of Flow and the Transition of Laminar Boundary Layer Into Turbulent. From Uchenyye Zapiski TsAGI, vol. VI, no. 6, 1975, pp. 130-147, Machine Translation, FTO-ID(RS)T-0284-78, prepared by Foreign Technology Division, Air Force Systems Command, April, 1978.

14. Bohn, A. J.; and Mangiarotty, R. A.: Wind Tunnel Study on the Effects of Acoustical Disturbances on Controlled Laminar Flow. AIAA Paper No. 79-0629, 1979.

15. Pfenninger, Werner; and Reed, Verlin D.: Laminar-Flow Research and Experiments. Astronautics and Aeronautics, July 1966, pp. 44-50.

16. Bushnell, Dennis M.; and Tuttle, Marie H.: Survey and Bibliography on Attainment of Laminar Flow Control in Air Using Pressure Gradient and Suction. Volume I. NASA RP-1035, 1979.

17. Hefner, Jerry N.; and Bushnell, Dennis M.: Status of Linear Boundary-Layer Stability Theory and the e^n Method, With Emphasis on Swept-Wing Applications, NASA TP-1645, April 1980.

18. Kachanov, Yu S.; Kozlov, V. V.; and Levchenko, V. Ya.: Occurrence of Tollmien-Schlichting Waves in the Boundary Layer Under the Effect of External Perturbations. Translated from Izvestiya Akademii Nauk SSSR, Mekhanika Zhidkosti i Gaza, no. 5, Sept.-Oct. 1978, pp. 85-94.

19. Mungar, P.: On the Sensitivity of Shear Layers to Sound. AIAA Paper No. 77-1369, 1977.

20. Miller, G.; and Callegari, A.: The Effects of Acoustical Disturbances on Boundary Layer Transition. NYU/DAS #78/01, New York University, Jan. 1978.

21. Obremski, H. J.; Morkovin, M. V.; Landahl, M.; Wazzan, A. R.; Okamura, T. T.; and Smith, A. M. O.: A Portfolio of Stability Characteristics of Incompressible Boundary Layers. AGARDograph 134, Mar. 1969.

22. Murdock, John W.: A Numerical Study of Nonlinear Effects on Boundary-Layer Stability. AIAA J., vol. 15, no. 8, Aug. 1977, pp. 1167-1173.

23. Murdock, John W.; and Taylor, Thomas D.: Numerical Investigation of Nonlinear Wave Interaction in a Two-Dimensional Boundary Layer. In Laminar-Turbulent Transition, AGARD-CP-224, 1977, pp. 4-1 to 4-8.

24. Illingworth, C. R.: The Effects of a Sound Wave on the Compressible Boundary Layer on a Flat Plate. J. Fluid Mech., vol. 3, pt. 5, 1958, pp. 471-493.

25. White, Frank M.: Viscous Fluid Flow. McGraw-Hill Book Co., 1974.

26. Radbill, John R.; and McCue, Gary A.: Quasilinearization and Nonlinear Problems in Fluid and Orbital Mechanics. American Elsevier Pub. Co., Inc., 1970.

27. Schlichting, Hermann: Boundary Layer Theory. McGraw-Hill Book Co. Inc., first and second English editions, 1955, 1960.

28. Struminskii, V. V.: Nonlinear Stability Theory of the Boundary Layer. In Heat and Mass Transfer in Boundary Layers, ed. by N. Afgan, Z. Zaric, and P. Anastasijevic, Pergamon Press, 1972, pp. 459-474.

29. Schlichting, Hermann: Boundary Layer Theory. McGraw-Hill Book Co. Inc., third English edition, 1968.

30. Ross, J. A.; Barnes, F. H.; Burns, J. G.; and Ross, M. A. S.: The Flat Plate Boundary Layer. Part 3. Comparison of Theory with Experiment. J. of Fluid Mech., vol. 43, pt. 4, 1970, pp. 819-832.

31. Kinsler, Lawrence E.; and Frey, Austin R.: Fundamentals of Acoustics. Second ed., John Wiley and Sons, Inc., 1962.

32. White, Frederick E.; and Teas, Donald C.: References to Contemporary Papers on Physics. J. of the Acoust. Soc. of Am., vol. 64, Supplement 2, Winter 1978.

33. White, Frederick E.; and Teas, Donald C.: References to Contemporary Papers on Physics. J. of the Acoust. Soc. of Am., vol. 65, Supplement 2, Summer 1979.

34. Nayfeh, Ali H.; Kaiser, John E.; and Telionis, Demetri P.: Acoustics of Aircraft Engine-Duct Systems. AIAA J., vol. 13, no. 2, 1975, pp. 130-153.

35. Reethof, Gerhard: Turbulence-Generated Noise in Pipe Flow. Ann. Rev. Fluid Mech., vol. 10, 1978, pp. 333-367.

36. Lambert, R. F.; and Steinbrueck, E. A.: Acoustic Synthesis of a Flowduct Area Discontinuity. J. Acoust. Soc. Am., vol. 67, no. 1, Jan. 1980, pp. 59-65.

37. Dong, S. B.; and Liu, C. Y.: A Finite-Element Analysis of Sound Propagation in a Nonuniform Moving Medium. J. Acoust. Soc. Am., vol. 66, no. 2, Aug. 1979, pp. 548-555.

38. Grimm, Denny W.; and Hurst, C. J.: A Geometric Acoustics Approach to the Study of Sound Propagation in Ducts Containing Sheared Flows. J. Acoust. Soc. Am., vol. 66, no. 6, Dec. 1979, pp. 1867-1875.

39. El-Sharkawy, A. I.; and Nayfeh, Ali H.: Effect of an Expansion Chamber on the Propagation of Sound in Circular Ducts. J. Acoust. Soc. Am., vol. 63, no. 3, Mar. 1978, pp. 674-687.

47. Morse, Philip M.; and Ingard, K. Uno: Theoretical Acoustics. McGraw-Hill Book Co., 1968.

48. Meyer, Erwin; and Neumann, Ernst-Georg (John M. Taylor, Jr., transl.): Physical and Applied Acoustics. Academic Press, 1972.

49. Skudrzyk, Eugen: The Foundations of Acoustics. Springer-Verlag, 1971.

50. Mechel, von F.; Schilz, W.; and Dietz, J.: Akustische Impedanz Einer Luftdurchströmten Offnung. Acustica, vol. 15, nó. 4, 1965, pp. 199-206.

51. Bechert, D.; Michel, U.; and Pfizenmair, E.: Recent Advances Concerning an Understanding of Sound Transmission Through Engine Nozzles and Jets. NASA TM-75454, 1978.

52 Ronneberger, D.: Experimentelle Untersuchungen Zum Akustischen Reflexionsfaktor Von Unstetigen Querschnittsänderungen In Einem Luftdurchströmten Rohr. Acustica, vol. 19, 1967/68, pp. 222-235.

53 Schopper, M. R.: Interaction of Aerodynamic Noise With Laminar Boundary Layers in Supersonic Wind Tunnels. NASA CR-3621, 1982.

40 Forsythe, George E.; Malcolm, Michael A.; and Moler, Cleve B.: Computer Methods for Mathematical Computations. Prentice-Hall, Inc., 1977.

41. LaFara, Robert L.: Computing Methods for Science and Engineering. Hayden Book Co., Inc., 1973.

42 Malik, M. R.; and Orszag, S. A.: Comparison of Methods for Prediction of Transition by Stability Analyses. AIAA J., vol. 18, no. 12, Dec. 1980, pp. 1485-1489.

43 Gaster, M.: A Note on the Relation Between Temporally-Increasing and Spatially-Increasing Disturbances in Hydrodynamic Stability. J. of Fluid Mech., vol. 14, pt. 2, 1962.

44 Gaster, M.: The Role of Spatially Growing Waves in the Theory of Hydrodynamic Stability. In progress in Aeronautical Sciences, vol. 6, ed. by Kuchemann, D. and Sterne, L. H. G., Pergamon Press, 1965, pp. 251-270.

45 Davis, M. R.: Design of Flat Plate Leading Edges to Avoid Flow Separation. AIAA J., vol. 18, no. 5, May 1980, pp. 598-600.

46 Cebeci, Tuncer; and Bradshaw, Peter: Momentum Transfer in Boundary Layers. Hemisphere Pub. Co., 1977.

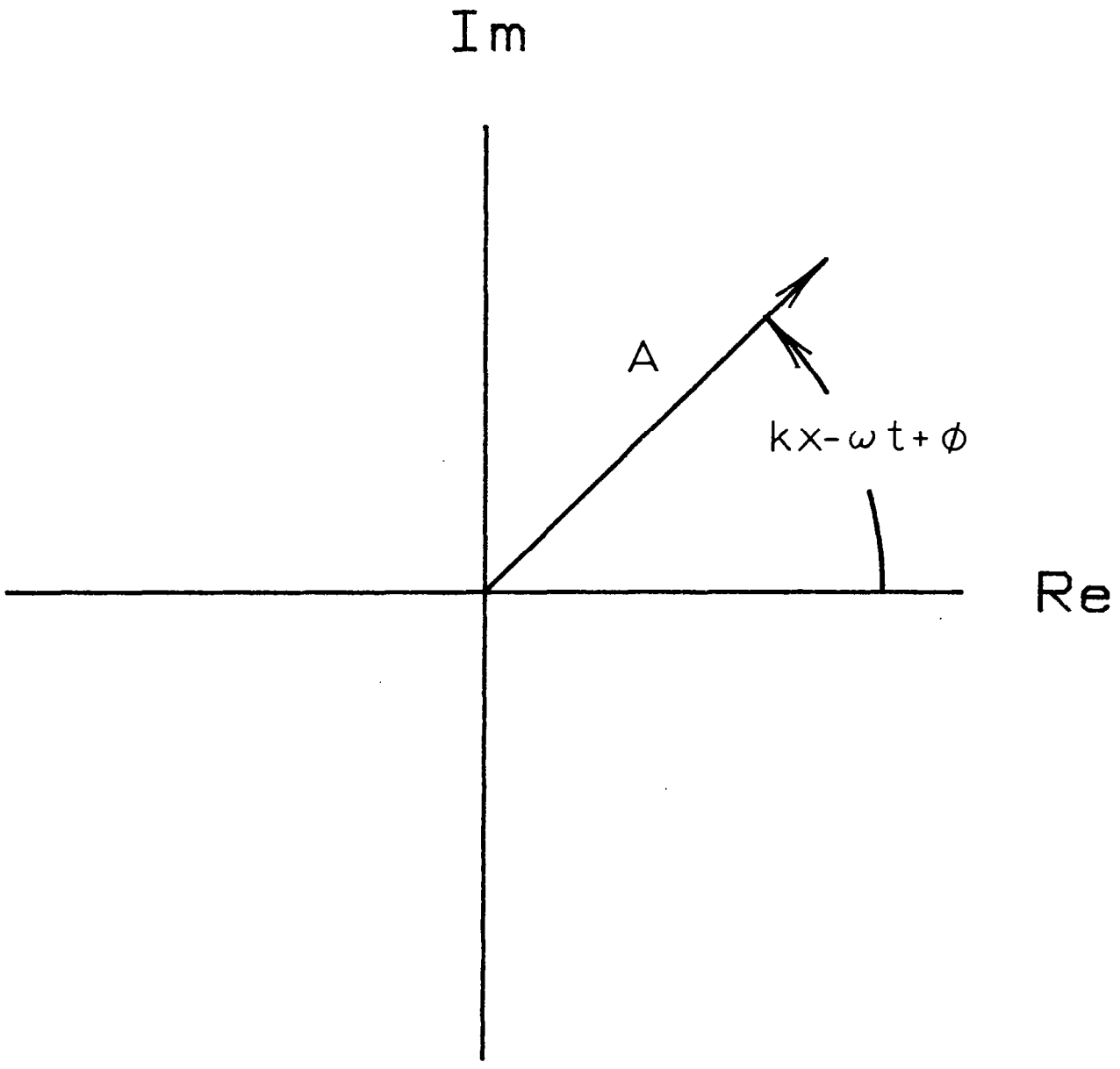

Figure 1.- Complex representation of the traveling wave $A\, e^{i(kx-\omega t+\phi)}$

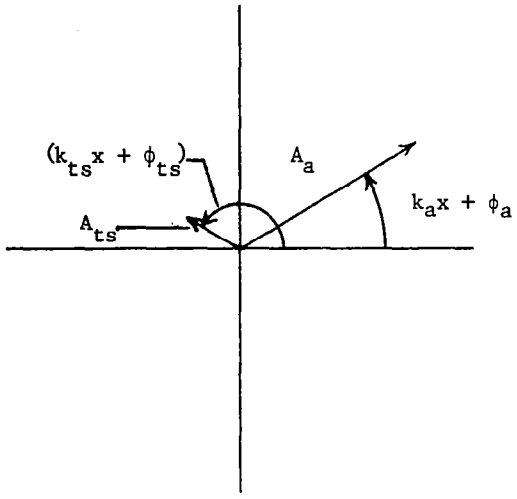

(a) Representation of acoustic and TS traveling waves.

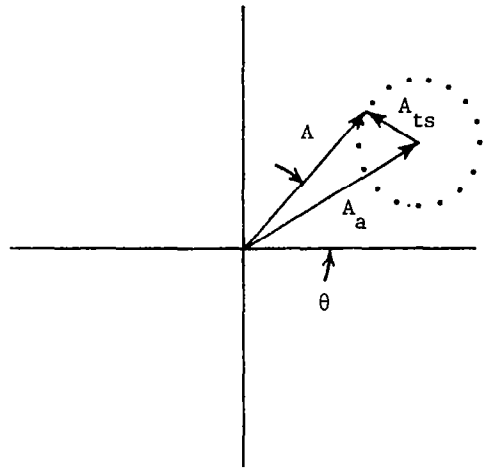

(b) Representation of wave sum. Dotted circle is approximate path of the tip of the sum vector A.

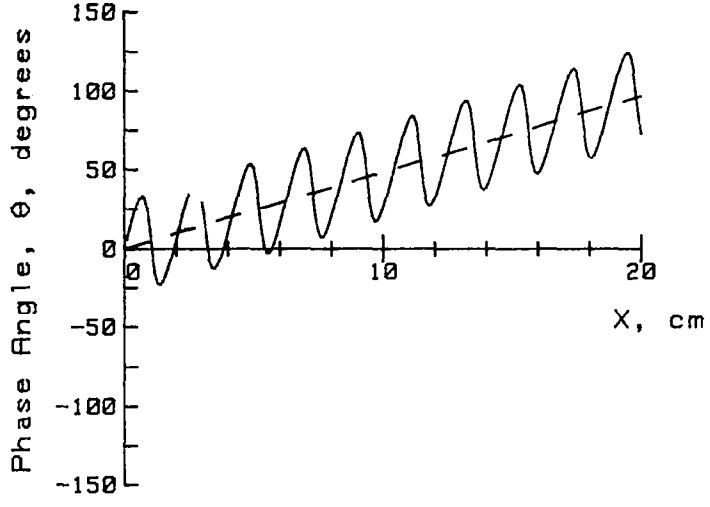

(c) Phase angle of wave sum; $A_{ts} \approx 0.5\ A_a$, $k_a = 10\pi/373$, $k_{ts} \approx 36.75\ k_a$, $\phi_a = \phi_{ts} = 0$.

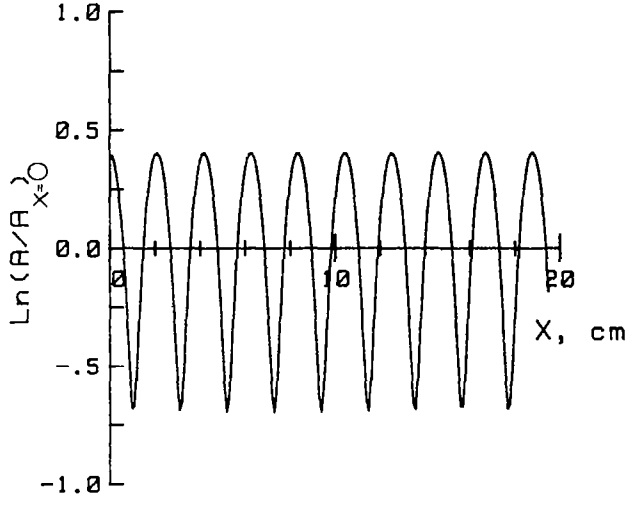

(d) Amplitude of wave sum.

Figure 2.- Complex representation of the sum of two traveling waves of the same frequency and resulting spatial variation of phase angle and amplitude.

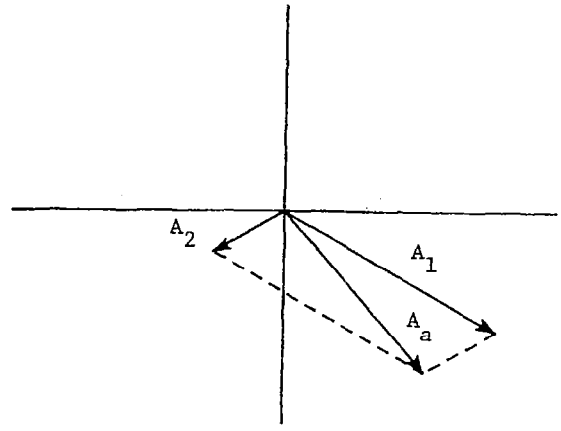

(a) Complex diagram; x=10. TS wave vector not shown.

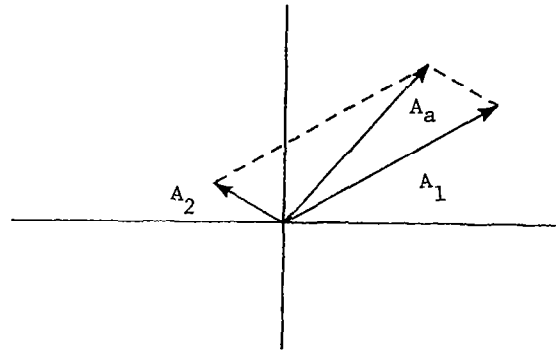

(b) Complex diagram; x=20. TS wave vector not shown.

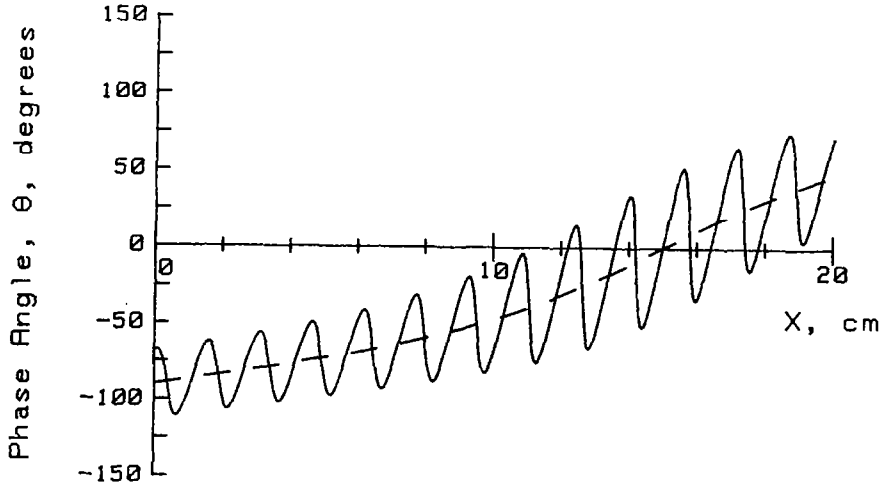

(c) Signal phase angle.

Figure 3.- Diagrams showing the effect of an upstream propagating acoustic wave on the signal phase angle and amplitude. $k_1 = -k_2 = 6$, $k_{ts} = 240$, $\phi_1 = \phi_2 = -90^{\circ}$, $\phi_{ts} = 0$, $A_1 = 1$, $A_2 = 0.3$, $A_{ts} = 0.5$.

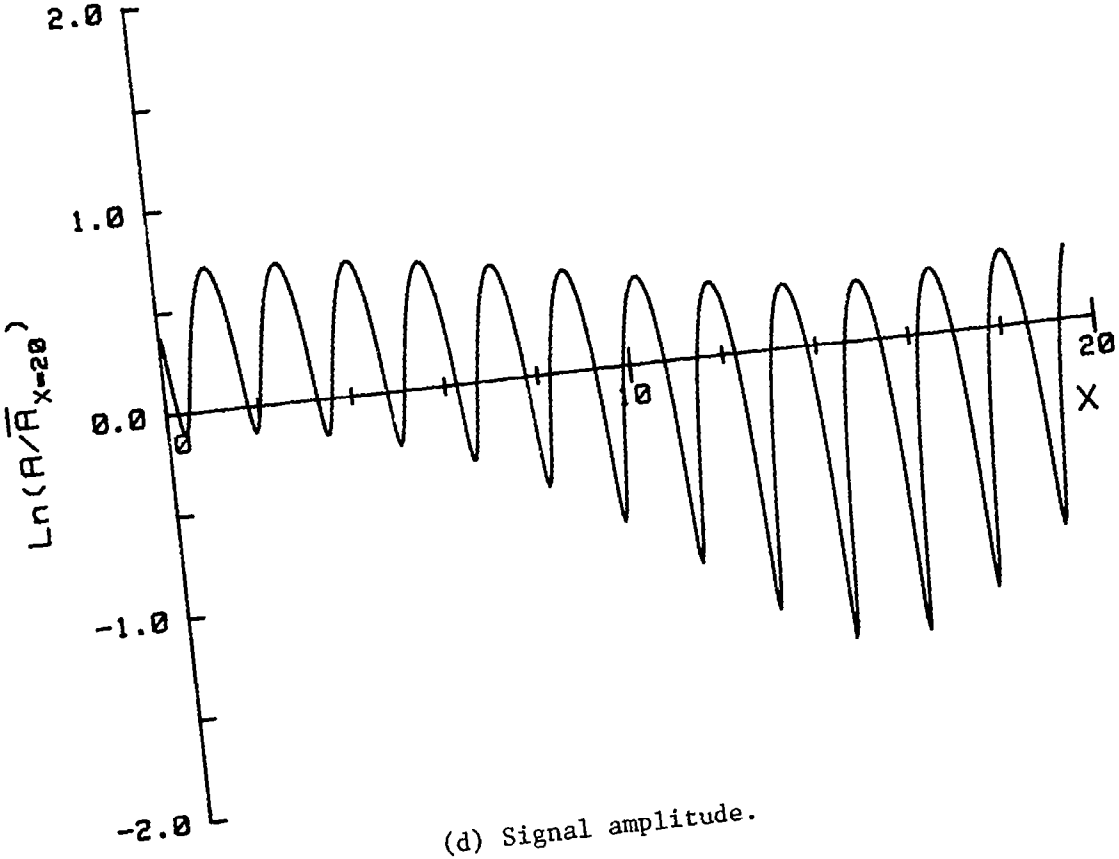

(d) Signal amplitude.

Figure 3.- Concluded.

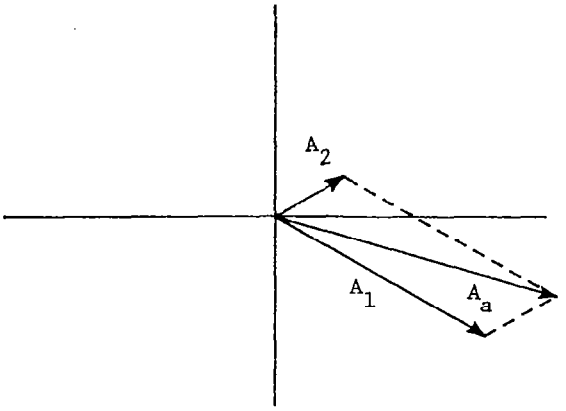

(a) Complex diagram; x=20. TS wave vector not shown.

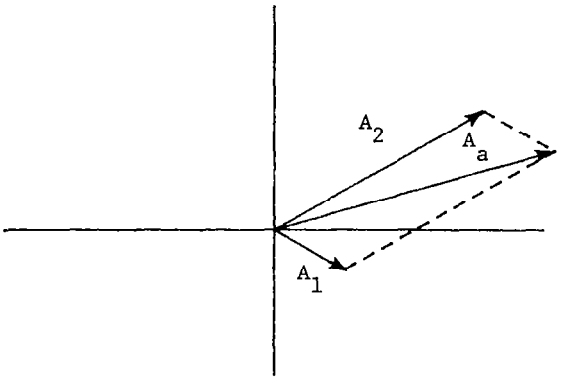

(b) Complex diagram; x=20. TS wave vector not shown.

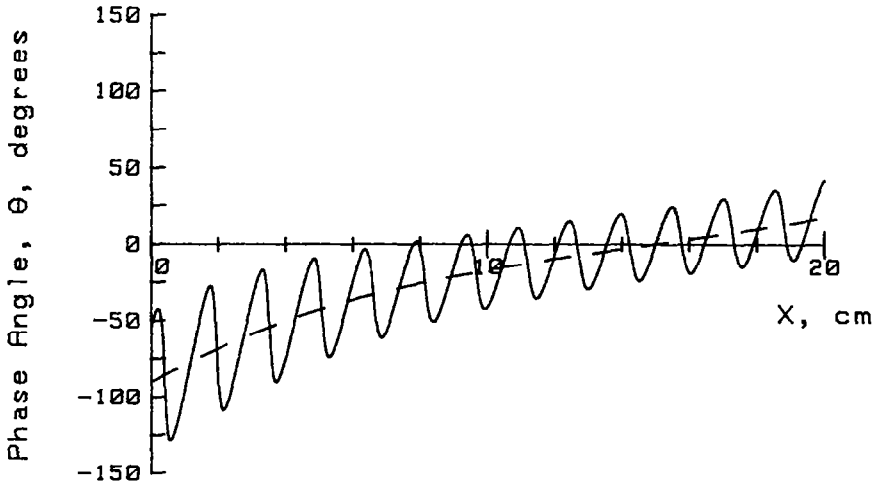

(c) Signal phase angle.

Figure 4.- Diagrams showing the effect of an upstream propagating acoustic wave on the signal phase angle and amplitude. Conditions same as in figure 3 except $\phi_2=90^{\circ}$.

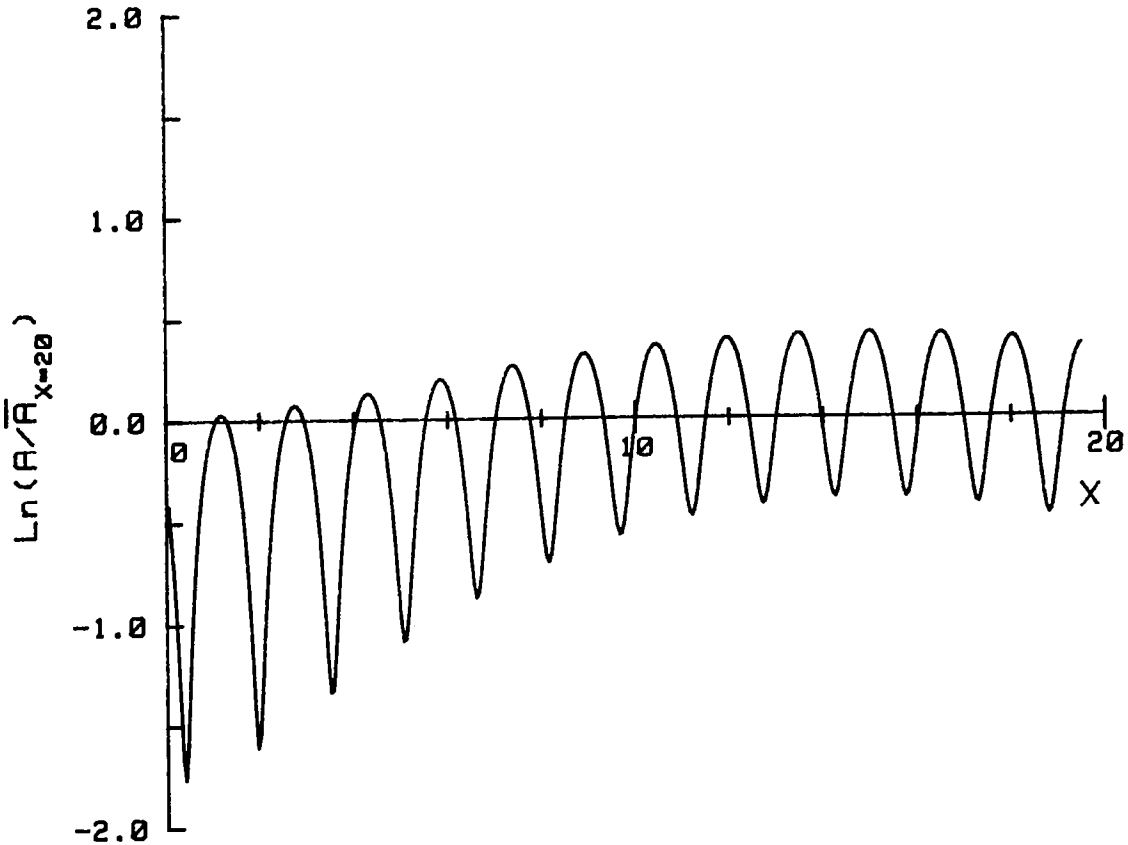

(d) Signal amplitude

Figure 4.- Concluded.

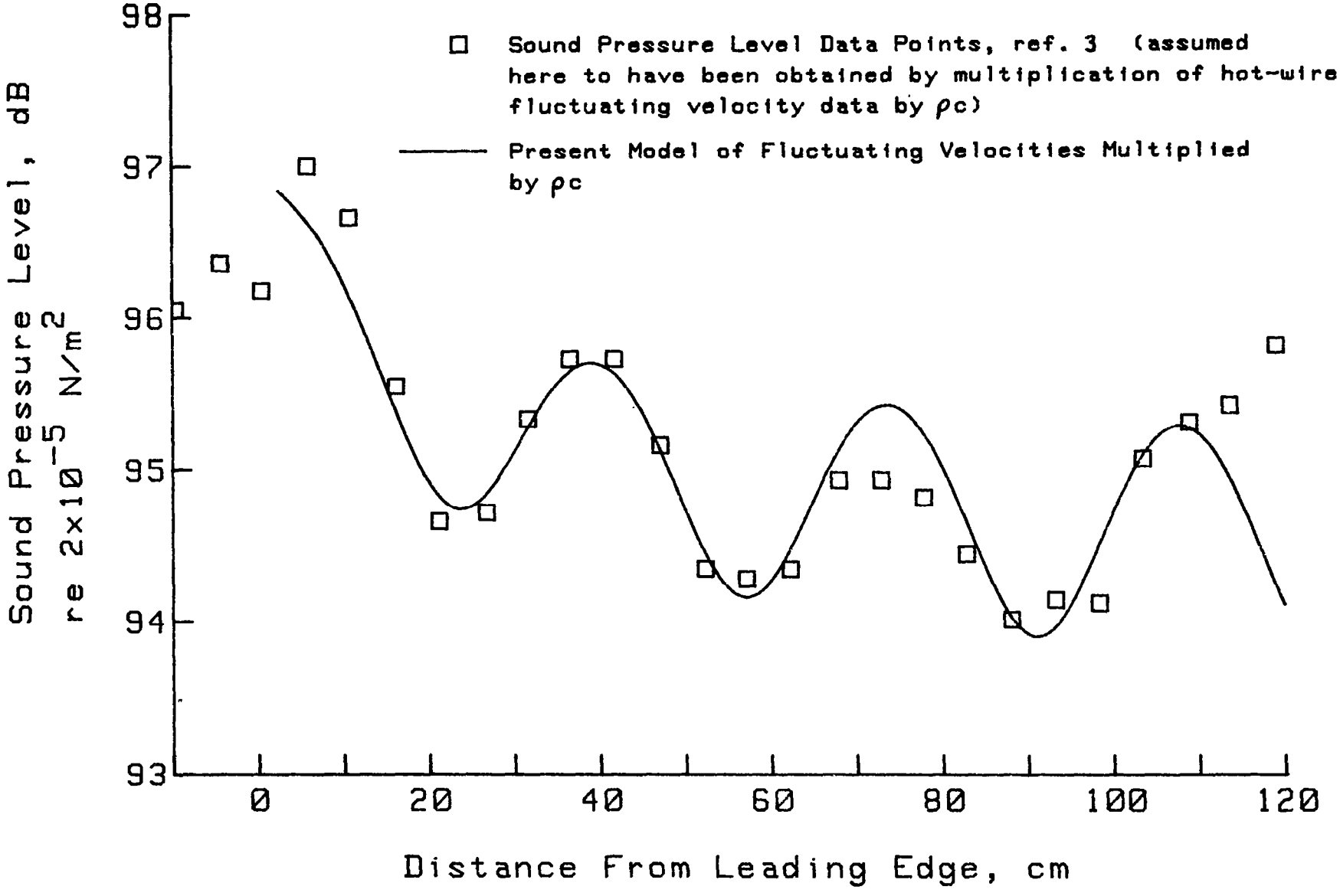

Figure 5.- Comparison of modeled freestream acoustic pressures with Shapiro's data. Pressures estimated from velocities using plane waves equation. Frequency of sound is 500 Hz.

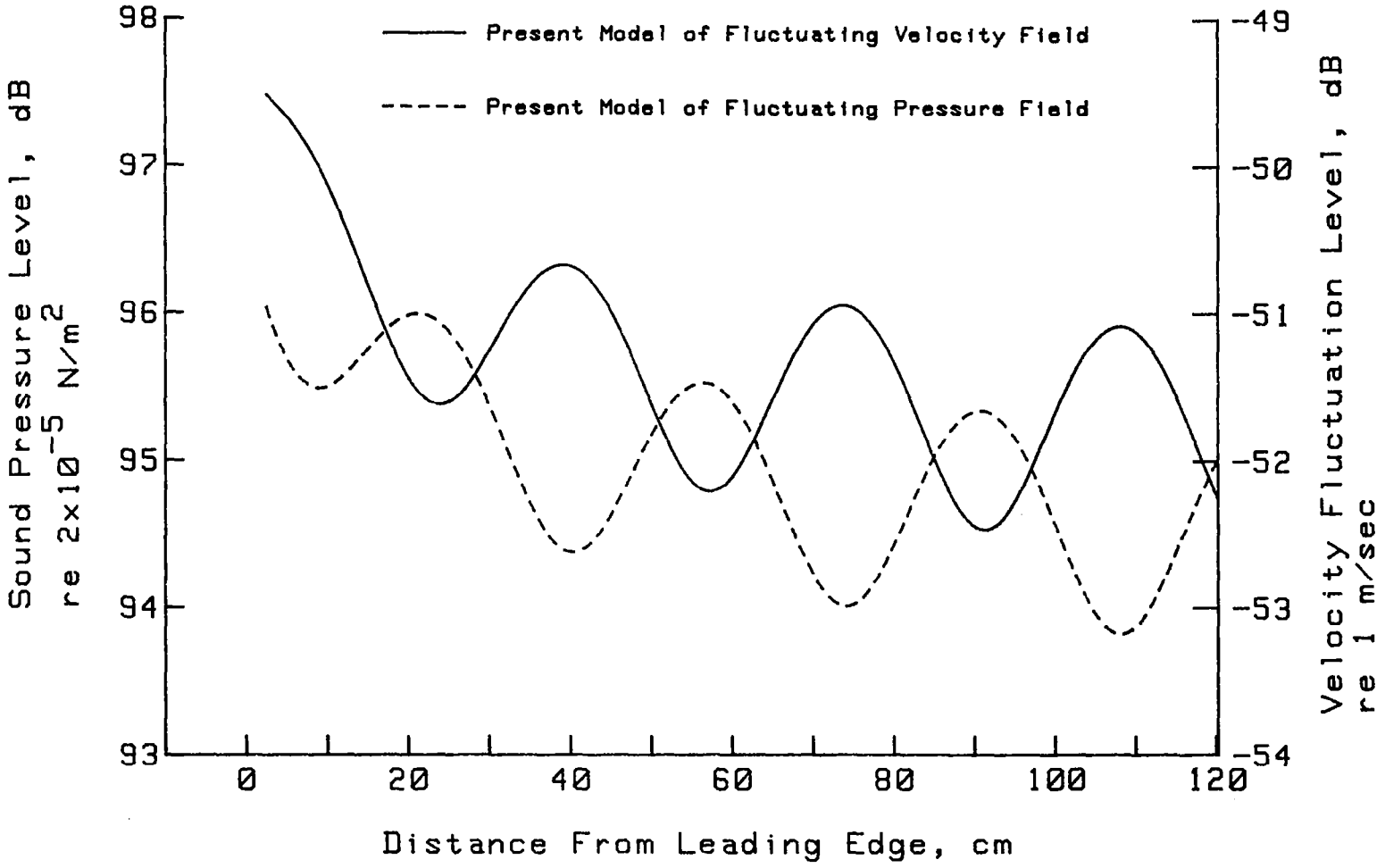

Figure 6.- Variation of modeled acoustic pressure and velocity along tunnel centerline.

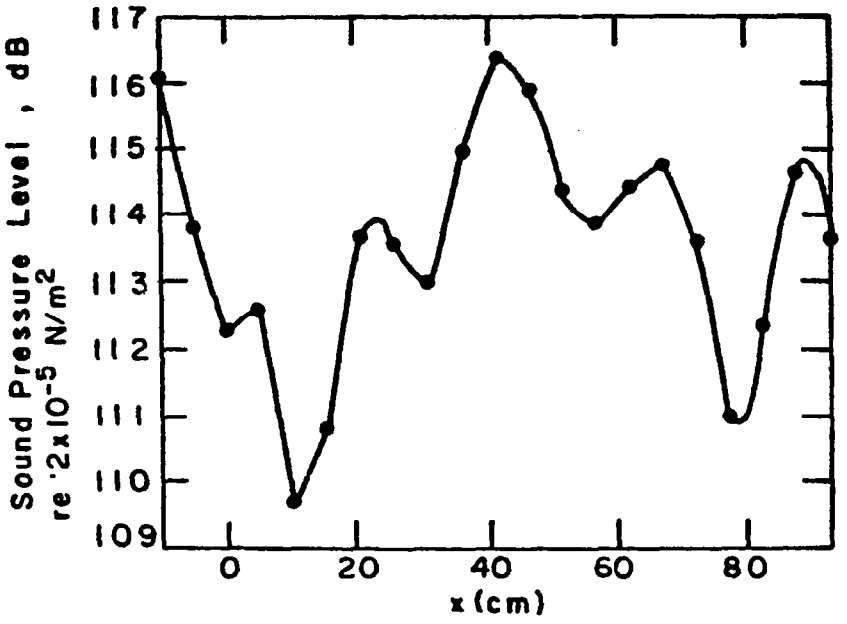

Figure 7.- Data from Shapiro, ref. 3, showing sound pressure level along tunnel centerline for a loudspeaker signal of 1000 Hz.

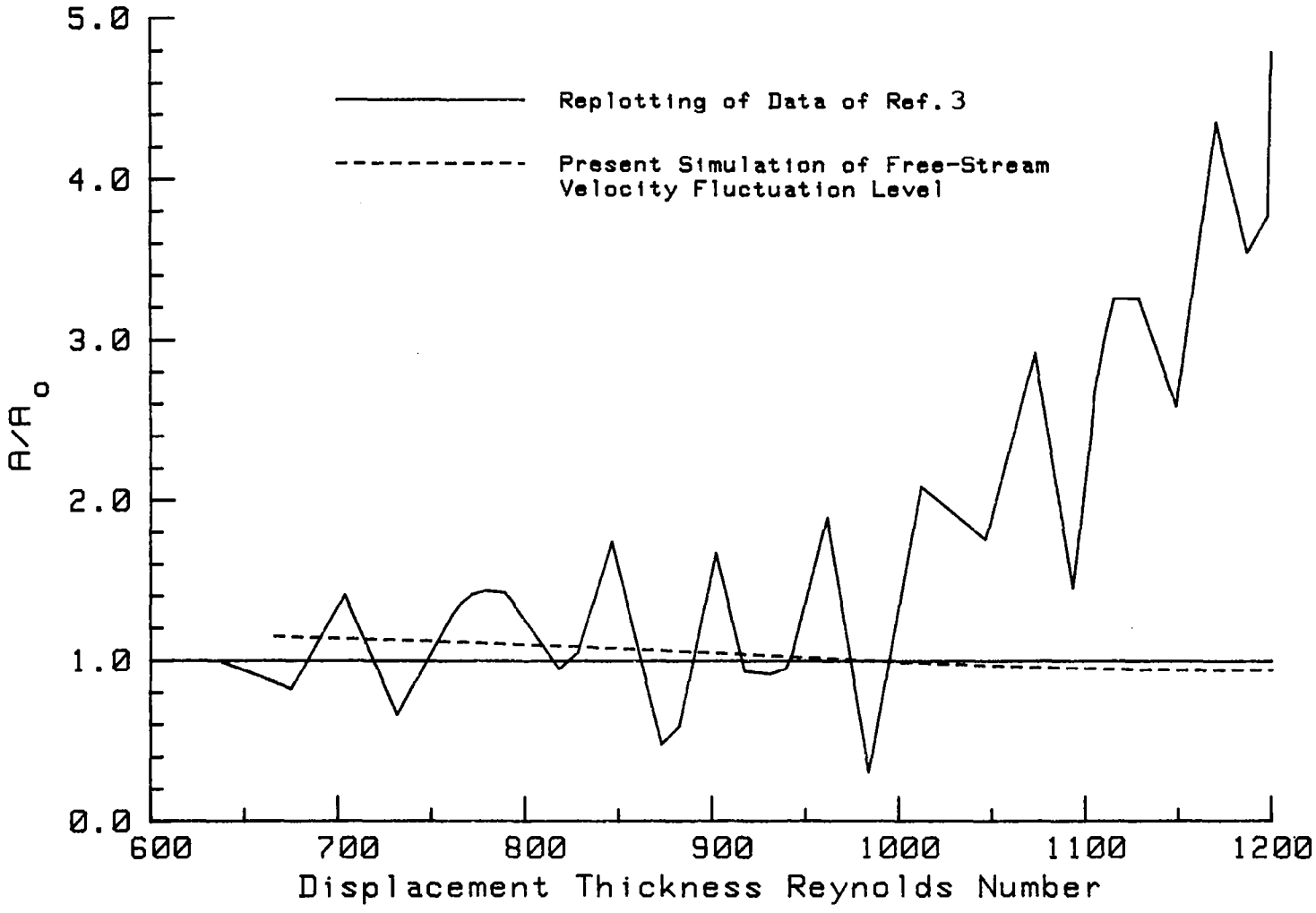

Figure 8 .- Low-Reynolds number boundary layer disturbance amplitude data and the modeled freestream disturbance level.

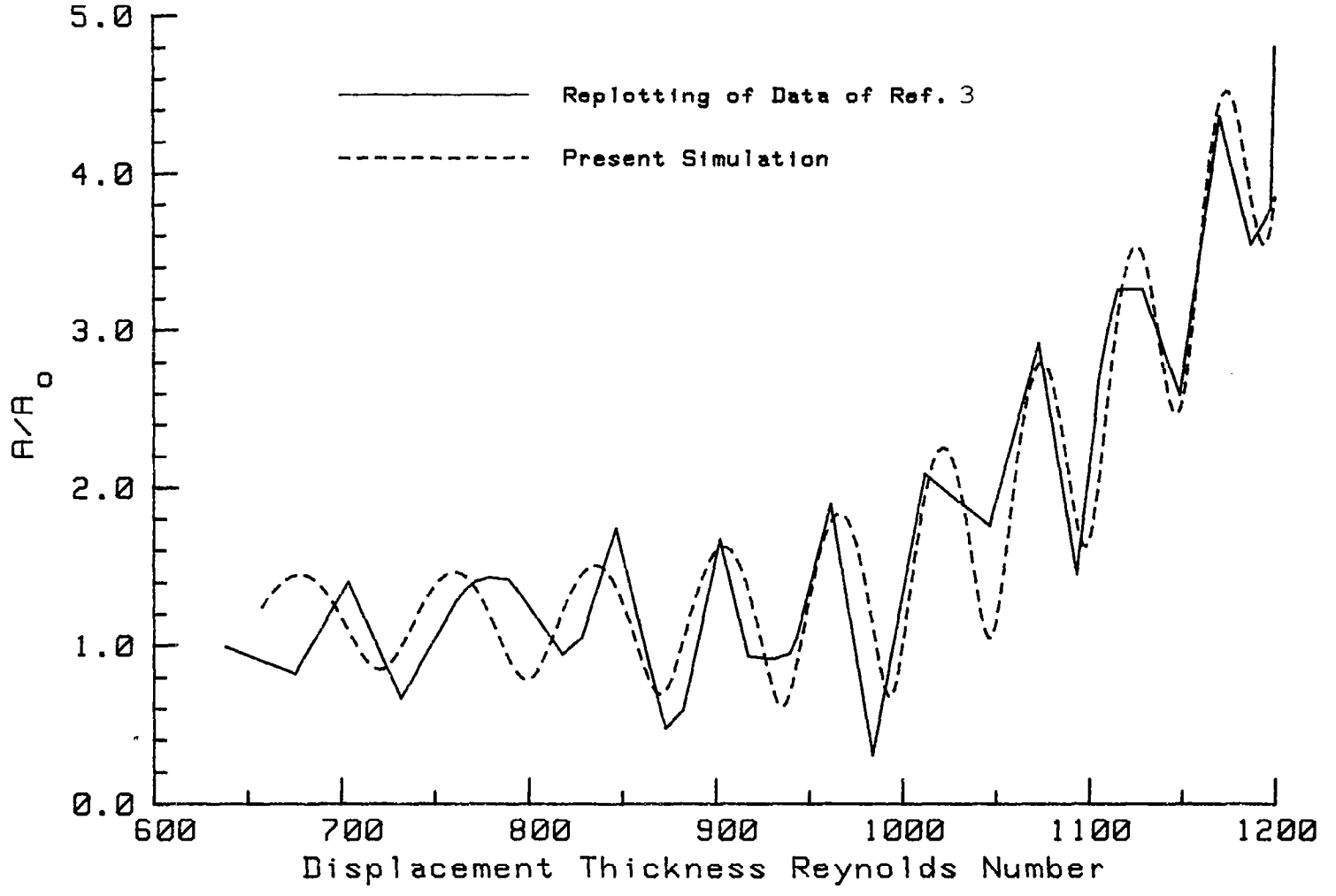

Figure 9 .- Comparison of low-Reynolds number boundary layer disturbance amplitude with modeled values.

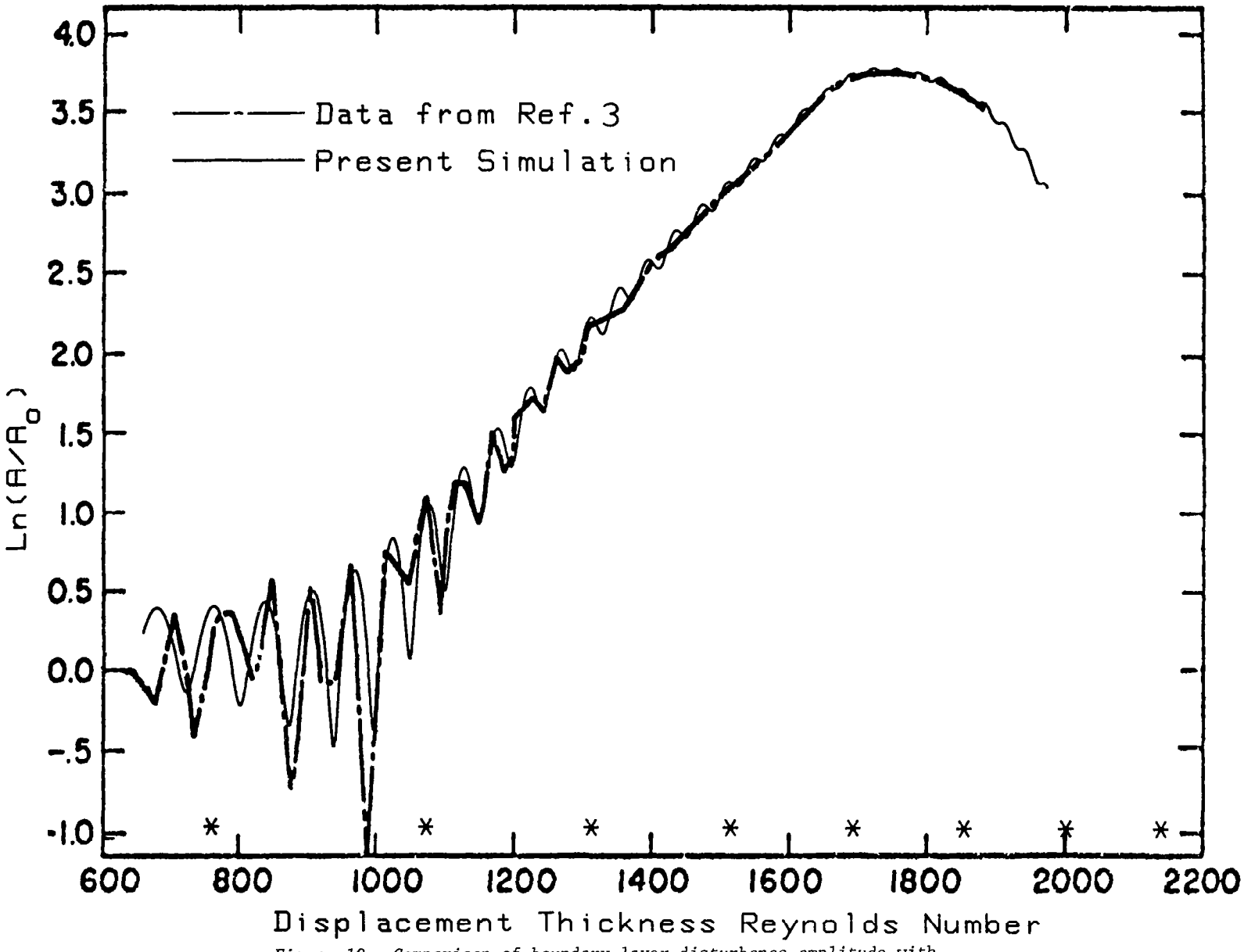

Figure 10.- Comparison of boundary layer disturbance amplitude with modeled values over complete Reynolds number range $\phi_3 = 0^o$.

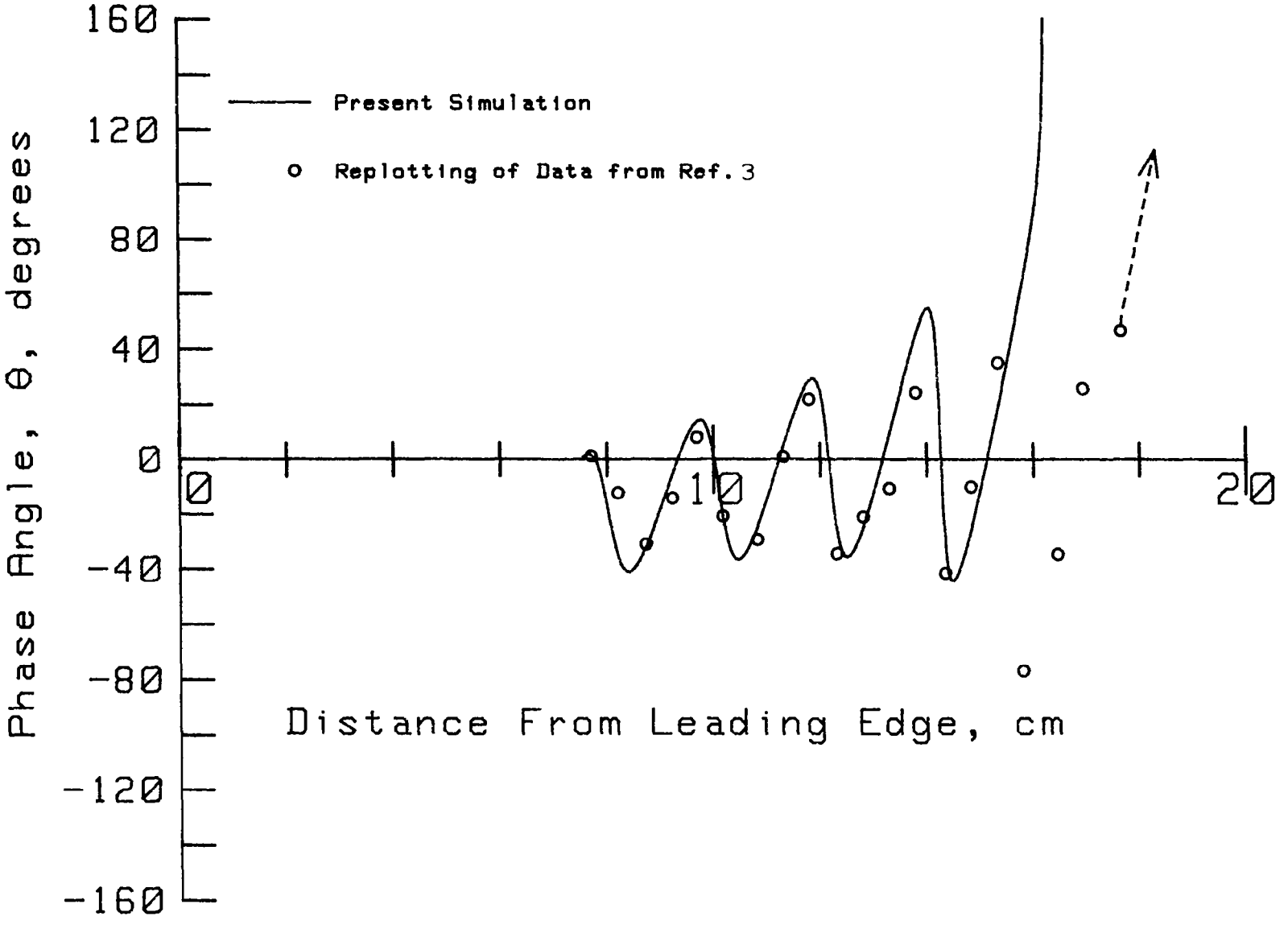

Figure 11.- Comparison of phase angle data with modeled values for distances less than 20 cm from leading edge. $\phi_3=180^{o}$.

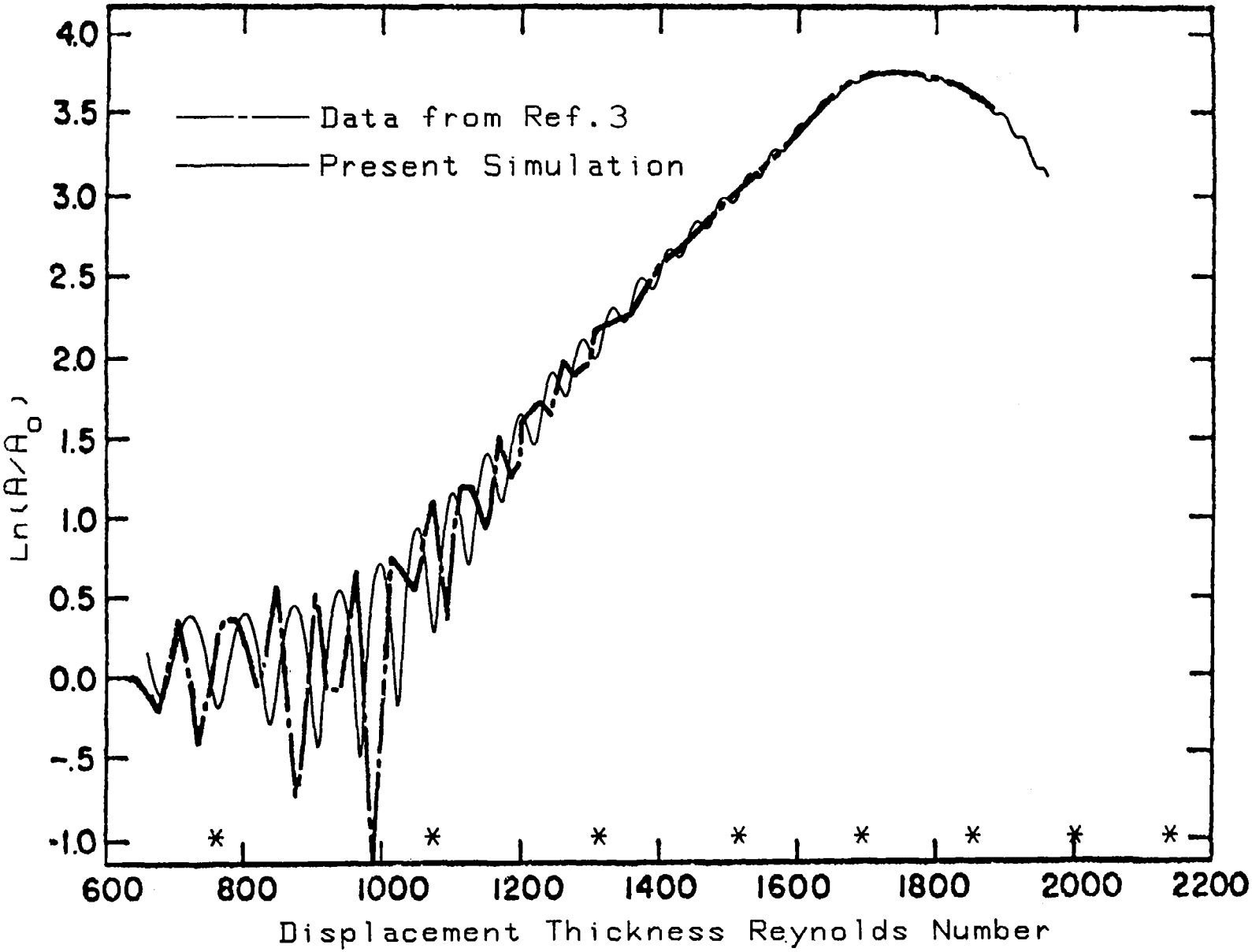

Figure 12.- Comparison of boundary layer disturbance amplitude with modeled values over complete Reynolds number range. $\phi_3 = 180^{\circ}$.

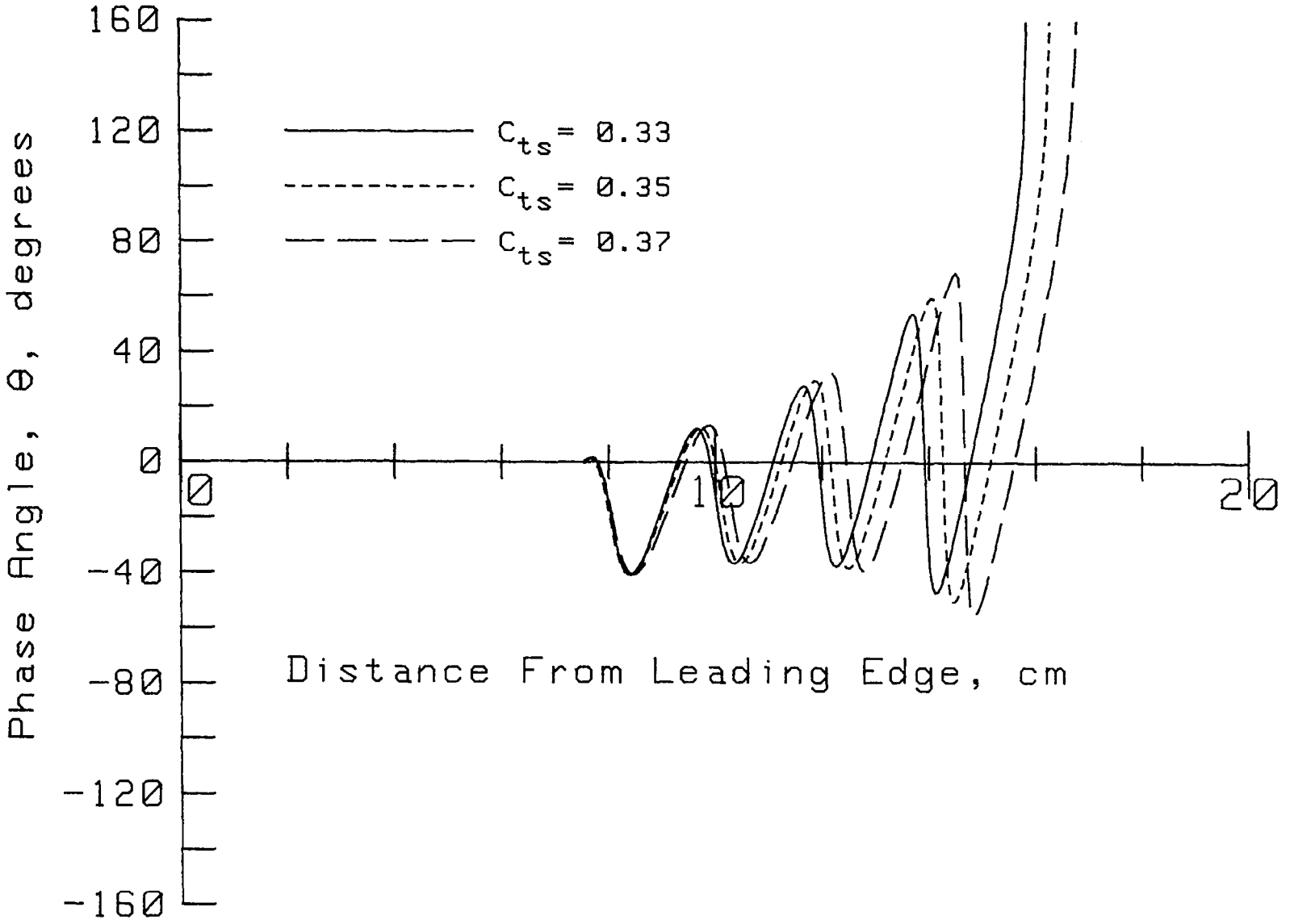

Figure 13.- The effect of TS wave phase speed on the periodicity of the phase angle for conditions upstream of the stability theory neutral point.

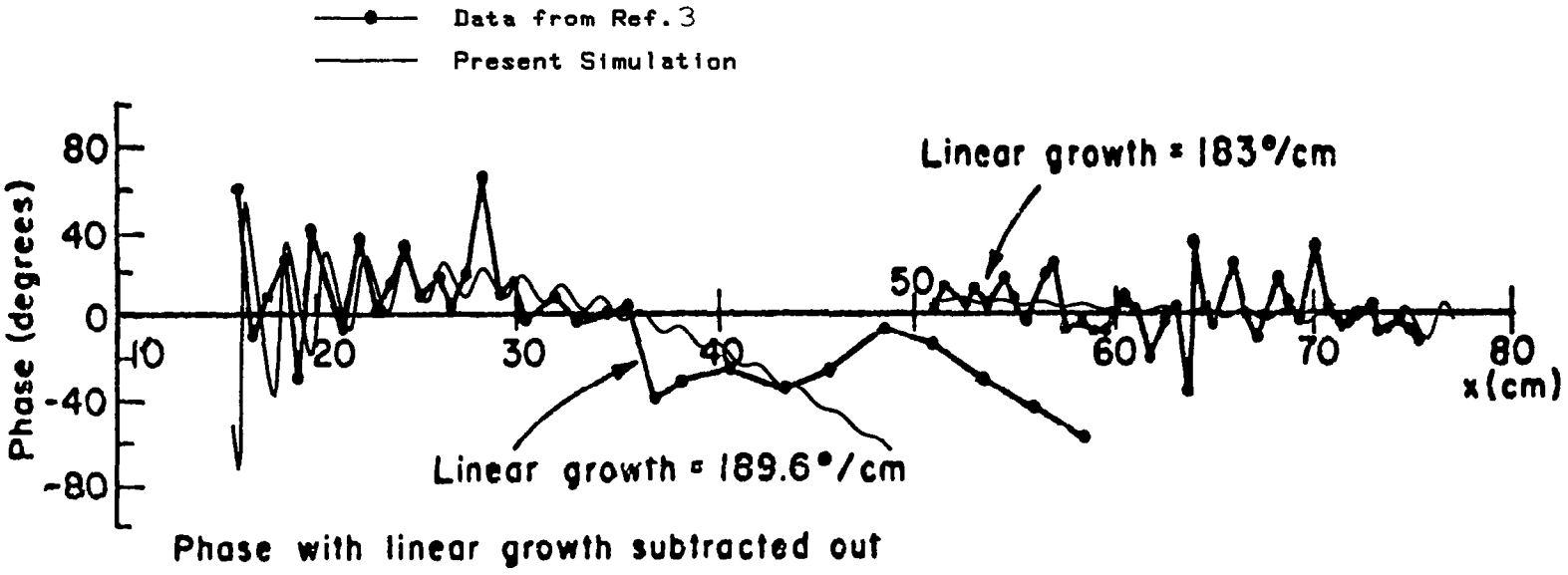

Figure 14.- Comparison of phase angle data with modeled values for the x=15 to 75 cm range.

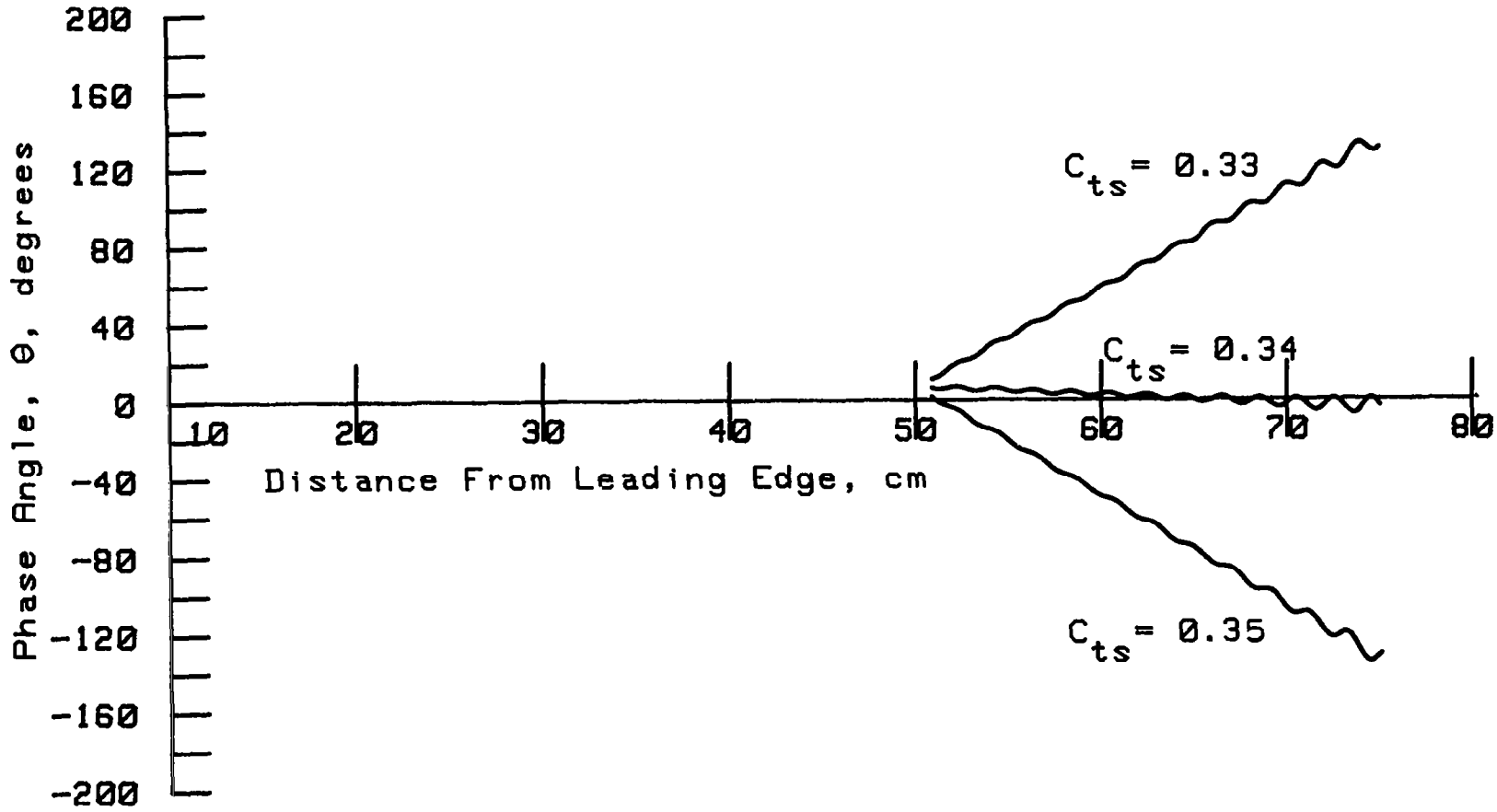

Figure 15.- The effect of the TS wave phase speed on the phase angle for conditions well downstream of stability theory neutral point. A linear growth rate of 183^{o}/cm has been subtracted.

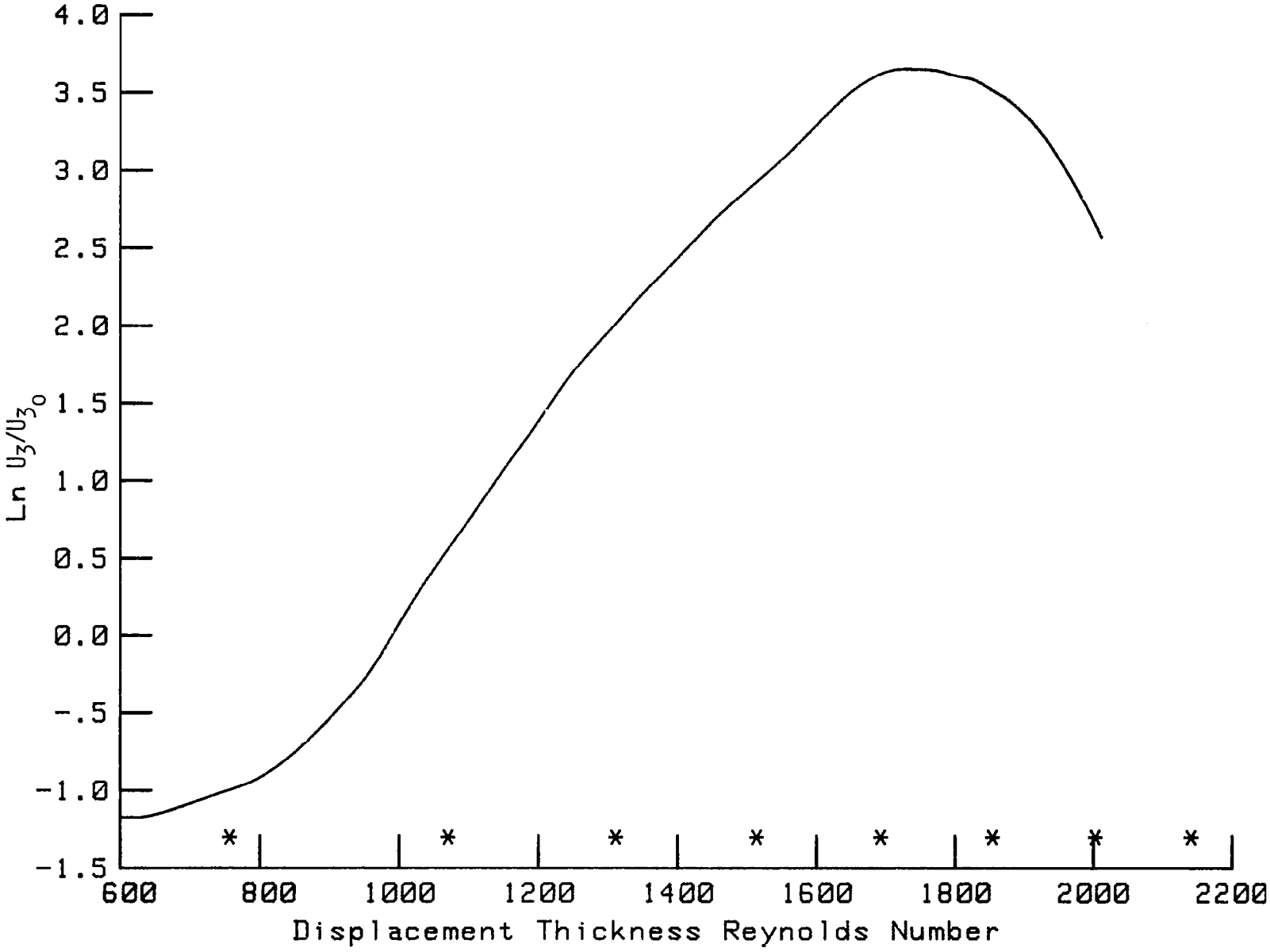

Figure 16.- TS wave amplitude growth curve as obtained from present analysis of Shapiro's data in reference 3.

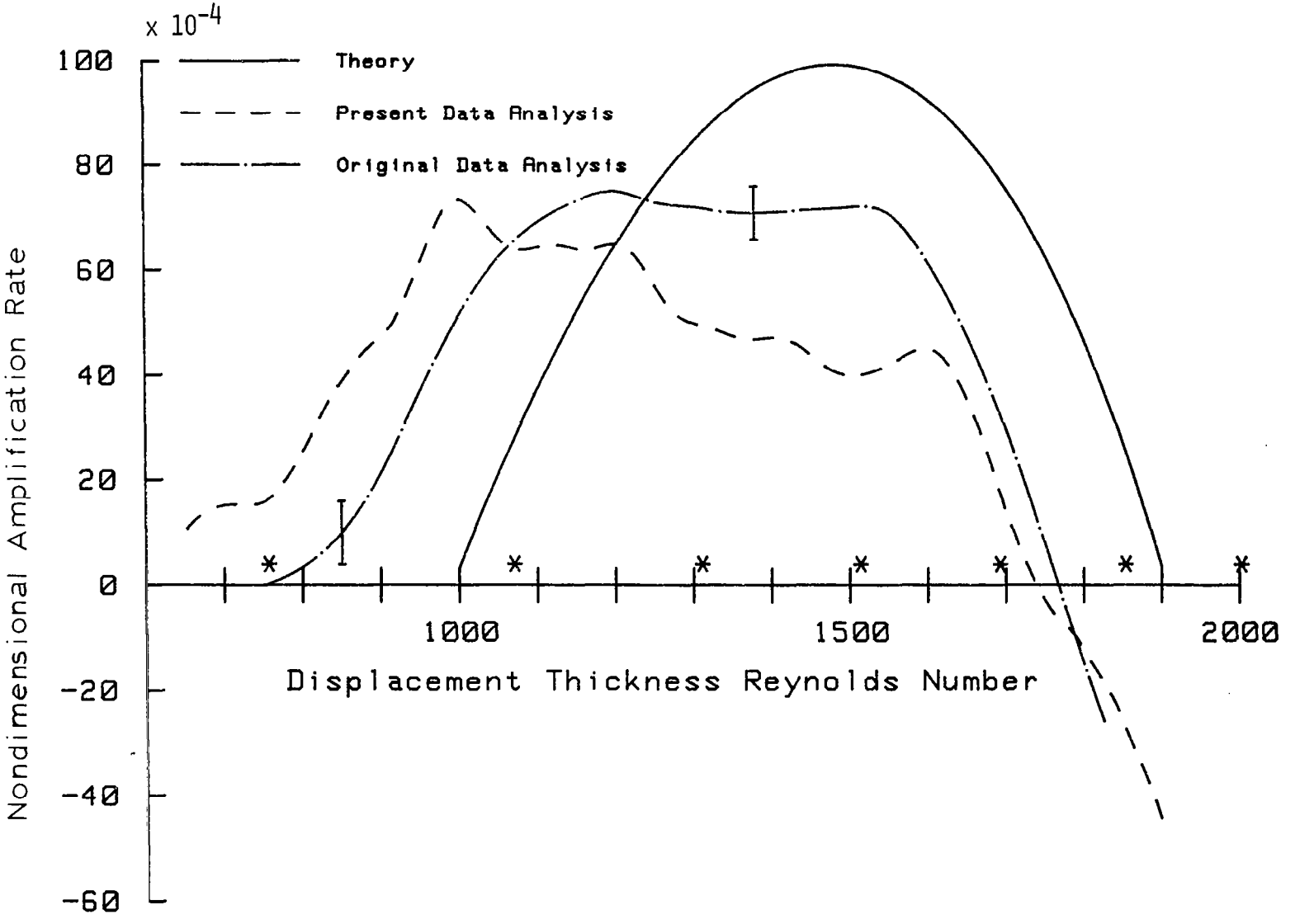

Figure 17.- Comparison of TS wave amplitude growth rates obtained from flat plate stability theory, from Shapiro's analysis of his data, and from present reevaluation of Shapiro's data.

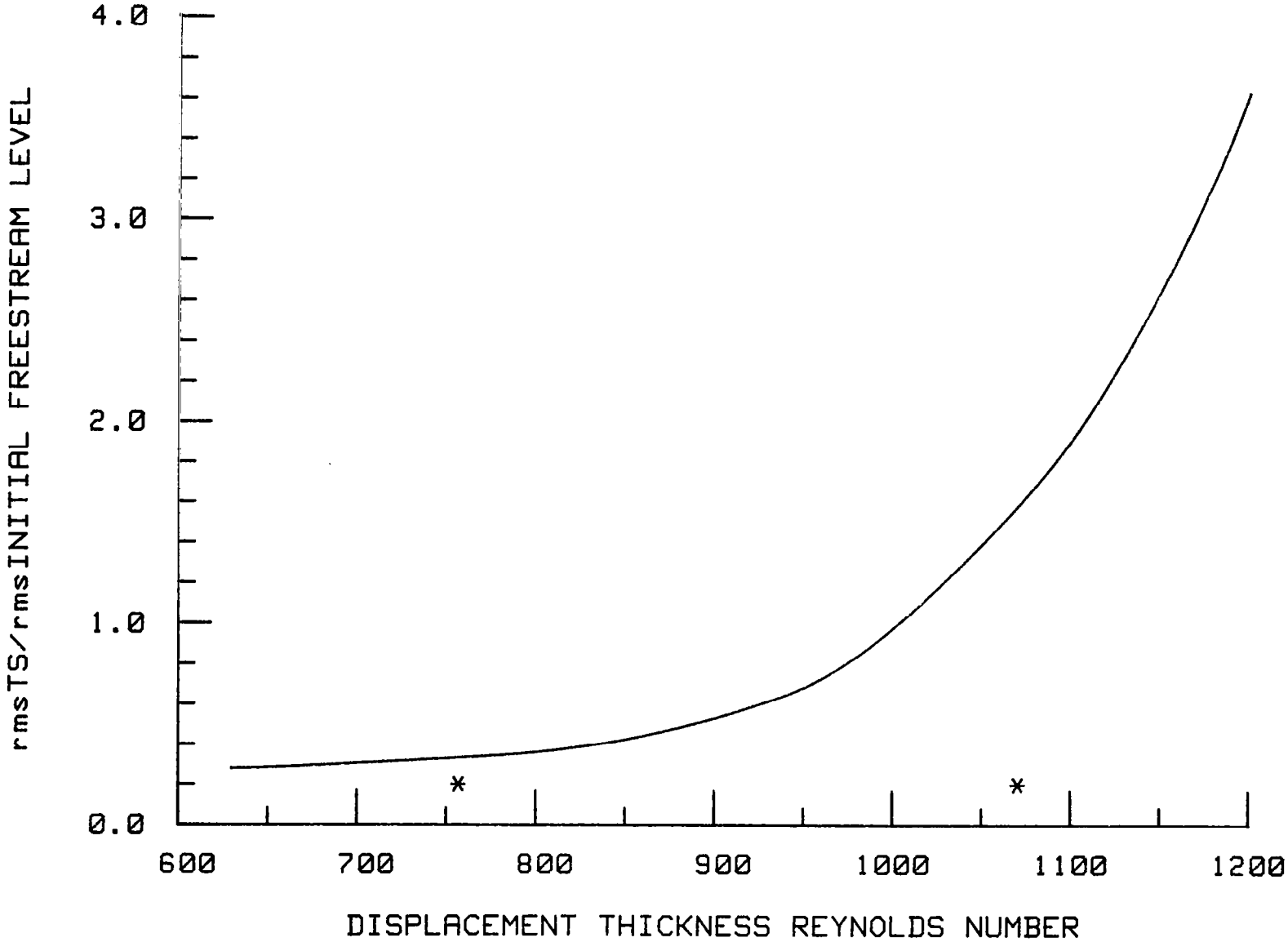

Figure 18.- Variation with Reynolds number of the ratio of the TS wave amplitude to the sound field amplitude at the plate's leading edge as evaluated from Shapiro's data (ref. 3).

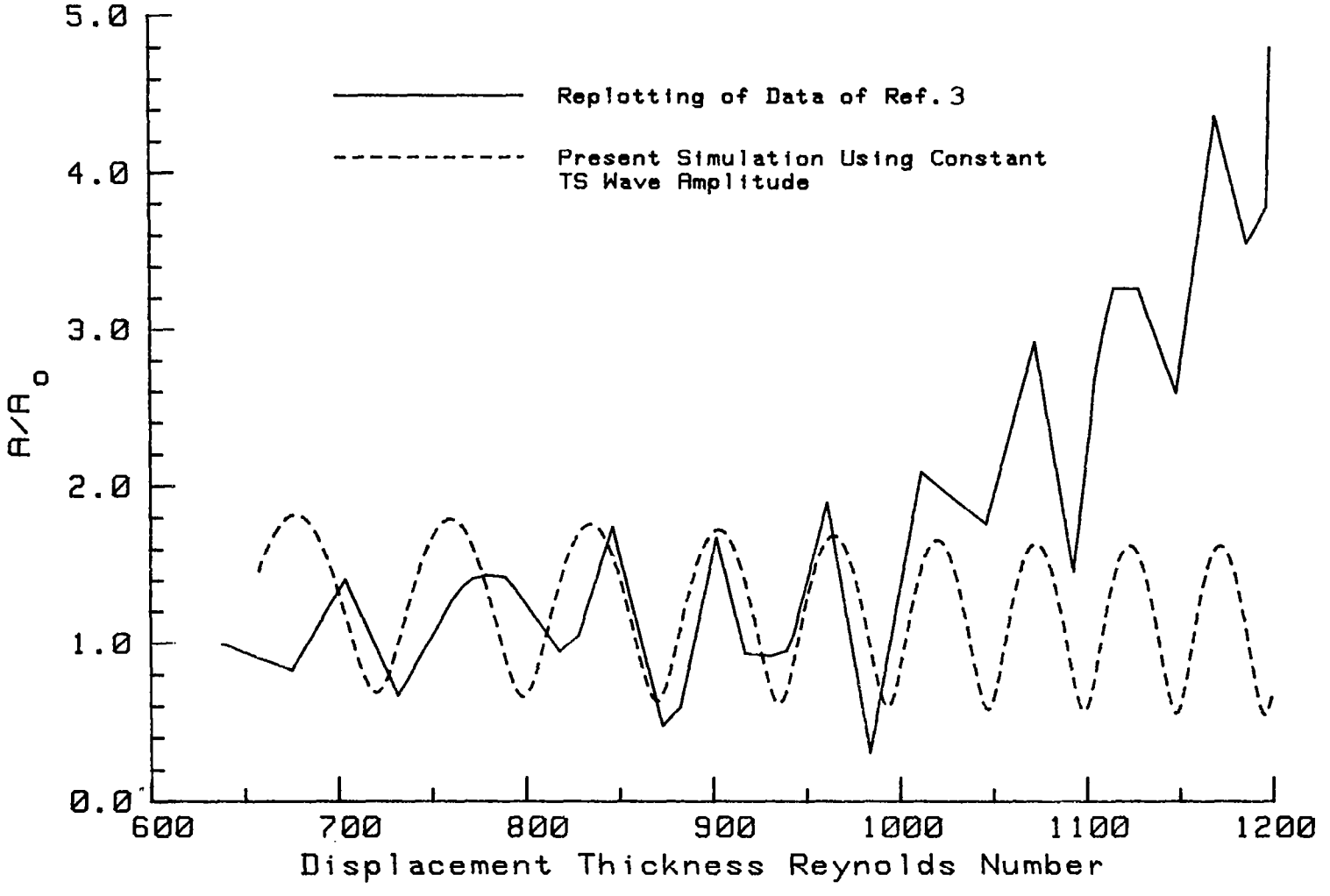

(a) Data and modeled amplitude variation with Reynolds number.

Figure 19.- Comparison of TS wave amplitude and phase angle data with modeled values using a constant TS wave amplitude.

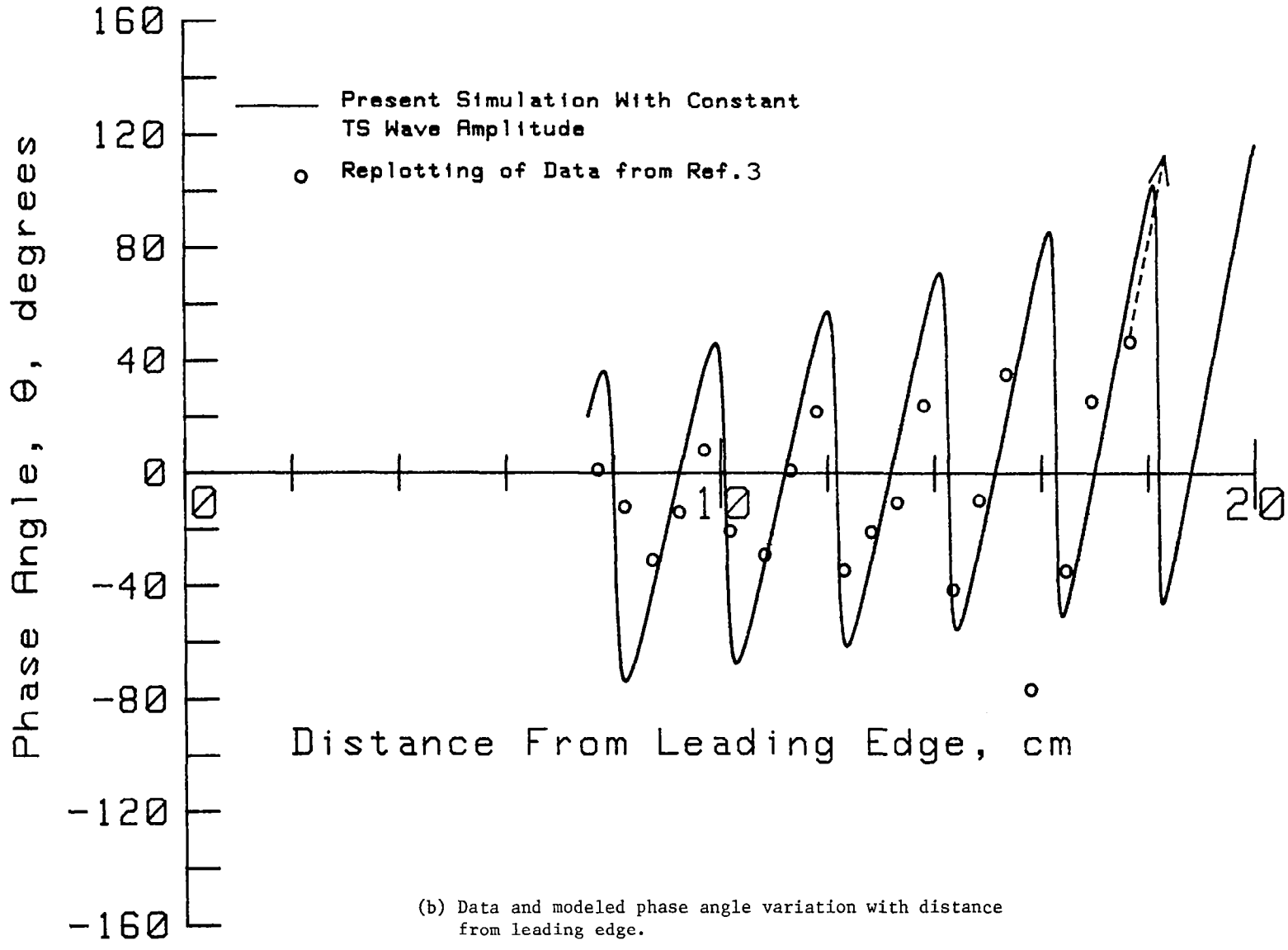

(b) Data and modeled phase angle variation with distance from leading edge.

Figure 19.- Concluded.

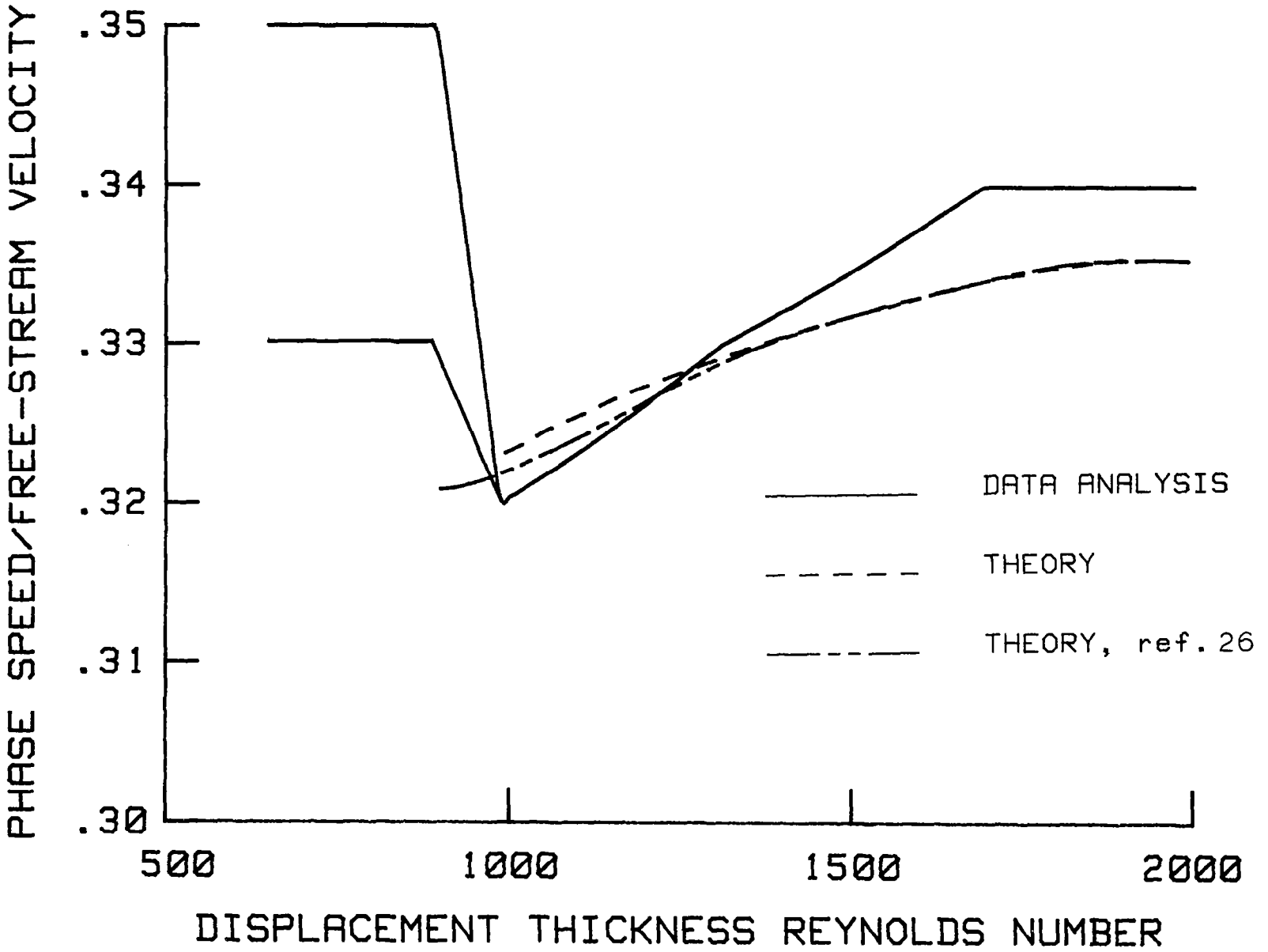

(a) Variation of wave speed with Reynolds number.

Figure 20. - Comparison of nondimensional TS wave speeds as obtained from Shapiro's phase angle data with theoretical flat plate boundary layer stability values.

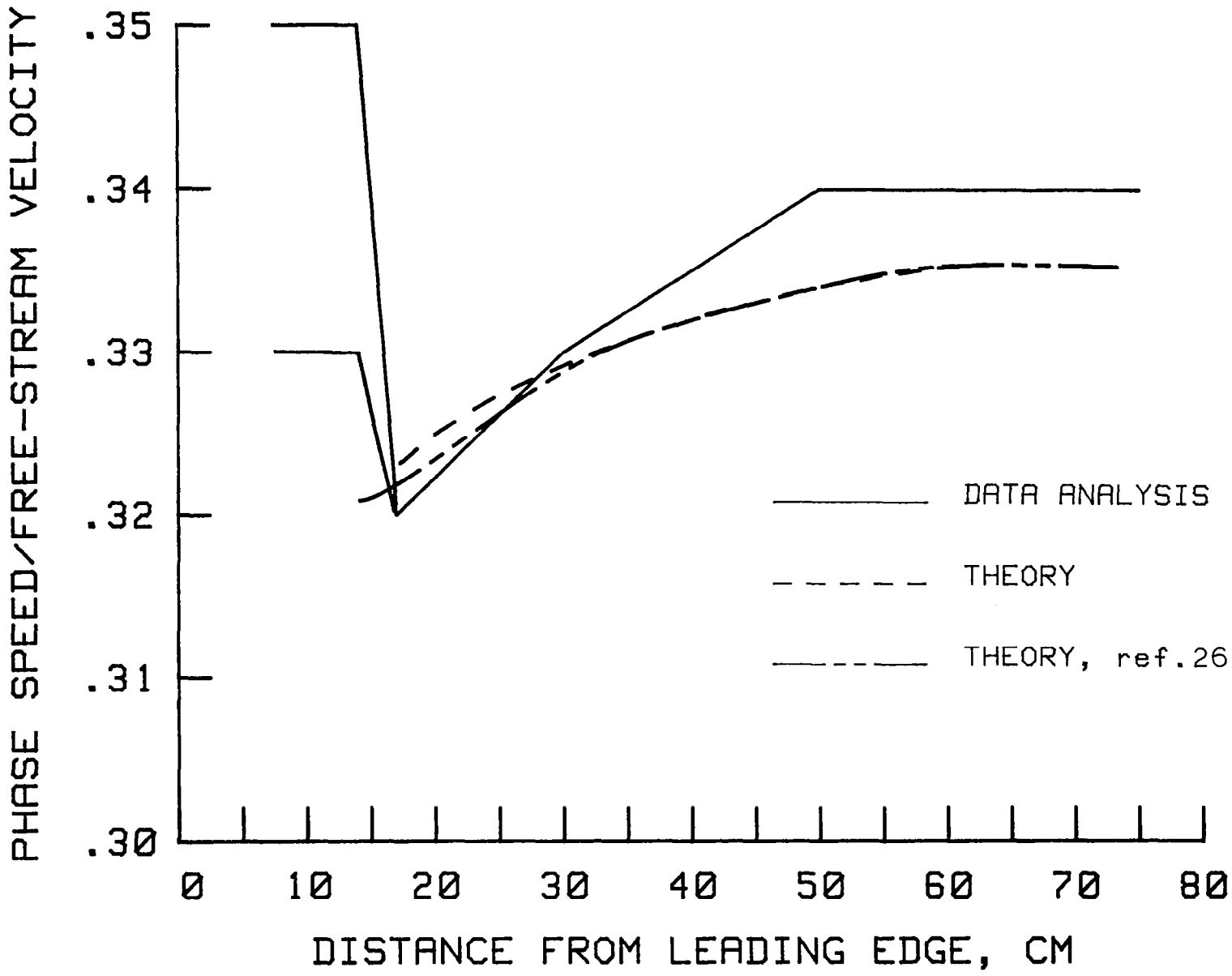

(b) Variation of wave speed with distance from leading edge.

Figure 20. - Concluded

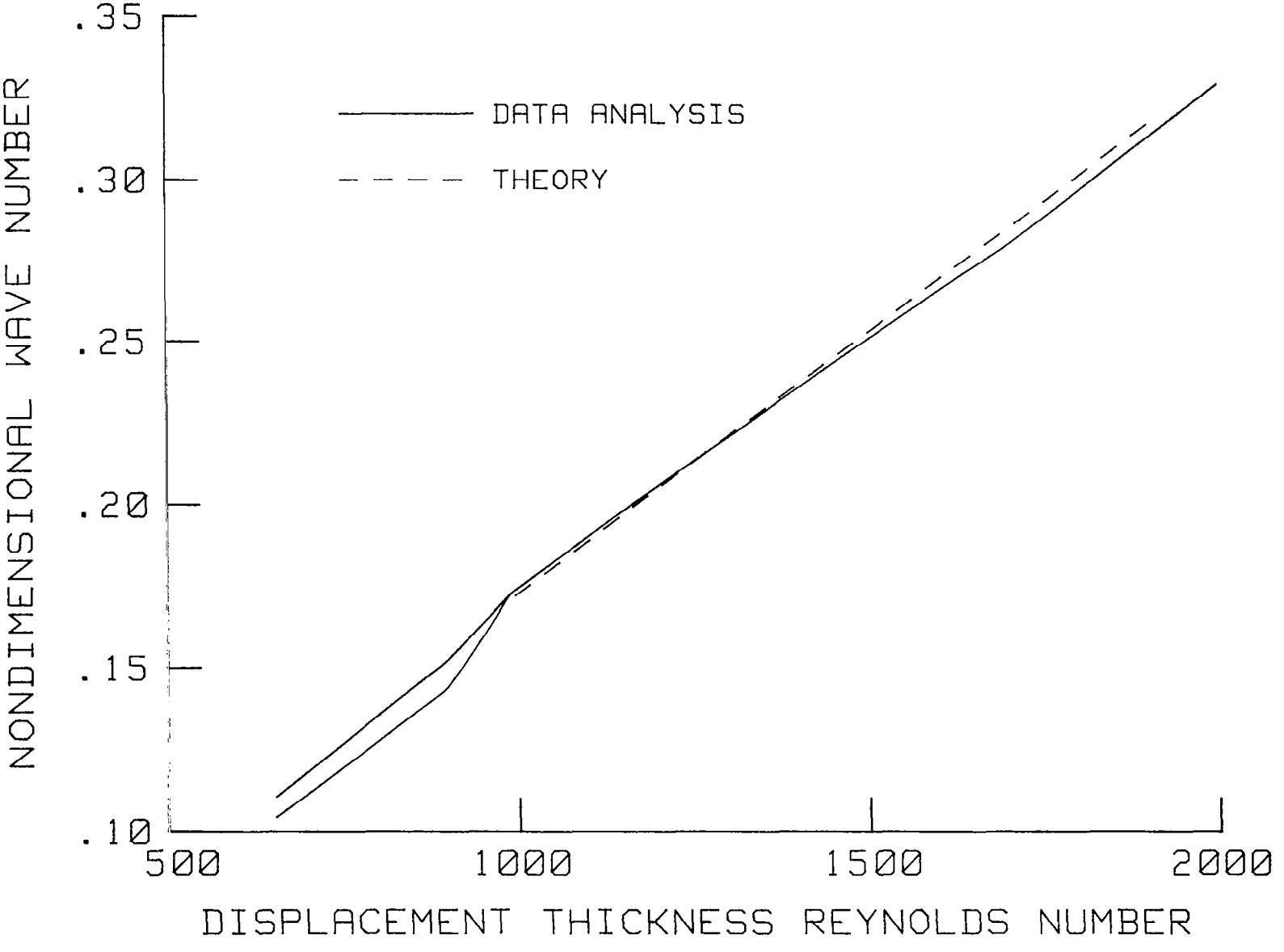

Figure 21. - Comparison of nondimensional wave numbers as obtained from Shapiro's phase angle data (ref. 3) with flat plate boundary layer stability values.

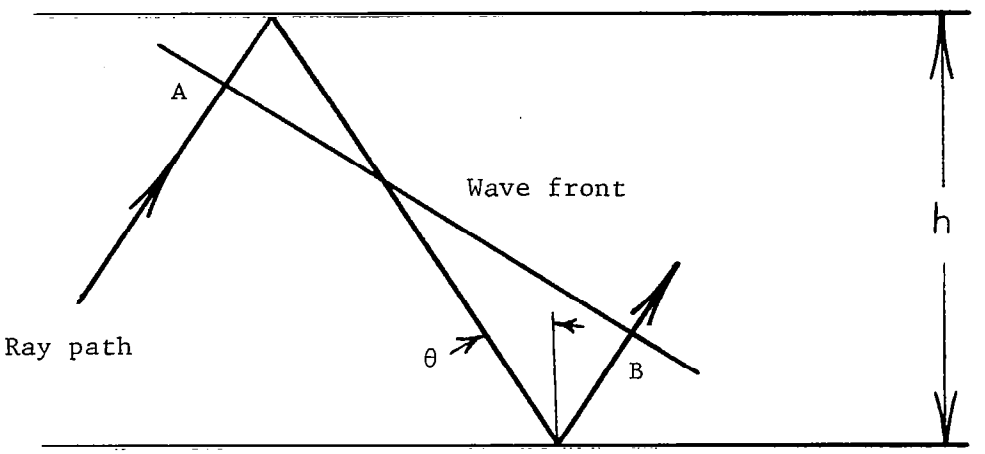

Figure 22. - Constructive interference of reflected wave path. Path length from A to B must be an integer multiple of the wavelength.

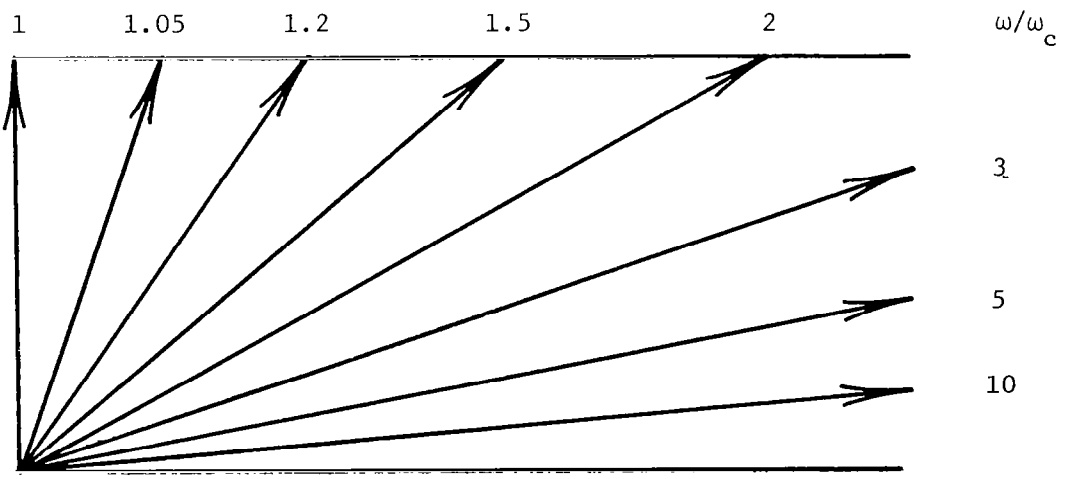

Figure 23. - Direction of propagation of sound waves for a given mode in a duct for different ratios of the frequency to the cutoff frequency of the mode, ω/ω_c.

1. Report No.	2. Government Accession No.	3. Recipient's Catalog No.
NASA CR-3620		

4. Title and Subtitle	5. Report Date
ANALYSIS OF AN EXISTING EXPERIMENT ON THE INTERACTION OF ACOUSTIC WAVES WITH A LAMINAR BOUNDARY LAYER	November 1982
	6. Performing Organization Code
7. Author(s)	8. Performing Organization Report No.
M. R. Schopper	
9. Performing Organization Name and Address	10. Work Unit No.
Systems and Applied Sciences Corporation 17 Research Drive Hampton, Virginia 23666	11. Contract or Grant No. NAS1-16572
	13. Type of Report and Period Covered
12. Sponsoring Agency Name and Address	Contractor Report
National Aeronautics and Space Administration Washington, DC 20546	14. Sponsoring Agency Code 505-31-23-03

15. Supplementary Notes

Langley Technical Monitor: Ivan E. Beckwith
Final Report

16. Abstract

The primary purpose of the present study is the reevaluation of the hot-wire anemometer amplitude data contained in the 1977 report of P. J. Shapiro entitled, "The Influence of Sound Upon Laminar Boundary Layer Instability." As shown here, the low-Reynolds number boundary layer disturbance data were misinterpreted and the present effort was made to improve the corresponding disturbance growth rate curves. The data are modeled as the sum of upstream and downstream propagating acoustic waves and a wave representing the Tollmien-Schlichting (TS) wave. The amplitude and phase velocity of the latter wave were then adjusted so that the total signal reasonably matched the amplitude and phase angle hot-wire data along the plate laminar boundary layer.

The phase velocity results agree well with theoretical two-dimensional TS phase speeds. The TS wave amplitude at the earliest measurement station was 0.25 times the sound field amplitude near the leading edge. The revised rates show growth occurring further upstream than Shapiro found. It appears that the premature growth is due to the adverse pressure gradient created by the shape of the plate. Basic elements of sound propagation in ducts and the experimental and theoretical acoustic-stability literature are reviewed.

17. Key Words (Selected by Author(s))	18. Distribution Statement
Boundary layer stability Boundary layer transition Wind tunnel acoustics	Unclassified-Unlimited Subject Category 34

19. Security Classif. (of this report)	20. Security Classif. (of this page)	21. No. of Pages	22. Price
Unclassified	Unclassified	108	A06

For sale by the National Technical Information Service, Springfield, Virginia 22161

NASA-Langley, 1982